

Consistent spectral approximation of Koopman operators using resolvent compactification

Dimitrios Giannakis¹ and Claire Valva²

¹ Department of Mathematics, Dartmouth College, Hanover, New Hampshire, USA

² Courant Institute of Mathematical Sciences, New York University, New York, New York, USA

E-mail: clairev@nyu.edu

Abstract. Koopman operators and transfer operators represent dynamical systems through their induced linear action on vector spaces of observables, enabling the use of operator-theoretic techniques to analyze nonlinear dynamics in state space. The extraction of approximate Koopman or transfer operator eigenfunctions (and the associated eigenvalues) from an unknown system is nontrivial, particularly if the system has mixed or continuous spectrum. In this paper, we describe a spectrally accurate approach to approximate the Koopman operator on L^2 for measure-preserving, continuous-time systems via a “compactification” of the resolvent of the generator. This approach employs kernel integral operators to approximate the skew-adjoint Koopman generator by a family of skew-adjoint operators with compact resolvent, whose spectral measures converge in a suitable asymptotic limit, and whose eigenfunctions are approximately periodic. Moreover, we develop a data-driven formulation of our approach, utilizing data sampled on dynamical trajectories and associated dictionaries of kernel eigenfunctions for operator approximation. The data-driven scheme is shown to converge in the limit of large training data under natural assumptions on the dynamical system and observation modality. We explore applications of this technique to dynamical systems on tori with pure point spectra and the Lorenz 63 system as an example with mixing dynamics.

Keywords: Koopman operators, transfer operators, measure-preserving systems, spectral approximation, kernel methods, data-driven techniques

AMS classification scheme numbers: 37A10, 37E99, 37G30

1. Introduction

The operator-theoretic formulation of ergodic theory characterizes dynamical systems through their induced action on linear spaces of observables, realized via composition operators, known as Koopman operators, and their duals, known as transfer or Ruelle–Perron–Frobenius operators [4, 29]. Dating back at least to work of Koopman and von Neumann in the 1930s [51, 52], this framework has proven to be a highly powerful analytical tool, allowing to translate problems about nonlinear dynamics, such as occurrence of ergodicity and mixing, to equivalent linear operator problems. Over approximately the past two decades, advances in computational capabilities, numerical methods, and data science have spurred considerable interest in the development of methodologies utilizing these operators for data-driven analysis and forecasting of observables. These methods offer a solid theoretical foundation combined with applicability under real-world data observation modalities, and have been successfully applied in diverse areas such as fluid dynamics, climate dynamics, and molecular dynamics among other fields; see, e.g., the surveys [12, 48, 60, 62].

Yet, despite considerable theoretical and methodological progress, fundamental questions remain, particularly with regards to the complex spectral characteristics of evolution operators associated with deterministic dynamics. Indeed, a measure-preserving flow is weak-mixing if and only if the Koopman operator on L^2 has a simple eigenvalue at 1, with a constant corresponding eigenfunction, and no other eigenvalues [80]. This means that when faced with systems of high dynamical complexity, numerical methods must be able to consistently approximate the continuous Koopman spectrum, which has been a major challenge. Even if the Koopman operator is diagonalizable, its spectrum is oftentimes not discrete (e.g., it forms a dense subset of the unit circle in the measure-preserving case), which also presents numerical challenges. The spectral properties associated with deterministic dynamics are in stark contrast to the behavior of stochastic systems, where the Kolmogorov and Fokker-Planck operators (the stochastic analogs of the Koopman and transfer operators, respectively) have typically discrete spectra due to the presence of diffusion.

In this paper, we propose a data-driven methodology for spectrally consistent approximation of Koopman and transfer operators in continuous-time measure-preserving ergodic flows that approximates the generator by a skew-adjoint operator with compact resolvent (and thus discrete spectrum). Our approach is based on a combination of ideas from two recent papers on Koopman operator approximation: The paper [26] introduced an approximation technique that regularizes the generator, V , of the unitary Koopman group $U^t = e^{tV}$ by pre- and post-composition with kernel integral operators mapping into reproducing kernel Hilbert spaces (RKHSs). This results in a family of compact, skew-adjoint operators V_τ , $\tau > 0$, which are diagonalizable and whose spectral measures converge to the spectral measure of V in the limit of vanishing regularization parameter τ . Meanwhile, in [71], Susuki, Mauroy, and Mezić developed a Koopman spectral analysis technique that focuses on the *resolvent* of the generator,

$R_z(V) = (z - A)^{-1}$, where $z \in \mathbb{C}$ is an element of the resolvent set of V . A key element of their approach is the use of the integral representation of the resolvent,

$$R_z(V) = \int_0^\infty e^{-zt} U^t dt, \quad \operatorname{Re} z > 0, \quad (1)$$

which provides a means for computing $R_z(V)$ via quadrature involving the unitary Koopman operators U^t without requiring access to the unbounded generator V .

Here, we use the compactification approach of [26] and the integral representation of the resolvent employed in [71] to build a compact operator $R_{z,\tau}$ which is the resolvent of a skew-adjoint operator. Using this construction, we obtain a family of skew-adjoint unbounded operators $V_{z,\tau}$ with compact resolvent that converge spectrally to V . We view this as a more natural approximation than the compact approximation V_τ from [26], which could be said to be over-regularized since V_τ is bounded whereas V is unbounded. More precisely, it is known that certain one-parameter families of skew-adjoint operators with compact resolvents exhibit holomorphic dependence of the eigenvalues and corresponding eigenspaces on the parameter, which is not true for families of compact operators due to the concentration of the spectrum near 0 [45, Remark 3.11]. Furthermore, our approximation is structure-preserving in the sense that $V_{z,\tau}$ generates a unitary evolution group analogously to V . In this paper, we also develop data-driven approximations of $V_{z,\tau}$ that are skew-adjoint and converge to $V_{z,\tau}$ in suitable asymptotic limits.

1.1. Review of data-driven methodologies

Since the early works of Mezić and Banaszuk [59, 61] and Dellnitz, Froyland, and Junge [28, 32] on Koopman and transfer operators, respectively, operator-theoretic techniques have emerged as a highly popular framework for analysis of data generated by dynamical systems, with a correspondingly large literature. In broad terms, one can categorize approximation techniques based the function space in which approximation is performed and the topology used to characterize convergence. For forecasting applications, convergence in strong or weak operator topologies is generally adequate since one is interested in approximating the action of the Koopman or transfer operators on specific forecast observables and/or functionals (e.g., expectation functionals). On the other hand, spectral decomposition techniques generally require stronger approximations to ensure convergence of the spectral measure and/or eliminate spectral pollution. For example, strong resolvent convergence, or generalized strong resolvent convergence, imply convergence of the spectral measure [10, 14] (without eliminating the possibility of spectral pollution; see remark 2.3). In any of these settings, the choice of function space is a key consideration affecting the convergence, robustness, and amount of information that can be extracted from numerical techniques, particularly in spectral analysis applications where the Koopman and transfer operator spectra depend strongly on the space of functions on which these operators are allowed to act. Below, we outline

some of the techniques that are more closely related to the methodology described in this paper.

The dynamic mode decomposition (DMD) was originally proposed by Schmid and Sesterhenn as a method for analysis of fluid mechanical snapshot data [69, 68], was interpreted by Rowley et al. [66] as a Koopman operator approximation technique, and is now perhaps the most popular technique for Koopman spectral analysis. It is closely related to linear inverse models [63, 75], whereby the Koopman operator is approximated by a finite-rank operator in a dictionary of linear observables. The raw DMD method provides limited convergence guarantees to the infinite-dimensional Koopman operator, and it has been modified and generalized in many ways since its inception. Among these modifications is the extended DMD (EDMD) technique of Williams et al. [81], which replaces the linear DMD dictionary by more general dictionaries of nonlinear observables to derive Galerkin methods for approximation of the Koopman operator on L^2 . The use of generalized dictionaries considerably increases the potential approximation power of the method, though the original EDMD formulation offered limited explicit mechanisms to control the asymptotic behavior of the approximation as the dictionary size increases. This becomes an especially pertinent issue in dynamical systems with invariant measures supported on geometrically complex, potentially unknown sets (e.g., nonlinear manifolds or fractal attractors), where it is not obvious how to choose a dictionary that will lead to a well-conditioned EDMD approximation.

Recently, Colbrook and Townsend [20] proposed a DMD-type algorithm called residual DMD (ResDMD) that employs a residual-based approach to eliminate spurious eigenvalues resulting, e.g., from spectral pollution or ill-conditioned EDMD dictionaries. Combined with a framework for approximation of the Koopman resolvent using high-order quadrature, ResDMD is also able to compute smoothed approximations of the spectral measure of the Koopman operator with convergence guarantees. Other variants of DMD such as mpDMD [19] and piDMD [2] preserve unitarity of the Koopman operator on L^2 for measure-preserving invertible transformations. Earlier work of Govindarajan et al. [39] developed approximations of the Koopman operator based on periodic approximations of the underlying state space dynamics; such Koopman operator approximations are automatically unitary. In the paper [53], Korda, Putinar, and Mezić developed a technique that employs the Christoffel-Darboux kernel in spectral space to consistently approximate the spectral measure of the Koopman operator for measure-preserving systems.

On the transfer operator side, popular approximation techniques are based on the Ulam method [77]. The Ulam method creates a finite-rank approximation of the transfer operator by partitioning the state space into a finite collection of subsets, and building a Markov matrix from associated transition probabilities under the dynamics. Essentially, the method can be viewed as a Galerkin approximation in subspaces of L^p spanned by piecewise-constant functions. An advantage of the Ulam method is that it is positivity preserving; that is, the finite-rank approximate operator maps positive functions to positive functions which is a key structural property of transfer operators. The Ulam

method has been shown to yield spectrally consistent approximations for particular classes of systems such as expanding maps and Anosov diffeomorphisms on compact manifolds [32]. In some cases, spectral computations from the Ulam method have been shown to recover eigenvalues of transfer operators on anisotropic Banach spaces adapted to the expanding/contracting subspaces of such systems [9]; however, these results depend on carefully chosen state space partitions that may be hard to construct in high dimensions and/or under unknown dynamics. Various modifications of the basic Ulam method have been proposed that are appropriate for high-dimensional applications; e.g., set-oriented methods [28] and sparse grid techniques [43]. Recent techniques for transfer operator approximation have employed smoothing by kernel integral operators [33] and regularization of optimal transport plans [50, 44].

Another family of approaches has emphasized the use of data-driven dictionaries for Koopman/transfer operator approximation. Among these is a technique called diffusion forecasting [6], which approximates Koopman and transfer operators (or their Kolmogorov/Fokker Planck analogs in stochastic systems) using a data-driven basis of L^2 obtained via the diffusion maps algorithm [16]. Leveraging spectral convergence results for kernel integral operators [74, 79], this approach was shown to produce a well-conditioned consistent approximation as the amount of training data and basis function increases, thus avoiding issues associated with dictionary choice in *ad hoc* applications of EDMD. In [38, 35], the diffusion forecasting technique was adopted in a framework that approximates the generator V of measure-preserving ergodic flows on manifolds by an advection–diffusion operator $L_\tau = V - \tau\Delta$, where τ is a regularization parameter and Δ is a Laplace-type diffusion operator. Using a normalized diffusion maps basis appropriate for H^1 Sobolev regularity, a Galerkin method was developed for the eigenvalue problem of L_τ which was found to perform well for systems with pure point spectrum such as ergodic rotations on tori. While promising numerical results were also obtained for mixing systems, [38, 35] did not address the question of consistent approximation of the continuous Koopman spectrum.

Arguably, the most straightforward case for analyzing the spectral properties of diffusion-regularized generators such as L_τ occurs when the regularizing operator Δ commutes with V . The papers [23, 35] showed that such a commuting operator Δ can be obtained from the infinite-delay limit of a family of kernel integral operators constructed using delay-coordinate maps [67, 72]. This result indicates that incorporating delays is useful for improving the efficiency of Koopman eigenfunction approximation in data-driven bases, though the infinite-delay limit was found to be trivial if V is the generator of a weak-mixing system. Earlier work [5, 11, 37] had independently explored incorporating delay coordinates (possibly with weights [5]) in diffusion maps and Koopman operator approximation techniques and found that the approach helps reveal slowly decorrelating observables under complex dynamics. Further asymptotic analysis [36] related such slowly-decorrelating observables to the ϵ -approximate Koopman spectrum.

The methods outlined above perform approximation of Koopman operators on L^p

spaces, oftentimes associated with invariant measures. In recent years, a distinct line of work has emerged that focuses on approximation of Koopman operators on RKHSs [1, 24, 26, 42, 46, 49, 54, 65, 64]. Unlike L^2 spaces whose elements are equivalence classes of functions, RKHSs are function spaces with continuous pointwise evaluation functionals. This allows leveraging techniques from learning theory [22] to perform spectral analysis and forecasting of observables. At the same time, a challenge with RKHS techniques is that, aside from special cases such as translations on groups, a general RKHS \mathcal{H} is not invariant under the action of the Koopman operator, making the choice of reproducing kernel a delicate matter. At a minimum, the kernel should be chosen such that the Koopman operator on \mathcal{H} is densely defined and closable. Provided that such a kernel can be found (which is, in general, non-trivial [42]), the Koopman operator on \mathcal{H} will typically be unbounded, introducing theoretical and numerical complications.

1.2. Reproducing kernel Hilbert space compactification

As a motivation of our approach, we summarize in more detail the RKHS-based Koopman approximation framework proposed in [26]. Rather than identifying RKHSs tailored to particular dynamical systems, [26] employed a different approach that starts from a one-parameter family of reproducing kernels k_τ , $\tau > 0$, satisfying mild regularity assumptions, and uses the corresponding integral operators to perturb the Koopman generator such that it is a compact operator on the corresponding RKHS. In more detail, for a continuous-time, measure-preserving ergodic flow on a state space X with invariant measure μ and generator V on $L^2(\mu)$, the compactification approach of [26] builds a one-parameter family of skew-adjoint compact operators $W_\tau : \mathcal{H}_\tau \rightarrow \mathcal{H}_\tau$, where $W_\tau = P_\tau V P_\tau^*$ and $P_\tau : L^2(\mu) \rightarrow \mathcal{H}_\tau$ is an integral operator mapping into the RKHS \mathcal{H}_τ ,

$$P_\tau f = \int_X p_\tau(\cdot, x) f(x) d\mu(x).$$

The operators W_τ turn out to be unitarily equivalent to $V_\tau = G_\tau^{1/2} V G_\tau^{1/2}$, $G_\tau \equiv P_\tau^* P_\tau$, acting on $L^2(\mu)$. The latter, were shown to be compact, skew-adjoint operators converging in strong resolvent sense (and thus spectrally) to the generator V as $\tau \rightarrow 0$.

The compactness of V_τ and W_τ makes these operators amenable to finite-rank approximation by projection onto finite-dimensional subspaces of $L^2(\mu)$ and \mathcal{H}_τ , respectively, spanned by eigenvectors of G_τ . Eigendecomposition of the projected operators then yields approximate Koopman eigenvalues and eigenfunctions which were shown to lie in the ϵ -approximate point spectrum of the Koopman operator for a tolerance ϵ that depends on an RKHS-induced Dirichlet energy functional. In particular, eigenfunctions of the projected V_τ or W_τ with small Dirichlet energy as $\tau \rightarrow 0$ were shown to be approximately cyclical, slowly decorrelating observables under potentially mixing dynamics. Moreover, being elements of RKHSs, the eigenfunctions of W_τ can be used in conjunction with the Nyström method in supervised-learning models for

predicting the evolution of observables. Since V_τ and W_τ are skew-adjoint operators, the associated evolution operators e^{tV_τ} and e^{tW_τ} are automatically unitary on $L^2(\mu)$ and \mathcal{H}_τ , respectively. Unitarity of e^{tV_τ} and e^{tW_τ} is structurally consistent with unitarity of the unperturbed Koopman operator $U^t = e^{tV}$.

Yet, despite these attractive features, the RKHS compactification schemes of [26] suffer from two potential shortcomings. First, the compactness and skew-adjointness of V_τ and W_τ means that the spectra of these operators are confined to bounded intervals in the imaginary line containing 0. This leads to a high concentration of eigenvalues and frequent eigenvalue crossings as τ is varied (see, e.g., [26, Fig. 3]), contributing to sensitivity of the spectra of V_τ/W_τ with respect to τ , and hindering the identification of continuous curves of eigenvalues and eigenfunctions. Note that advection–diffusion operators of the type L_τ from section 1.1 do not suffer from this issue since they are unbounded operators whose spectra are not confined to the imaginary line (though note that these methods rely on the support of the invariant measure having sufficient regularity to appropriately define a diffusion operator Δ). Another possible shortcoming of [26] pertains to the way the action of the generator V is approximated in data-driven settings. Their approach utilizes finite-difference schemes applied to time-ordered data, and while the error of these approximations can be controlled in the limit of vanishing sampling interval using RKHS regularity, finite-differencing is generally detrimental to noise robustness. Avoiding a finite-difference approximation would also facilitate the processing of data at variable time intervals.

1.3. Contributions of this work

Combining ideas from [26] and [71], we develop a data-driven Koopman spectral analysis technique for continuous-time, measure-preserving ergodic flows that is based on a compactification of the resolvent $R_z(V)$ of the generator. The primary distinguishing features of this approach are outlined below. Figure 1 summarizes the main steps of the scheme in a flowchart.

- (i) *Spectral convergence.* By smoothing $R_z(V)$ with kernel integral operators G_τ , $\tau > 0$, we build a family of compact operators $R_{z,\tau} : L^2(\mu) \rightarrow L^2(\mu)$ that converge strongly to $R_z(V)$. For any nonzero real number z , the $R_{z,\tau}$ are resolvents of skew-adjoint unbounded operators $V_{z,\tau}$ on $L^2(\mu)$ whose spectral measures converge strongly to V (see theorem 3.5). By standard properties of the functional calculus, the $V_{z,\tau}$ generate unitary evolution groups $\{U_{z,\tau}^t := e^{tV_{z,\tau}}\}_{t \in \mathbb{R}}$ that converge strongly to the Koopman group, i.e., $\lim_{\tau \rightarrow 0^+} U_{z,\tau}^t f = U^t f$ for any observable $f \in L^2(\mu)$ and evolution time $t \in \mathbb{R}$. These results hold for systems of arbitrary (pure-point, continuous, mixed) spectral characteristics, and do not require differentiable structure for the support of the invariant measure.
- (ii) *Structure preservation.* The regularized generators $V_{z,\tau}$ preserve two important properties V : they are skew-adjoint and unbounded. As just mentioned, skew-adjointness makes these operators amenable to analysis via the spectral theorem

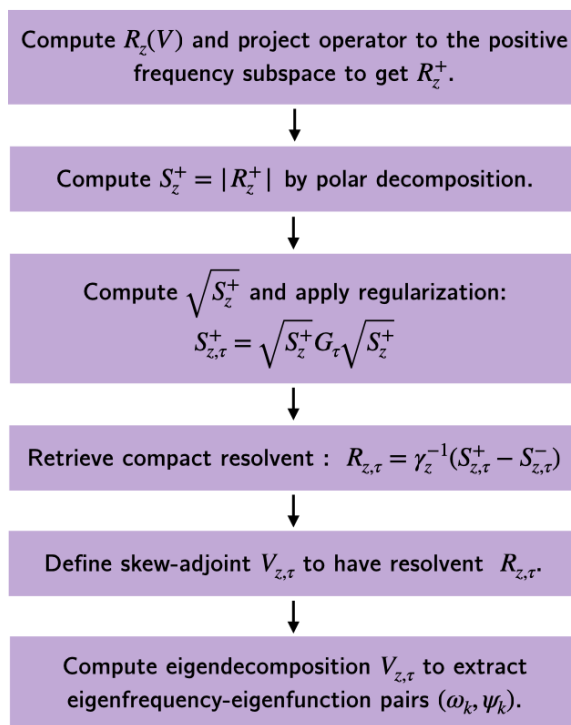


Figure 1. Overview of the resolvent compactification scheme for spectral approximation of the Koopman generator V described in the paper.

and functional calculus for normal operators on Hilbert spaces. Moreover, in our view, unboundedness of $V_{z,\tau}$ represents an improvement over the compactification schemes of [26] as it avoids issues associated with concentration of eigenvalues on bounded intervals containing 0 (see section 1.2). Additionally, the unboundedness of $V_{z,\tau}$ can provide a practical benefit in the analysis of Koopman eigenfrequencies obtained from a given dynamical system. As eigenfrequencies do not cluster at zero, it can be easier to identify and interpret the lower frequencies that may be of interest.

- (iii) *Consistent data-driven approximation.* We approximate $V_{z,\tau}$ by finite-rank, skew-adjoint operators acting on eigenspaces of the smoothing operators G_τ . In data-driven applications, the finite-rank operators are represented in a well-conditioned basis of kernel eigenvectors computed from trajectory data with convergence guarantees in the large-data limit. In particular, the use of kernel eigenvectors avoids issues due to ad hoc choice of dictionaries, and the basis vectors are well-adapted to invariant measures supported on geometrically complex sets (e.g., fractal attractors) embedded in high-dimensional ambient spaces. Other approximation steps include numerical quadrature to approximate the resolvent integral in (1) and low-rank projection to constrain the numerically approximated eigenfunctions of $V_{z,\tau}$ to either positive- or negative-frequency subspaces of $L^2(\mu)$. The scheme converges in the successive limits of increasing number of samples N , integral

quadrature nodes Q , kernel eigenvectors L , and rank parameter $M \leq L$, followed by decreasing the regularization parameter τ to 0.

- (iv) *No finite differencing.* Through the use of the integral representation (1) for the resolvent, our approach obviates the need to perform finite-difference approximations of the generator (as done, e.g., in [38, 35, 26]). Rather than being directly dependent on the temporal sampling interval of the data, which is oftentimes difficult to control in practical applications, our approximation utilizes numerical quadrature methods for evaluating the integral for $R_z(V)$ in (1). This provides a flexible framework for controlling approximation accuracy by varying z in relation to the sampling interval and the timespan of the training data. Additionally, the integral representation of the resolvent opens the possibility of using recently developed high-order resolvent-based schemes for approximation of spectral measures [18].
- (v) *Identification of slowly decorrelating observables.* Eigendecomposition of $V_{z,\tau}$ reveals slowly decorrelating observables of the dynamical system and their associated characteristic frequencies. When the generator V possesses non-trivial point spectrum, the spectra of $V_{z,\tau}$ contain sequences of eigenvalues converging to each of the eigenvalues of V (including in situations when the point spectrum of V is not discrete), and the corresponding eigenspaces of $V_{z,\tau}$ converge to Koopman eigenspaces. When the spectrum of V has a non-trivial continuous component (i.e., the span of its eigenvectors is not dense in $L^2(\mu)$) the spectra of $V_{z,\tau}$ contain eigenfunctions that behave as approximate Koopman eigenfunctions. These eigenfunctions reveal slowly decorrelating observables under potentially mixing dynamics. In section 6, we present numerical experiments illustrating the properties of these eigenfunctions in systems with pure point spectrum (ergodic rotation and skew-rotation on \mathbb{T}^2), and mixing (Lorenz 63 (L63) system).

1.4. Plan of the paper

In section 2 we introduce the class of dynamical systems under study and state the problem of spectral approximation of Koopman and transfer operators that will be the focus of the paper. In section 3, we describe our mathematical framework for Koopman spectral analysis by resolvent compactification, and state and prove our main theoretical results. In section 4, we construct finite-rank approximations of our compactification scheme. This is followed by a description of its data-driven numerical implementation in section 5. Section 6 presents our numerical experiments to the ergodic torus rotation, skew rotation, and L63 system. The main text ends in section 7 with a brief conclusory discussion. Appendix A contains an overview of the kernel construction employed in the operators G_τ . Appendix B contains plots of analytically known Koopman eigenfunctions on the torus for comparison with the numerical results in section 6.

2. Problem statement

In this section, we introduce the class of dynamical systems (section 2.1) and the Koopman spectral analysis problem we wish to study (sections 2.2 and 2.3). Aside from a few exceptions, which we will explicitly point out, our setup and notation follow closely [26].

2.1. Dynamical system

We consider a continuous-time, continuous flow $\Phi^t : \mathcal{M} \rightarrow \mathcal{M}$, $t \in \mathbb{R}$, on a metric space \mathcal{M} . The flow is assumed to have an ergodic invariant Borel probability measure μ with compact support $X \subseteq \mathcal{M}$. We also assume that there is a compact set $M \subseteq \mathcal{M}$ which is forward-invariant (i.e., $\Phi^t(M) \subseteq M$ for any $t \geq 0$) and contains X . As noted in [26], many dynamical systems encountered in applications belong in this class, including ergodic flows on compact manifolds with regular invariant measures (in which case $\mathcal{M} = M = X$), dissipative ordinary differential equations on noncompact manifolds (e.g., the L63 system [57], where $\mathcal{M} = \mathbb{R}^3$, M is an absorbing ball [56], and X a fractal attractor [76]), and dissipative partial equations with inertial manifolds [21] (where \mathcal{M} is an infinite-dimensional function space). We should point out that [26] required that the compact set M be a C^1 manifold and that the restricted flow $\Phi^t|_M$ is C^1 . These conditions were introduced in order to ensure the well-definition of certain approximations involving the generator (whose domain includes C^1 functions). As mentioned in section 1, the approximations developed in this work do not require direct access to the generator, and thus we may drop C^1 regularity assumptions.

The flow Φ^t induces a group of unitary Koopman operators on the Hilbert space $H = L^2(\mu)$ that act by composition, $U^t f = f \circ \Phi^t$. By Stone's theorem on strongly continuous 1-parameter unitary groups [70], the Koopman group $U = \{U^t\}_{t \in \mathbb{R}}$ has a skew-adjoint generator $V : D(V) \rightarrow H$ defined on a dense subspace $D(V) \subseteq H$ as

$$Vf = \lim_{t \rightarrow 0} \frac{U^t f - f}{t},$$

where the limit is taken in the $L^2(\mu)$ norm. The generator completely characterizes the Koopman group, in the sense that any other strongly continuous one-parameter group on H with generator V is identical to U . Moreover, V reconstructs the Koopman operator at any time $t \in \mathbb{R}$ by exponentiation, $U^t = e^{tV}$, defined via the Borel functional calculus.

We note that the adjoint of $U^t : H \rightarrow H$ coincides with the time- t transfer operator $P^t : H \rightarrow H$, $P^t f = f \circ \Phi^{-t}$; that is, $(U^t)^* = U^{-t} = P^t$. Thus, working with the Koopman vs. transfer operator on H is merely a matter of convention, though it should be kept in mind that in other function spaces and/or under non-unitary dynamics the Koopman and transfer operator families are generally different. For detailed expositions of operator-theoretic aspects of ergodic theory we refer the reader to [4, 29].

In what follows, $\langle f, g \rangle = \int_X f^* g d\mu$ and $\|f\|_H = \langle f, f \rangle$ are the standard inner product and norm of H , respectively, where the inner product is taken conjugate-linear in the first argument. Moreover, $\mathbf{1} : \mathcal{M} \rightarrow \mathbb{R}$ is the function on \mathcal{M} equal to 1 everywhere, and $\tilde{H} = \{f \in H : \langle \mathbf{1}, f \rangle \equiv \int_{\mathcal{M}} f d\mu = 0\}$ is the closed subspace of H consisting of zero-mean functions with respect to the invariant measure. We equip the space of continuous functions on M with the standard Banach space norm $\|f\|_{C(M)} = \max_{x \in M} |f(x)|$, and define the closed subspace $\tilde{C}(M) = \{f \in C(M) : \int_M f d\mu = 0\}$ analogously to $\tilde{H} \subset H$. We define $\iota : C(M) \rightarrow H$ as the bounded linear map that maps continuous functions on M into their corresponding equivalence classes in H . We will denote the space of bounded linear maps on a Banach space \mathbb{E} as $B(\mathbb{E})$, and $\|A\|$ will be the operator norm of $A \in B(\mathbb{E})$. Limits in the norm topology and strong operator topology of $B(\mathbb{E})$ will be denoted as \xrightarrow{n} and \xrightarrow{s} , respectively. Given an operator $A : D(A) \rightarrow \mathbb{E}$ defined on a subspace $D(A) \subseteq \mathbb{E}$, $\rho(A)$ and $\sigma(A)$ will denote the resolvent set and spectrum of A , respectively. Given a topological space \mathbb{X} , $\mathcal{B}(\mathbb{X})$ will denote the Borel σ -algebra generated by the open subsets of \mathbb{X} .

2.2. Spectral decomposition of measure-preserving ergodic flows

By the spectral theorem for skew-adjoint operators, the spectrum of the generator V is a closed subset of the imaginary line, $\sigma(V) \subseteq i\mathbb{R}$, and there exists a projection-valued measure (PVM) $E : \mathcal{B}(i\mathbb{R}) \rightarrow B(H)$ decomposing the generator and Koopman operators via the spectral integrals

$$V = \int_{i\mathbb{R}} \lambda dE(\lambda), \quad U^t = \int_{i\mathbb{R}} e^{t\lambda} dE(\lambda). \quad (2)$$

A fundamental result in ergodic theory [40] states that there is a U^t -invariant splitting $H = H_p \oplus H_c$ into orthogonal subspaces H_p and H_c and a decomposition $E = E_p + E_c$ into PVMs $E_p : \mathcal{B}(i\mathbb{R}) \rightarrow B(H_p)$ and $E_c : \mathcal{B}(i\mathbb{R}) \rightarrow B(H_c)$, where E_p is discrete (i.e., there is a countable set $\sigma_p(V) \subseteq \sigma(V)$ such that $E_p(i\mathbb{R} \setminus \sigma_p(V)) = 0$), and E_c is continuous, (i.e., E_c has no atoms).

The set $\sigma_p(V)$ consists of the eigenvalues of V which are also atoms of E_p ; that is, given $\lambda \in i\mathbb{R}$ we have $E_p(\{\lambda\}) \neq 0$ iff $\lambda \in \sigma_p(V)$, in which case there is a corresponding eigenvector $\psi \in H$ such that $V\psi = \lambda\psi$. Correspondingly, H_p admits an orthonormal basis $\{\psi_l\}_{l \in \mathbb{Z}}$ consisting of generator eigenfunctions that satisfy $V\psi_l = i\omega_l\psi_l$ for $i\omega_l \in \sigma_p(V)$. We call the real numbers ω_l eigenfrequencies. Since V is a real operator, i.e., $(Vf)^* = V(f^*)$ for every $f \in D(V)$, it is natural to order the eigenvectors and corresponding eigenfrequencies such that $\psi_{-l} = \psi_l^*$ and $\omega_{-l} = -\omega_l$. Moreover, since μ is an ergodic invariant measure under Φ^t , every eigenvalue $i\omega_l$ is simple.

From (2), we see that the Koopman evolution of an observable $f \in H_p$ is expressible as

$$U^t f = \sum_{l \in \mathbb{Z}} e^{i\omega_l t} c_l \psi_l, \quad c_l = \langle \psi_l, f \rangle, \quad (3)$$

where the summands are periodic in time t with period $2\pi/\omega_l$. It should be noted that the discreteness of E_p does not imply that $\sigma_p(V)$ is a discrete set; in fact, so long as $\sigma_p(V)$ contains two rationally independent elements (such as in the case of an ergodic rotation on the 2-torus; see (57)), $\sigma_p(V)$ is a dense subset of the imaginary line. As noted in section 1.1, this presents numerical challenges and typically necessitates some form of regularization of V for stable computation of the eigenvalues in $\sigma_p(V)$ and the corresponding eigenfunctions. See [26, figure 5] for an illustration of poor behavior of naive discretizations of the generator of an ergodic rotation on \mathbb{T}^2 that occur even when using a well-conditioned Fourier basis.

Unlike the quasiperiodic evolution from (3), observables in the continuous spectrum subspace H_c exhibit a decay of correlations characteristic of weak-mixing dynamics. Specifically, defining the temporal cross-correlation function $C_{fg} : \mathbb{R} \rightarrow \mathbb{C}$ of two observables $f, g \in H$ as $C_{fg}(t) = \langle f, U^t g \rangle$, it can be shown that if g lies in H_c ,

$$\lim_{T \rightarrow \infty} \frac{1}{T} \int_0^T |C_{fg}(t)| dt = 0, \quad \forall f \in H; \quad (4)$$

see, e.g., the proof of the Mixing Theorem in [40, p. 39]. If the system is weak-mixing, i.e., $\lim_{T \rightarrow \infty} \frac{1}{T} \int_0^T |\mu(A \cap \Phi^{-t}(B)) - \mu(A)\mu(B)| dt = 0$ for any two sets $A, B \in \mathcal{B}(X)$, then we have $H_c = \tilde{H}$ and (4) holds for any mean-zero observable $g \in \tilde{H}$.

2.3. Spectral approximation by operators with discrete spectrum

Equation (4), in conjunction with the fact that H_c has, by definition, no basis of Koopman eigenfunctions, raises the question of what should be appropriate generalizations of the Koopman eigenfunction basis of H_p that are able to capture the evolution of arbitrary observables in H (including, in particular, observables in the continuous spectrum subspace H_c) in a manner that behaves approximately like the decomposition in (3). Following [26], we will build such bases by eigendecomposition of a family of operators that are skew-adjoint and diagonalizable (and thus have associated orthonormal eigenfunctions), and converge spectrally to the generator V in a limit of vanishing regularization parameter. To that end, we recall the following notions of convergence of skew-adjoint operators [14, 27].

Definition 2.1 (Convergence of skew-adjoint operators). Let $A : D(A) \rightarrow \mathbb{H}$ be a skew-adjoint operator on a Hilbert space \mathbb{H} and $A_\tau : D(A_\tau) \rightarrow \mathbb{H}$ a family of skew-adjoint operators indexed by τ , with resolvents $R_z(A) = (zI - A)^{-1}$ and $R_z(A_\tau) = (zI - A_\tau)^{-1}$ respectively.

- (i) The family A_τ is said to converge in strong resolvent sense to A as $\tau \rightarrow 0^+$, denoted $A_\tau \xrightarrow{\text{sr}} A$, if for some (and thus, every) $z \in \mathbb{C} \setminus i\mathbb{R}$ the resolvents $R_z(A_\tau)$ converge strongly to $R_z(A)$; that is, $\lim_{\tau \rightarrow 0^+} R_z(A_\tau)f = R_z(A)f$ for every $f \in \mathbb{H}$.
- (ii) The family A_τ is said to converge in strong dynamical sense to A as $\tau \rightarrow 0^+$, denoted $A_\tau \xrightarrow{\text{sd}} A$ if, for every $t \in \mathbb{R}$, the unitary operators e^{tA_τ} converge strongly to e^{tA} ; that is, $\lim_{\tau \rightarrow 0^+} e^{tA_\tau}f = e^{tA}f$ for every $f \in \mathbb{H}$.

It can be shown, e.g., [27, Proposition 10.1.8], that strong resolvent convergence and strong dynamical convergence are equivalent notions. For our purposes, this implies that if a family of skew-adjoint operators converges to the Koopman generator V in strong resolvent sense, the unitary evolution groups generated by these operators consistently approximate the Koopman group generated by V .

Strong resolvent convergence and strong dynamical convergence imply the following form of spectral convergence, e.g., [26, Proposition 13].

Theorem 2.2. *With the notation of definition 2.1, let $\tilde{E} : \mathcal{B}(i\mathbb{R}) \rightarrow B(\mathbb{H})$ and $\tilde{E}_\tau : \mathcal{B}(i\mathbb{R}) \rightarrow B(\mathbb{H})$ be the spectral measures of A and A_τ , respectively, i.e., $A = \int_{i\mathbb{R}} \lambda d\tilde{E}(\lambda)$ and $A_\tau = \int_{i\mathbb{R}} \lambda d\tilde{E}_\tau(\lambda)$. Then, the following hold.*

- (i) *For every element $\lambda \in \sigma(A)$ of the spectrum of A , there exists a sequence $\tau_1, \tau_2, \dots \searrow 0$ and elements $\lambda_n \in \sigma(A_{\tau_n})$ of the spectra of A_{τ_n} such that $\lim_{n \rightarrow \infty} \lambda_n = \lambda$.*
- (ii) *For every bounded continuous function $h : i\mathbb{R} \rightarrow \mathbb{C}$, as $\tau \rightarrow 0^+$ the operators $h(A_\tau) = \int_{i\mathbb{R}} h(\lambda) d\tilde{E}_\tau(\lambda)$ converge strongly to $h(A) = \int_{i\mathbb{R}} h(\lambda) d\tilde{E}(\lambda)$.*
- (iii) *For every bounded Borel-measurable set $\Theta \in \mathcal{B}(i\mathbb{R})$ such that $\tilde{E}(\partial\Theta) = 0$ (i.e., the boundary of Θ does not contain eigenvalues of A_τ), as $\tau \rightarrow 0^+$ the projections $\tilde{E}_\tau(\Theta)$ converge strongly to $\tilde{E}(\Theta)$.*

In what follows, we will build a family of densely-defined operators $V_{z,\tau} : D(V_{z,\tau}) \rightarrow H$, $D(V_{z,\tau}) \subset H$, parameterized by $z, \tau > 0$ with the following properties.

- (P1) $V_{z,\tau}$ is skew-adjoint.
- (P2) $V_{z,\tau}$ has compact resolvent.
- (P3) $V_{z,\tau}$ is real, $(V_{z,\tau}f)^* = V_{z,\tau}(f^*)$ for all $f \in D(V)$.
- (P4) $V_{z,\tau}$ annihilates constant functions, $V_{z,\tau}\mathbf{1} = 0$.
- (P5) For each $z > 0$, $V_{z,\tau} \xrightarrow{\text{sr}} V$ as $\tau \rightarrow 0^+$.

By properties (P1) and (P2), the spectrum of $V_{z,\tau}$ consists entirely of isolated eigenvalues with finite multiplicities, and there is an orthonormal basis $\{\psi_{l,\tau}\}_{l \in \mathbb{Z}}$ of H consisting of eigenfunctions,

$$V_{z,\tau}\psi_{l,\tau} = i\omega_{l,\tau}\psi_{l,\tau}, \quad (5)$$

where $\omega_{l,\tau} \in \mathbb{R}$ are eigenfrequencies such that $\sigma(V_{z,\tau}) = \{i\omega_{l,\tau}\}_{l \in \mathbb{Z}}$. Moreover, by (P3) and (P4), the eigenfunctions and eigenfrequencies can be chosen such that

$$\omega_{-l,\tau} = -\omega_{l,\tau}, \quad \psi_{-l,\tau} = \psi_{l,\tau}^*, \quad \omega_{0,\tau} = 0, \quad \psi_{0,\tau} = \mathbf{1}. \quad (6)$$

Note the similarity with the corresponding properties of Koopman eigenfunctions ψ_l and eigenfrequencies ω_l from section 2.2. Finally, by property (P5) and the equivalence of strong resolvent convergence and strong dynamical convergence, for any $f \in H$ we have,

$$U^t f = \lim_{\tau \rightarrow 0^+} \sum_{l \in \mathbb{Z}} e^{i\omega_{l,\tau} t} c_{l,\tau} \psi_{l,\tau}, \quad c_{l,\tau} = \langle \psi_{l,\tau}, f \rangle. \quad (7)$$

We view (7) as a generalization of the Koopman evolution of observables in the point spectrum subspace H_p in (3).

Remark 2.3 (Spectral exactness). Two important notions in spectral approximation of linear operators are spectral inclusion and spectral exactness. Following [3, 10], we will say that a family of operators $(A_n)_{n \in \mathbb{N}}$ with $A_n : D(A_n) \rightarrow \mathbb{E}$ on a Banach space \mathbb{E} approximating an operator $A : D(A) \rightarrow \mathbb{E}$ is spectrally inclusive if for every $\lambda \in \sigma(A)$ there is a sequence of elements $\lambda_n \in \sigma(A_n)$ such that $\lim_{n \rightarrow \infty} \lambda_n = \lambda$. We will say that the approximation A_n has spectral pollution if there exists a complex number $\lambda \notin \sigma(A)$ (called here a spurious eigenvalue) and an infinite subset $I \subseteq \mathbb{N}$ such that $\lambda_n \rightarrow \lambda$ for $n \in I$. On the basis of theorem 2.2(i), our spectral approximation of the generator V by the family of operators $V_{z,\tau}$ is spectrally inclusive. However, it is not necessarily free of spurious eigenvalues, and this remains a possible avenue for algorithm improvement.

3. Resolvent compactification framework

In this section, we describe a procedure for building the operator family $V_{z,\tau}$ that satisfies properties (P1)–(P4) laid out in section 2.3. Central to our construction will be the use of kernel integral operators to compactify the resolvent of V ; we introduce these operators and state their properties in section 3.1. Our approach will make use of an orthogonal splitting of H into subspaces associated with negative, zero, and positive frequencies; we describe this splitting in section 3.2. In section 3.3, we describe the resolvent compactification procedure leading to $V_{z,\tau}$, and in section 3.4 we state and prove our main theoretical result, theorem 3.5. In section 3.5, we discuss a procedure for identifying slowly decorrelating observables from the eigenfunctions of $V_{z,\tau}$, and establish connections between the corresponding eigenvalues and the approximate point spectrum of the Koopman operator. We note that for the purposes of our compactification scheme, the resolvent parameter z will be required to be strictly positive, rather than an arbitrary complex number in the resolvent set of V .

3.1. Kernel integral operators

We consider a family of kernel functions $p_\tau : \mathcal{M} \times \mathcal{M} \rightarrow \mathbb{R}$, $\tau > 0$, with the following properties.

- (K1) p_τ is measurable, and it is continuous on $M \times M$.
- (K2) p_τ is Markovian with respect to μ ; i.e., $p_\tau \geq 0$ and for every $x \in M$ the normalization condition $\int_X p_\tau(x, \cdot) d\mu = 1$ holds.
- (K3) The integral operators $G_\tau : H \rightarrow H$ with $G_\tau f = \int_X p_\tau(\cdot, x) f(x) d\mu(x)$ form a strongly continuous semigroup; i.e., $G_\tau G_{\tau'} = G_{\tau+\tau'}$ for every $\tau, \tau' > 0$ and $\lim_{\tau \rightarrow 0^+} G_\tau f = f$ for every $f \in H$.
- (K4) G_τ is strictly positive; i.e., $\langle f, G_\tau f \rangle > 0$ for every nonzero $f \in H$.
- (K5) G_τ is ergodic; i.e., $G_\tau f = f$ for all $\tau > 0$ iff f is constant μ -a.e.

Note that every such kernel p_τ is necessarily symmetric, $p_\tau(x, x') = p_\tau(x', x)$, and the corresponding integral operator G_τ is self-adjoint and of trace class. Examples of kernels meeting these conditions are heat kernels on manifolds and translation-invariant kernels on compact abelian groups induced by positive functions on the dual group; e.g., [25]. The paper [26] describes a procedure that derives the family p_τ from a suitable un-normalized kernel $k : \mathcal{M} \times \mathcal{M} \rightarrow \mathbb{R}_+$ (e.g., a Gaussian kernel on $\mathcal{M} = \mathbb{R}^d$, $k(x, x') = e^{-\|x-x'\|^2/\epsilon^2}$) through a sequence of normalization steps. We summarize this approach in appendix Appendix A as we will use it in our numerical experiments in section 6.

Remark 3.1. Ref. [26] required, in addition to the properties listed above, that the kernel p_τ is positive-definite, i.e., for any finite collection of points $x_1, \dots, x_n \in \mathcal{M}$ the $n \times n$ kernel matrix $\mathbf{G} = [G_{ij}]$ with elements $G_{ij} = [p_\tau(x_i, x_j)]$ is positive. This condition implies that p_τ has an associated RKHS \mathcal{H}_τ which can be used to define compact approximations of the generator (see section 1.2). Here, our focus is on approximations of the generator acting on $L^2(\mu)$, which do not require positive definiteness of p_τ . See section 7 for a discussion of possible extensions of our scheme to RKHS-based approximations when the kernel p_τ is positive-definite.

For our purposes, the importance of Markovianity and ergodicity of G_τ is that these operators are contractive and share with the Koopman group U^t the subspace of H spanned by μ -a.e. constant functions as a one-dimensional common eigenspace. The latter implies, in particular, that the subspace $\tilde{H} \subset H$ of zero-mean functions is invariant under G_τ , just as it is under U^t . The importance of the continuity of p_τ on $M \times M$ and strict positivity of G_τ lies in the fact that every eigenfunction of these operators has a continuous representative. Specifically, if $\phi_j \in H$ is an eigenfunction satisfying $G_\tau \phi_j = \lambda_j^\tau \phi_j$, where the eigenvalue λ_j^τ is strictly positive, it follows by continuity of p_τ and compactness of X that the function $\varphi_j : M \rightarrow \mathbb{C}$ with $\varphi_j(x) = \lambda_j^{-\tau} \int_X p_\tau(x, \cdot) \phi_j d\mu$ is a continuous representative of the $L^2(\mu)$ element ϕ_j . As a result, associated with the semigroup G_τ is an orthonormal basis $\{\phi_0, \phi_1, \dots\}$ of H with representatives $\varphi_j \in C(M)$ and strictly positive corresponding eigenvalues $\lambda_0^\tau = 1 > \lambda_1^\tau \geq \lambda_2^\tau \geq \dots \searrow 0^+$ of finite multiplicity. Henceforth, we will choose the basis functions such that every ϕ_j is real and $\phi_0 = 1$ μ -a.e.

3.2. Frequency-sign-definite subspaces

We split H into negative-, zero-, and positive-frequency subspaces,

$$H = H_- \oplus H_0 \oplus H_+,$$

defined as $H_- = \Pi_- H$, $H_0 = \Pi_0 H$, and $H_+ = \Pi_+ H$, respectively, using the spectral projections $\Pi_- = E(i(-\infty, 0))$, $\Pi_0 = E(\{0\}) = \langle \mathbf{1}, \cdot \rangle \mathbf{1}$, and $\Pi_+ = E(i(0, \infty))$. By ergodicity, H_0 is one-dimensional and $\Pi_0 = \langle \mathbf{1}, \cdot \rangle \mathbf{1}$. Given any bounded, measurable function $f : i\mathbb{R} \rightarrow \mathbb{C}$, we have that $f(V) \in B(H)$ commutes with any of Π_- , Π_0 , or Π_+ ,

so that $f(V) = f_-(V) + f_0(V) + f_+(V)$, where

$$f_\bullet(V) = \Pi_\bullet f(V) = f(V) \Pi_\bullet = \Pi_\bullet f(V) \Pi_\bullet$$

and Π_\bullet stands for any of Π_- , Π_0 , or Π_+ . This means, in particular, that for every $z \in \rho(V)$, the resolvent $R_z(V)$ decomposes as

$$R_z(V) = R_z^-(V) + R_z^0(V) + R_z^+(V), \quad (8)$$

where $R_z^\bullet(V) = \Pi_\bullet R_z(V)$. In (8), $R_z^0(V)$ is trivially a rank-1 operator,

$$R_z^0(V) = \frac{1}{z} \langle \mathbf{1}, \cdot \rangle \mathbf{1}, \quad (9)$$

As such, to arrive at a compact approximation of $R_z(V)$ one only needs to compactify $R_z^+(V)$ and $R_z^-(V)$. In fact, by virtue of the following lemma, it suffices to consider only one of these two operators.

Lemma 3.2. *The map $J : H \rightarrow H$ that maps $f \in H$ to its complex conjugate, $Jf := f^*$, is an antilinear, isometric isomorphism between H_+ and H_- . In particular, J intertwines the projections Π_+ and Π_- , i.e., $J \circ \Pi_+ = \Pi_- \circ J$.*

Proof. See section 3.6. □

It follows from lemma 3.2 that $J \circ R_z^+(V) = R_z^-(V) \circ J$ and thus

$$R_z^-(V) = J \circ R_z^+(V) \circ J. \quad (10)$$

We can therefore compactify $R_z^+(V)$ and use (10) to obtain a compactification of $R_z^-(V)$.

Before closing this subsection, we note that the decomposition (8) can be equivalently expressed as a direct sum of operators,

$$R_z(V) = R_z^-(V)|_{H_-} \oplus R_z^0(V)|_{H_0} \oplus R_z^+(V)|_{H_+},$$

where $R_z^\bullet(V)|_{H_\bullet}$ are linear maps from H_\bullet into itself given by restriction of $R_z^\bullet(V)$. In what follows, will be making use of either version of the decomposition of $R_z(V)$ (as well as similar decompositions of other operators) as convenient without change of notation.

3.3. Construction of the compactified resolvent

By a version of the spectral mapping theorem for the resolvents of generators of strongly continuous evolution semigroups [30, Theorem IV.1.13], we have that for any $z \in \rho(V)$

$$\sigma(R_z(V)) \setminus \{0\} = \left\{ \frac{1}{z - \lambda} : \lambda \in \sigma(V) \right\}.$$

This means that for $z > 0$ the resolvent spectrum $\sigma(R_z(V))$ is a subset of the circle of radius $1/z$ centered at the point $1/(2z)$ on the positive real line; see fig. 2. We shall denote this circle by C_z . Denoting the closed semicircle in C_z located in the upper half

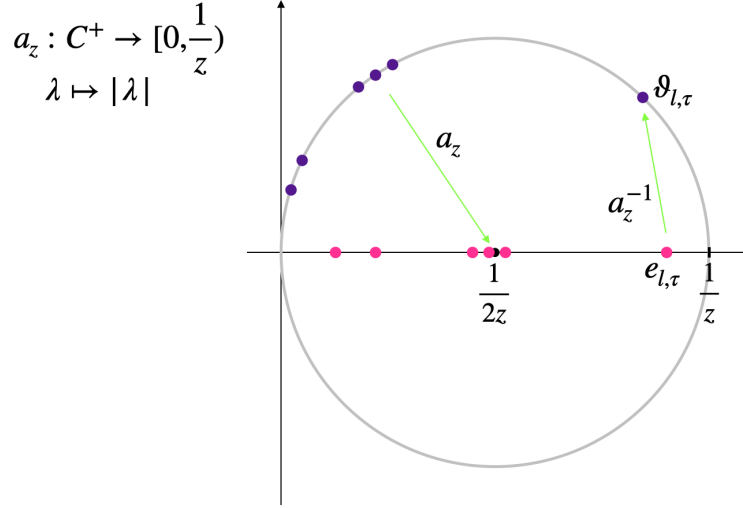


Figure 2. Schematic of the spectrum of the resolvent $R_z(V)$ for $z > 0$ and the bijective correspondence of the spectrum of the projected resolvent $R_z^+(V)$ (which is a subset of the semicircle C_z^+ with center $(2z)^{-1}$ and radius z^{-1}) and the spectrum of its modulus $S_z^+ = |R_z^+(V)|$ (which is a subset of the interval $[0, z^{-1}]$). This correspondence is realized through the function $a_z : C_z^+ \rightarrow [0, z^{-1}]$ with $a_z(\lambda) = |\lambda|$ (see (14) for an explicit formula for a_z^{-1}). Upon compactification, $S_z^+ \mapsto S_{z,\tau}^+$, the operator $S_{z,\tau}^+$ acquires a discrete set of eigenvalues $e_{l,\tau} \in [0, z^{-1}]$ (magenta dots). These eigenvalues are mapped into C_z^+ by an application of a_z^{-1} , leading to the eigenvalues $\vartheta_{l,\tau}$ of the compactified resolvent $R_{z,\tau}^+$ (purple dots).

of the complex plane by $C_z^+ := \{\lambda \in C_z : \text{Im } \lambda \geq 0\}$, we have, by the spectral mapping theorem, the inclusion

$$\sigma(R_z^+(V)) \subseteq C_z^+. \quad (11)$$

Similarly, the projected resolvent $R_z^-(V)$ to the negative-frequency subspace H_- satisfies $\sigma(R_z^-(V)) \subseteq C_z^-$ with $C_z^- := \{\lambda \in C_z : \text{Im } \lambda \leq 0\}$. For later convenience, given $z > 0$ we define $\beta_z : \tilde{C}_z \rightarrow i\mathbb{R}$ on $\tilde{C}_z := C_z \setminus \{0\}$ as

$$\beta_z(\lambda) = \frac{1}{\lambda} + z. \quad (12)$$

The latter, is a left inverse of the resolvent function $R_z : i\mathbb{R} \rightarrow \tilde{C}_z \subset \mathbb{C}$ with $R_z(\lambda) = (z - \lambda)^{-1}$, so that $\beta_z(R_z(V)) = V$.

Next, let $a_z : C_z^+ \rightarrow [0, z^{-1}]$ be the modulus function on C_z^+ with $a_z(\lambda) = |\lambda|$. By (11), we can express the modulus of $R_z^+(V)$ as

$$S_z^+ := |R_z^+(V)| = \sqrt{(R_z^+(V))^* R_z^+(V)} = a_z(R_z^+(V)). \quad (13)$$

In particular, since a_z is a bijective function, we can recover $R_z^+(V)$ from its modulus i.e.,

$$R_z^+(V) = a_z^{-1}(S_z^+),$$

where

$$a_z^{-1}(x) = xe^{i(\frac{\pi}{2} + \sin^{-1}(xz))}, \quad x \in [0, z^{-1}]. \quad (14)$$

Note that we can obtain S_z^+ by computing a polar decomposition for $R_z^+(V)$,

$$R_z^+(V) = W_z S_z^+,$$

where $W_z \in B(H)$ is a partial isometry.

We are now ready to compactify $R_z^+(V)$ by compactifying its modulus. Specifically, given Markov operators $G_\tau \in B(H)$ satisfying properties (K1)–(K5), we define the trace class, positive operators

$$S_{z,\tau}^+ = \sqrt{S_z^+} G_\tau \sqrt{S_z^+}, \quad (15)$$

and the compact operators

$$R_{z,\tau}^+ = a_z^{-1}(S_{z,\tau}^+). \quad (16)$$

Note that the well-definition of $R_{z,\tau}^+$ in (16) relies on the fact that the spectra of $S_{z,\tau}^+$ are subsets of $[0, z^{-1}]$ (i.e., the domain of definition of a_z^{-1}) since G_τ are contractive operators. In particular, for each $z, \tau > 0$, $S_{z,\tau}^+$ is a positive, trace class operator with spectrum contained in $[0, z^{-1}]$, range contained in H_+ , and nullspace containing H_- and H_0 . We can thus view $S_{z,\tau}^+$ as an operator on H_+ that admits an eigendecomposition

$$S_{z,\tau}^+ \psi_{l,\tau} = e_{l,\tau} \psi_{l,\tau}, \quad l \in \mathbb{N},$$

where the eigenvalues $e_{l,\tau}$ lie in $[0, z^{-1}]$ (with 0 as the only possible accumulation point) and the corresponding eigenfunctions $\psi_{l,\tau}$ form an orthonormal basis of H_+ . By (16), the $\psi_{l,\tau}$ are also eigenfunctions of $R_{z,\tau}^+$, corresponding to the eigenvalues

$$\vartheta_{l,\tau} = a_z^{-1}(e_{l,\tau}) \in C_z^+.$$

The following lemma will ensure later on that the $\vartheta_{l,\tau}$ have well-defined corresponding eigenfrequencies.

Lemma 3.3. *The eigenvalues $\vartheta_{l,\tau}$ of $R_{z,\tau}^+$ are nonzero.*

Proof. Since the resolvent function $R_z : i\mathbb{R} \rightarrow \mathbb{C}$ maps $[0, \infty)$ to $C_z^+ \setminus \{0\}$, 0 is not an eigenvalue of $R_z(V)$ and thus it is also not an eigenvalue of S_z^+ . Therefore, for every nonzero $f \in H_+$, $S_z^{1/2} f$ is nonzero and $S_{z,\tau}^+ f$ is nonzero so long as $G_\tau S_z^{1/2} f$ is nonzero. The latter follows from the fact that G_τ is a strictly positive operator (property (K4)), and we conclude that $S_{z,\tau}^+ f \neq 0$ and thus that every eigenvalue $e_{l,\tau}$ of $S_{z,\tau}^+$ is strictly positive. Therefore, every eigenvalue $\vartheta_{l,\tau} = a_z^{-1}(e_{l,\tau})$ of $R_{z,\tau}^+$ is nonzero. \square

We can build a compact approximation $R_{z,\tau}^-$ of the negative-frequency resolvent $R_z^-(V)$ by defining

$$S_z^- = |R_z^-(V)|$$

and carrying out analogous steps to (13)–(16) used to obtain $R_{z,\tau}^+$, replacing S_z^+ by S_z^- . Analogously to (10), this operator satisfies

$$R_{z,\tau}^- = J \circ R_{z,\tau}^+ \circ J. \quad (17)$$

Thus, we can conveniently write down an eigendecomposition

$$R_{z,\tau}^- \vartheta_{l,\tau} = \vartheta_{l,\tau} \psi_{l,\tau}, \quad l \in \{-1, -2, \dots\},$$

with eigenvalues $\vartheta_{l,\tau} \in C_z^-$ and corresponding orthonormal eigenfunctions $\psi_{l,\tau} \in H_-$ using the eigendecomposition of $R_{z,\tau}^+$:

$$\vartheta_{l,\tau} = \vartheta_{-l,\tau}^*, \quad \psi_{l,\tau} = \psi_{-l,\tau}^*, \quad l \in \{-1, -2, \dots\}.$$

Using (9), (16), and (17), we define, for each $z, \tau > 0$, $R_{z,\tau} : H \rightarrow H$ as the compact operator given by

$$R_{z,\tau} = R_{z,\tau}^- + R_z^0 + R_{z,\tau}^+. \quad (18)$$

This operator will serve as our compact approximation of the resolvent $R_z(V)$. Defining $\psi_{0,\tau} = \mathbf{1}$, $\vartheta_{0,\tau} = z^{-1}$, and using the eigendecompositions of $R_{z,\tau}^+$ and $R_{z,\tau}^-$ just described along with lemma 3.3, we deduce that $R_{z,\tau}$ is diagonal in the orthonormal eigenbasis $\{\psi_{l,\tau}\}_{l \in \mathbb{Z}}$ of H with corresponding eigenvalues $\{\vartheta_{l,\tau}\}_{l \in \mathbb{Z}}$ lying in $C_z \setminus \{0\}$. Correspondingly,

$$V_{z,\tau} := \beta_z(R_{z,\tau}) \quad (19)$$

is an unbounded skew-adjoint operator on H with compact resolvents $R_{\tilde{z}}(V_{z,\tau})$, $\tilde{z} \in \rho(V_{z,\tau})$. For $\tilde{z} = z$, the resolvent $R_z(V_{z,\tau})$ is equal to $R_{z,\tau}$. In particular, $V_{z,\tau}$ admits the eigendecomposition in (5) for the eigenfunctions $\psi_{l,\tau}$ and the eigenfrequencies

$$\omega_{l,\tau} = \frac{1}{i} \beta_z(\vartheta_{l,\tau}) = \frac{1}{i} \left(\frac{1}{\vartheta_{l,\tau}} + z \right). \quad (20)$$

Remark 3.4. An alternative way of compactifying S_z^+ would be to define $\tilde{S}_{z,\tau}^+ = G_\tau^{1/2} S_z G_\tau^{1/2}$. This operator is positive, compact, and its spectrum is contained in $[0, z^{-1}]$ (in fact, $\sigma(\tilde{S}_{z,\tau}^+) = \sigma(S_{z,\tau}^+)$), and thus $\tilde{R}_{z,\tau}^+ = a_z^{-1}(\tilde{S}_{z,\tau}^+)$ is a well-defined compact approximation of $R_z^+(V)$. However, unless S_z and G_τ happen to commute, $\tilde{S}_{z,\tau}^+$ does not map H_+ into itself, and is thus it is not suitable for providing an eigenbasis of this subspace.

3.4. Spectral convergence

Our main spectral approximation result is as follows.

Theorem 3.5. *For each $z > 0$, the operators $V_{z,\tau}$ in (19) satisfy properties (P1)–(P5). As a result, as $\tau \rightarrow 0^+$, $V_{z,\tau}$, converges spectrally to V in the sense of theorem 2.2.*

Proof. Properties (P1)–(P3) follow by construction of $V_{z,\tau}$. Property (P4) follows from the fact that $\psi_{\tau,0} = \mathbf{1}$ and $\omega_{\tau,0} = 0$.

To establish property (P5), fix a nonzero $f \in H_+$, and note that since a_z^{-1} is a continuous function on the closed interval $[0, z^{-1}]$, for any $\epsilon > 0$, there exists a

polynomial $p : [0, z^{-1}] \rightarrow \mathbb{C}$ such that $\|a_z^{-1} - p\|_\infty < \epsilon/(3\|f\|_H)$. We have

$$\begin{aligned}
 & \| (R_z(V) - R_z(V_{z,\tau}))f \|_H \\
 &= \| (R_z^+(V) - R_{z,\tau}^+)f \|_H \\
 &= \| (a_z^{-1}(S_z^+) - a_z^{-1}(S_{z,\tau}^+))f \|_H \\
 &= \| (a_z^{-1}(S_z^+) - p(S_z^+) + p(S_z^+) - p(S_{z,\tau}^+) + p(S_{z,\tau}^+) - a_z^{-1}(S_{z,\tau}^+))f \|_H \\
 &\leq \| a_z^{-1}(S_z^+) - p(S_z^+) \| \|f\|_H + \| (p(S_z^+) - p(S_{z,\tau}^+))f \|_H + \| p(S_{z,\tau}^+) - a_z^{-1}(S_{z,\tau}^+) \| \|f\|_H \\
 &< \frac{2}{3}\epsilon + \| (p(S_z^+) - p(S_{z,\tau}^+))f \|_H.
 \end{aligned}$$

Since, as $\tau \rightarrow 0^+$, G_τ converges strongly to the identity, we have that $S_{z,\tau}^+ \xrightarrow{s} S_z^+$ and thus $p(S_{z,\tau}^+) \xrightarrow{s} p(S_z^+)$. In particular, there exists $\delta > 0$ such that for all $\tau \in (0, \delta)$, $\| (p(S_z^+) - p(S_{z,\tau}^+))f \|_H < \epsilon/3$, and thus

$$\| (R_z(V) - R_z(V_{z,\tau}))f \|_H < \epsilon.$$

It therefore follows that $R_z(V_{z,\tau}) \xrightarrow{s} R_z(V)$ on H_+ . The case $f \in H_-$ follows from the fact that $J \circ (R_z^-(V) - R_{z,\tau}^-)f = (R_z^+(V) - R_{z,\tau}^+) \circ Jf$. The case $f \in H_0$ is trivial. \square

As noted in section 2.3, an immediate corollary of theorem 3.5 is that the unitary evolution groups $\{U_{z,\tau}^t := e^{tV_{z,\tau}}\}_{t \in \mathbb{R}}$ generated by $V_{z,\tau}$ converge to the Koopman group $\{U^t\}_{t \in \mathbb{R}}$ in the strong operator topology of H . In particular, for every $t \in \mathbb{R}$ and $f \in H$, we have (cf. (7))

$$U^t f = \lim_{\tau \rightarrow 0^+} U_\tau^t f, \quad U_\tau^t f = \sum_{l \in \mathbb{Z}} e^{i\omega_l \tau t} \langle \psi_{l,\tau}, f \rangle \psi_{l,\tau}. \quad (21)$$

Equation (21) indicates that, collectively, the eigenvalues and eigenfunctions of $U_{z,\tau}^t$ well-approximate the action of the Koopman operator U^t on observables in H .

3.5. Slowly decorrelating observables and ϵ -approximate Koopman spectra

In a number of applications, e.g. [33], one is interested in identifying observables $f \in \tilde{H}$ with slow decay of their time-autocorrelation function,

$$C_f(t) \equiv C_{ff}(t) = \langle f, U^t f \rangle. \quad (22)$$

Note that in (22) we have taken f to have zero mean. For observables $f \in H$ with $\bar{f} \equiv \int_{\mathcal{M}} f d\mu \neq 0$ one would consider the anomaly correlation $C_{f'}$, computed via (22) for $f' = f - \bar{f}$. For a Koopman eigenfunction $\psi \in \tilde{H}$ with unit norm and corresponding eigenfrequency $\omega \in \mathbb{R}$, the autocorrelation function behaves as a pure complex phase,

$$C_\psi(t) = e^{i\omega t}, \quad (23)$$

whose modulus $|C_\psi(t)| = 1$ does not decay as $|t|$ increases. In systems with mixing dynamics, non-trivial such elements of \tilde{H} do not exist (see section 2.2), so it is natural to seek observables ψ that satisfy (23) approximately in some sense.

Due to the strong dynamical convergence in (21), the eigenfunctions of $\psi_{l,\tau}$ of $U_{z,\tau}^t$ are natural candidate observables to have slow decay of their time-autocorrelation modulus $|C_{\psi_{l,\tau}}(t)|$. However, one should keep in mind that, in general, strong convergence of $U_{z,\tau}^t$ to U^t does not imply that any given eigenpair $(\omega_{l,\tau}, \psi_{l,\tau})$ will approximately satisfy (23) with high accuracy. Our approach is therefore to identify appropriate eigenpairs from the spectra of $V_{z,\tau}$ *a posteriori*, by means of the following procedure.

Given a time parameter $T_c > 0$, and a candidate eigenpair (ω, ψ) with $\omega \in \mathbb{R}$ and ψ a unit vector in H , we compute the non-negative number

$$\varepsilon_{T_c}(\omega, \psi) = \max_{t \in [-T_c, T_c]} \operatorname{Re} (1 - e^{-i\omega t} C_\psi(t)). \quad (24)$$

Note that $\varepsilon_{T_c}(\omega, \psi) = 0$ for all $T_c \geq 0$ whenever ψ is a Koopman eigenfunction satisfying (23); otherwise $\varepsilon_{T_c}(\omega, \psi) \in (0, 1]$. Moreover, we have $\varepsilon_{T_c}(\omega, \psi) = \varepsilon_{T_c}(-\omega, \psi^*)$. Based on these facts, for a given T_c , we can order the eigenpairs $\{(\omega_{l,\tau}, \psi_{l,\tau})\}_{l \in \mathbb{Z}}$ from the spectrum of $V_{z,\tau}$ as

$$(\omega_{0,\tau}, \psi_{0,\tau}), (\omega_{1,\tau}, \psi_{1,\tau}), (\omega_{-1,\tau}, \psi_{-1,\tau}), (\omega_{2,\tau}, \psi_{2,\tau}), (\omega_{-2,\tau}, \psi_{-2,\tau}), \dots,$$

where $0 = \varepsilon_{T_c}(\omega_{0,\tau}, \psi_{0,\tau}) \leq \varepsilon_{T_c}(\omega_{\pm 1,\tau}, \psi_{\pm 1,\tau}) \leq \varepsilon_{T_c}(\omega_{\pm 2,\tau}, \psi_{\pm 2,\tau}) \leq \dots \leq 1$. In fact, ordering the eigenpairs in terms of $\varepsilon_{T_c}(\omega_{l,\tau}, \psi_{l,\tau})$ is closely related to identifying elements in the ε -approximate spectrum of the Koopman operator, as we now describe.

First, we recall (e.g., [13, 14]) that the ε -approximate spectrum $\sigma_{\text{ap},\varepsilon}(A)$ of a closed operator $A : D(A) \rightarrow \mathbb{H}$ on a Hilbert space \mathbb{H} is the set of complex numbers λ for which there exists a nonzero element $f \in \mathbb{H}$ such that

$$\|Af - \lambda f\|_{\mathbb{H}} < \varepsilon \|f\|_{\mathbb{H}};$$

in other words, $\lambda \in \sigma_{\text{ap},\varepsilon}(A)$ can be thought as behaving as an element of the point spectrum up to tolerance ε . As ε increases, $\sigma_{\text{ap},\varepsilon}(A)$ forms an increasing family of open subsets of the complex plane such that $\bigcup_{\varepsilon > 0} \sigma_{\text{ap},\varepsilon}(A) = \mathbb{C}$. Moreover, if A is normal and bounded then $\bigcap_{\varepsilon > 0} \sigma_{\text{ap},\varepsilon}(A) = \sigma(A)$. In that case, $\sigma_{\text{ap},\varepsilon}(A)$ coincides with the ε -pseudospectrum of A , the latter defined as the set of complex numbers λ such that $\|(A - \lambda)^{-1}\| > 1/\varepsilon$, with the convention that $\|(A - \lambda)^{-1}\| = \infty$ when $\lambda \in \sigma(A)$ [73].

One readily verifies that the eigenpairs $(\omega_{l,\tau}, \psi_{l,\tau})$ from (21) satisfy

$$\|U^t \psi_{l,\tau} - e^{i\omega_{l,\tau} t} \psi_{l,\tau}\|_H^2 \leq \varepsilon_{T_c}(\omega_{l,\tau}, \psi_{l,\tau})$$

It therefore follows that $e^{i\omega_{l,\tau} t}$ lies in the closure $\overline{\sigma_{\text{ap},\varepsilon}(U^t)}$ of the ε -approximate point spectrum of the Koopman operator U^t for tolerance $\varepsilon = \sqrt{2\varepsilon_{T_c}(\omega_{l,\tau}, \psi_{l,\tau})}$ for every time $t \in [-T_c, T_c]$.

Intuitively, we would like that $\varepsilon_{T_c}(\psi_{l,\tau})$ is small for large values of T_c ; that is, $\psi_{l,\tau}$ should behave approximately like a Koopman eigenfunction uniformly over large time intervals. Moreover, since U_τ^t is a unitary (and hence normal, bounded) operator, the

same conclusions hold for the ϵ -pseudospectrum. While criteria for selecting T_c will depend on the application at hand (e.g., T_c could be chosen on the basis of relevant prior knowledge about the system such as decorrelation and/or Lyapunov timescales), any given T_c induces an ordering the eigenfunctions in terms of $\epsilon_{T_c}(\psi_{l,\tau})$ that we find useful in practice.

3.6. Proof of lemma 3.2

We recall Stone's formula for computing the action of the spectral measure $\hat{E} : \mathcal{B}(\mathbb{R}) \rightarrow B(\mathbb{H})$ of a self-adjoint operator $A : D(A) \rightarrow \mathbb{H}$ on a Hilbert space \mathbb{H} (e.g., [27, Chapter 9]),

$$\frac{1}{2}(\hat{E}((a, b)) + \hat{E}([a, b]))f = \lim_{\epsilon \rightarrow 0^+} \int_{[a, b]} (R_{\lambda+i\epsilon}(A) - R_{\lambda-i\epsilon}(A))f d\lambda, \quad \forall f \in \mathbb{H},$$

where $-\infty < a < b < \infty$ and $A = \int_{\mathbb{R}} \lambda d\tilde{E}(\lambda)$. Using this result for $\mathbb{H} = \tilde{H}$, $A = \tilde{V}/i$ with $\tilde{V} = V|_{\tilde{H}}$ (i.e., \tilde{V} is the restriction of the generator on the subspace $\tilde{H} \subset H$ of zero-mean observables), and the spectral measure $\tilde{E} : \mathcal{B}(i\mathbb{R}) \rightarrow B(\tilde{H})$ of \tilde{V} , we get

$$\frac{1}{2}(\hat{E}((a, b)) + \hat{E}([a, b]))f = \lim_{\epsilon \rightarrow 0^+} \int_{i[a, b]} (R_{\lambda+\epsilon}(\tilde{V}) - R_{\lambda-\epsilon}(\tilde{V}))f d\lambda, \quad \forall f \in \tilde{H}.$$

Next, choosing a sequence b_n of positive numbers increasing to infinity which are not eigenfrequencies of \tilde{V} , and noting that $a = 0$ is not an eigenvalue of \tilde{V} , we have

$$\frac{1}{2}(\tilde{E}(i(0, b_n)) + \tilde{E}(i[0, b_n])) = \tilde{E}(i[a, b_n]) \quad (25)$$

and thus, for any $f \in \tilde{H}$,

$$\begin{aligned} \Pi_+ f &= \lim_{n \rightarrow \infty} \tilde{E}(i[0, b_n])f = \lim_{n \rightarrow \infty} \lim_{\epsilon \rightarrow 0^+} \int_{i[0, b_n]} (R_{\lambda+\epsilon}(\tilde{V}) - R_{\lambda-\epsilon}(\tilde{V}))f d\lambda, \\ \Pi_- f &= \lim_{n \rightarrow \infty} \tilde{E}(i[-b_n, 0])f = \lim_{n \rightarrow \infty} \lim_{\epsilon \rightarrow 0^+} \int_{i[-b_n, 0]} (R_{\lambda+\epsilon}(\tilde{V}) - R_{\lambda-\epsilon}(\tilde{V}))f d\lambda. \end{aligned} \quad (26)$$

Meanwhile, we have

$$\begin{aligned} (\tilde{E}(i[-b_n, 0]) \circ J)f &= \tilde{E}(i[-b_n, 0])f^* \\ &= \lim_{\epsilon \rightarrow 0^+} \int_{i[-b_n, 0]} \left(\frac{1}{(\lambda - \epsilon) - \tilde{V}} - \frac{1}{(\lambda + \epsilon) - \tilde{V}} \right) f^* d\lambda \\ &= \left(\lim_{\epsilon \rightarrow 0^+} \int_{i[-b_n, 0]} \left(\frac{1}{(-\lambda - \epsilon) - \tilde{V}} - \frac{1}{(-\lambda + \epsilon) - \tilde{V}} \right) f d\lambda \right)^* \\ &= \left(\lim_{\epsilon \rightarrow 0^+} \int_{i[0, b_n]} \left(\frac{1}{(\lambda - \epsilon) - \tilde{V}} - \frac{1}{(\lambda + \epsilon) - \tilde{V}} \right) f d\lambda \right)^* \\ &= (J \circ \tilde{E}(i[0, b_n]))f. \end{aligned}$$

With the above and (26), we obtain

$$(\Pi_- \circ J)f = \lim_{n \rightarrow \infty} (\tilde{E}(i[-b_n, 0]) \circ J)f = \lim_{n \rightarrow \infty} (J \circ \tilde{E}(i[0, b_n]))f = (J \circ \Pi_+)f,$$

proving the lemma.

4. Finite-rank approximation

Invariably, usage of the regularized generators $V_{z,\tau}$ from (19) in practical applications requires access to spectrally consistent finite-rank approximations of these operators. In this section, we address the problem of building such finite-rank approximations in a manner that is amenable to data-driven approximation. In section 5, we will take the finite-rank objects built here and translate them into those computable in a data-driven manner. For readers content with the construction in section 3, one may find the overview in algorithm 1 sufficient.

4.1. Spectral approximation of compact operators and practical obstructions

Our objective is to build a sequence of operators on H that (i) are resolvents of finite-rank, skew-adjoint operators; and (ii) converge strongly to $R_{z,\tau}$ from (18). The following result (e.g., [14, sections 3.6 and 5.1]) will provide a working definition of spectrally convergent approximations of compact operators that we will employ in our construction.

Theorem 4.1. *Let $A : \mathbb{E} \rightarrow \mathbb{E}$ be a compact operator on a Banach space \mathbb{E} and A_1, A_2, \dots a sequence of compact operators on \mathbb{E} that converges compactly to A ; that is, $A_n \xrightarrow{s} A$ and for every bounded sequence $f_1, f_2, \dots \in \mathbb{E}$ the sequence $(A - A_n)f_n$ has compact closure. Then, the following hold for every nonzero eigenvalue λ of A and every open neighborhood $O \subseteq \mathbb{C}$ such that $\sigma(A) \cap O = \{\lambda\}$:*

- (i) *There exists $n_* \in \mathbb{N}$ such that for all $n > n_*$ the set $\sigma(A_n) \cap O$ contains at most m eigenvalues of A_n , where m is the multiplicity of λ . Moreover, the multiplicities of these eigenvalues sum to m , and every $\lambda_n \in \sigma(A_n) \cap O$ converges to λ as $n \rightarrow \infty$.*
- (ii) *The spectral projections to the eigenspaces corresponding to $\sigma(A_n) \cap O$ converge strongly to the spectral projection to the eigenspace of A corresponding to λ .*

As motivation for our approach, we begin by noting that a tentative way of building approximations of $R_{z,\tau}$ would be to approximate the compact operators $S_{z,\tau}^+$ and $S_{z,\tau}^-$ separately by projection onto finite-dimensional subspaces $H_{+,L} \subset H_+$ and $H_{-,L} \subset H_-$; that is, employ $\hat{S}_{z,\tau,L}^+ := \Pi_{+,L} S_{z,\tau}^+ \Pi_{+,L}$ and $\hat{S}_{z,\tau,L}^- := \Pi_{-,L} S_{z,\tau}^- \Pi_{-,L}$ as approximations of $S_{z,\tau}^+$ and $S_{z,\tau}^-$, respectively, where $\Pi_{\pm,L} : H \rightarrow H$ are orthogonal projections mapping onto H_{\pm} . With these operators, one could define $\hat{R}_{z,\tau,L}^+ = a_z^{-1}(\hat{S}_{z,\tau,L}^+)$ and $\hat{R}_{z,\tau,L}^- = J \circ \hat{R}_{z,\tau,L}^+ \circ J$ analogously to the construction of $R_{z,\tau}^+$ and $R_{z,\tau}^-$ from section 3.3, respectively, and assemble a finite-rank resolvent

$$\hat{R}_{z,\tau,L} = \hat{R}_{z,\tau,L}^- \oplus R_z^0 \oplus \hat{R}_{z,\tau,L}^+, \quad (27)$$

acting on $H_{-,L} \oplus H_0 \oplus H_{+,L}$, with a corresponding finite-rank, skew-adjoint approximate generator $\hat{V}_{z,\tau,L} = \beta_z(\hat{R}_{z,\tau,L})$. Note that for well-definition of $\hat{R}_{z,\tau,L}$ via (27) it is important that $\hat{R}_{z,\tau,L}^+$ and $\hat{R}_{z,\tau,L}^-$ have H_+ and H_- as mutually orthogonal invariant subspaces, respectively. Arranging for the subspaces $H_{+,L}$ and $H_{-,L}$ to form increasing

families towards H_+ and H_- , respectively, would then imply that $\hat{R}_{z,\tau,L}$ converges strongly to $R_{z,\tau}$ as $L \rightarrow \infty$.

Despite its apparent simplicity, a shortcoming of this approach is that it is difficult to construct appropriate bases for the approximation spaces $H_{+,L}$ and $H_{-,L}$. In particular, aside from special cases involving integral operators G_τ that commute with Π_\pm , there are no kernel integral operator techniques known to us that can produce orthonormal bases of H_\pm via eigendecomposition (analogously to the eigenbases of H associated with G_τ). In the absence of such methods, we must content ourselves with approximations of $S_{z,\tau}^+$ and $S_{z,\tau}^-$ that do not preserve the invariance of the positive- and negative-frequency subspaces H_\pm under these operators. Building the resolvent and finite-rank generator from these approximations will require solution of an additional eigenvalue problem, as we describe in the following subsection.

4.2. Finite-rank approximation of the compactified resolvent and associated generator

Throughout this section, we restrict the compactified resolvent $R_{z,\tau}$ from (18) to the codimension-1 subspace $\tilde{H} \subset H$ of zero mean functions. This restriction is without loss, since we can trivially recover $R_{z,\tau}$ on H by adding to the restricted operator $R_{z,\tau}|_{\tilde{H}}$ the rank-1 operator $R_z^0(V)$ from (9).

Viewing, then, $R_{z,\tau}$ as an operator on \tilde{H} , it follows from the fact that $\|G_\tau f\|_{\tilde{H}} < \|f\|_{\tilde{H}}$ for any nonzero $f \in \tilde{H}$ that the spectra of $S_{z,\tau}^+$ and $S_{z,\tau}^-$ are strict, closed subsets of $[0, z^{-1}]$ that do not contain z^{-1} . Thus, using $a_z : C_z^+ \rightarrow [0, z^{-1}]$ from section 3.3 and similarly defining $\bar{a}_z : C_z^- \rightarrow [0, z^{-1}]$ as $\bar{a}_z(\lambda) = |\lambda|$, we have that $\sigma(R_{z,\tau}) = a_z^{-1}(\sigma(S_{z,\tau}^+)) \cup \bar{a}_z^{-1}(\sigma(S_{z,\tau}^-))$ is a subset of a closed arc in C_z that does not contain z^{-1} ; see Fig. 3 for a schematic illustration.

Let $\tilde{C}_z = C_z \setminus \{z^{-1}\}$ and consider the map $\gamma_z : \tilde{C}_z \rightarrow (-z^{-1}, z^{-1})$ defined as

$$\gamma_z(\lambda) = \begin{cases} |\lambda|, & \text{Im } \lambda \geq 0, \\ -|\lambda|, & \text{Im } \lambda < 0. \end{cases}$$

One readily verifies that γ_z is a continuous, injective mapping that maps $\sigma(R_{z,\tau})$ into the closed interval $I_{z,\tau} = [-e_{1,\tau}, e_{1,\tau}]$ (i.e., $I_{z,\tau}$ is the smallest interval containing $\sigma(-S_{z,\tau}^-) \cup \sigma(S_{z,\tau}^+)$). Moreover, we have $\gamma_z(R_{z,\tau}) = S_{z,\tau}^+ - S_{z,\tau}^-$ and thus

$$R_{z,\tau} = \gamma_z^{-1}(S_{z,\tau}^+ - S_{z,\tau}^-).$$

Note the explicit formula for the inverse of γ_z ,

$$\gamma_z^{-1}(x) = \begin{cases} a_z^{-1}(x), & x \in [0, z^{-1}), \\ (a_z^{-1}(-x))^*, & x \in (-z^{-1}, 0), \end{cases}$$

where a_z^{-1} was defined in (14). By continuity of γ_z^{-1} , we can build approximations of $R_{z,\tau}$ that are spectrally consistent in the sense of theorem 4.1 by first approximating

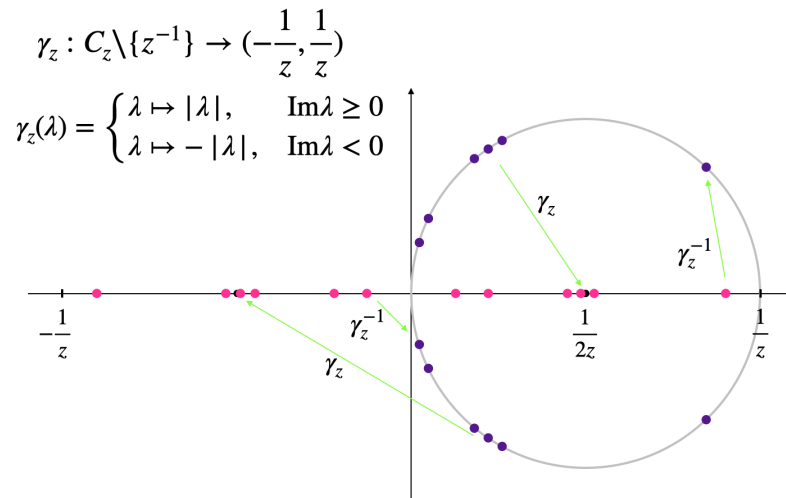


Figure 3. Schematic of the bijective correspondence of the spectrum of the compactified resolvent $R_{z,\tau}$ (illustrated with purple dots), which lies in the circular arc $C_z \setminus \{z^{-1}\}$, and the spectrum of the operator $S_{z,\tau}^+ - S_{z,\tau}^-$ (illustrated with magenta dots), which lies in the interval $(-z^{-1}, z^{-1})$. This correspondence is realized through the function γ_z as described in section 4.2.

$S_{z,\tau} \equiv S_{z,\tau}^+ - S_{z,\tau}^-$ by finite-rank operators with spectra contained in closed subintervals of $(-z^{-1}, z^{-1})$, and then applying γ_z^{-1} to these operators, as we now describe.

Using the kernel eigenbasis $\{\phi_j\}_{j=1}^\infty$ of \tilde{H} from section 3.1, define the L -dimensional approximation spaces $H_L = \text{span}\{\phi_1, \dots, \phi_L\}$ and the corresponding orthogonal projections $\Pi_L : \tilde{H} \rightarrow \tilde{H}$ with $\text{ran } \Pi_L = H_L$. Define also the finite-rank, projected resolvents $\tilde{R}_{z,L}^+ : \tilde{H} \rightarrow \tilde{H}$ as $\tilde{R}_{z,L}^+ = \Pi_L R_z^+(V) \Pi_L$, and the corresponding positive operators $\tilde{S}_{z,L}^+ := |\tilde{R}_{z,L}^+|$. We then have:

Lemma 4.2. *For any $L \in \mathbb{N}$, the spectrum of $\tilde{S}_{z,L}^+$ is contained in the interval $[0, z^{-1}]$.*

Proof. Since $\tilde{S}_{z,L}^+$ is self-adjoint, we have $\|\tilde{S}_{z,L}^+\| = \sqrt{\|(\tilde{S}_{z,L}^+)^2\|} = \sqrt{\|\tilde{R}_{z,L}^{+*} \tilde{R}_{z,L}^+\|}$. Moreover, for any $f \in \tilde{H}$, we have

$$\begin{aligned} \langle f, \tilde{R}_{z,L}^{+*} \tilde{R}_{z,L}^+ f \rangle &= \langle \Pi_L R_z^+(V) \Pi_L f, \Pi_L R_z^+(V) \Pi_L f \rangle \\ &\leq \langle R_z^+(V) \Pi_L f, R_z^+(V) \Pi_L f \rangle = \langle \Pi_L f, (S_z^+)^2 \Pi_L \rangle \\ &\leq \|S_z^+\|^4 \|f\|_H^2, \end{aligned}$$

and therefore $\|\tilde{R}_{z,L}^{+*} \tilde{R}_{z,L}^+\| \leq \|S_z^+\|^2$. We thus conclude that $\|\tilde{S}_{z,L}^+\| \leq \|S_z^+\|$ and $\sigma(\tilde{S}_{z,L}^+) \subseteq \sigma(S_z^+) \subset [0, z^{-1}]$ since S_z^+ is positive. \square

Analogously to S_z^+ from (13), we can obtain $\tilde{S}_{z,L}^+$ from a polar decomposition of $\tilde{R}_{z,L}^+$,

$$\tilde{R}_{z,L}^+ = W_{z,L} \tilde{S}_{z,L}^+,$$

where $W_{z,L} \in B(\tilde{H})$ is a partial isometry. Moreover, we introduce operators $\tilde{R}_{z,L}^-, \tilde{S}_{z,L}^- \in B(\tilde{H})$ associated with the negative-frequency subspace similarly. Using $\tilde{S}_{z,L}^+$ and $\tilde{S}_{z,L}^-$, we define the self-adjoint operators $S_{z,\tau,L}^+ : \tilde{H} \rightarrow \tilde{H}$ and $S_{z,\tau,L}^- : \tilde{H} \rightarrow \tilde{H}$ as

$$S_{z,\tau,L}^+ = \sqrt{\tilde{S}_{z,L}^+} G_\tau \sqrt{\tilde{S}_{z,L}^+}, \quad S_{z,\tau,L}^- = \sqrt{\tilde{S}_{z,L}^-} G_\tau \sqrt{\tilde{S}_{z,L}^-}. \quad (28)$$

By lemma 4.2 and the fact that Π_L are orthogonal projections, the spectra of $S_{z,\tau,L}^+$ and $-S_{z,\tau,L}^-$ are subsets of the positive and negative halves of $I_{z,\tau}$, respectively. However, note that $\text{ran } S_{z,\tau,L}^+$ and $\text{ran } S_{z,\tau,L}^-$ may not be linearly independent subspaces of H_L .

We would like to assemble a single operator that approximates $S_{z,\tau}$ from $S_{z,\tau,L}^+$ and $S_{z,\tau,L}^-$, while avoiding issues due to possible colinearity of $\text{ran } S_{z,\tau,L}^+$ and $\text{ran } S_{z,\tau,L}^-$ (e.g., creation of a non-trivial nullspace of $S_{z,\tau,L}^+ - S_{z,\tau,L}^-$ with formally infinite corresponding eigenfrequencies). With that in mind, we further reduce the rank of $S_{z,\tau,L}^+$ and $S_{z,\tau,L}^-$ and subtract the resulting operators to yield our final approximation of $S_{z,\tau}$. In what follows, $\Psi_\tau^{+,(M)} : \tilde{H} \rightarrow \tilde{H}$ will denote the orthogonal projection onto the M -dimensional subspace of \tilde{H} spanned by the leading M eigenfunctions of $S_{z,\tau}^+$, and $S_{z,\tau}^{+,(M)} : \tilde{H} \rightarrow \tilde{H}$ will be the rank- M operator $S_{z,\tau}^{+,(M)} = \Psi_\tau^{+,(M)} S_{z,\tau}^+ \Psi_\tau^{+,(M)}$. We similarly define $S_{z,\tau}^{-,(M)} = \Psi_\tau^{-,(M)} S_{z,\tau}^- \Psi_\tau^{-,(M)}$, where $\Psi_\tau^{-,(M)}$ is the orthogonal projection onto $\text{span}\{\psi_{1,\tau}^*, \dots, \psi_{M,\tau}^*\}$, and set $S_{z,\tau}^{(M)} = S_{z,\tau}^{+,(M)} - S_{z,\tau}^{-,(M)}$. For later convenience, we also define $\Psi_\tau^{(M)} = \Psi_\tau^{-,(M)} + \Psi_\tau^{+,(M)}$.

Let us write down an eigendecomposition

$$S_{z,\tau,L}^+ \xi_{j,\tau,L} = e_{j,\tau,L} \xi_{j,\tau,L}, \quad j \in \mathbb{N},$$

where the eigenvalues $e_{j,\tau,L}$ are ordered in decreasing order (note that $e_{j,\tau,L} = 0$ for all $j > L$), and the corresponding eigenfunctions $\xi_{j,\tau,L}$ are chosen to be orthonormal in \tilde{H} . By (17), $S_{z,\tau,L}^-$ admits the eigendecomposition

$$S_{z,\tau,L}^- \xi_{j,\tau,L}^* = e_{j,\tau,L} \xi_{j,\tau,L}^*.$$

Fixing a parameter $M \leq L$, we define the reduced-rank operators $S_{z,\tau,L}^{+,(M)}$ and $S_{z,\tau,L}^{-,(M)}$ as

$$S_{z,\tau,L}^{+,(M)} = \Xi_{\tau,L}^{(M)} S_{z,\tau,L}^+ \Xi_{\tau,L}^{(M)}, \quad S_{z,\tau,L}^{-,(M)} = \bar{\Xi}_{\tau,L}^{(M)} S_{z,\tau,L}^- \bar{\Xi}_{\tau,L}^{(M)}, \quad (29)$$

where $\Xi_{\tau,L}^{(M)} : \tilde{H} \rightarrow \tilde{H}$ and $\bar{\Xi}_{\tau,L}^{(M)} : \tilde{H} \rightarrow \tilde{H}$ are the orthogonal projections onto $\text{span}\{\xi_{1,\tau,L}, \dots, \xi_{M,\tau,L}\}$ and $\text{span}\{\xi_{1,\tau,L}^*, \dots, \xi_{M,\tau,L}^*\}$, respectively. We then introduce the operators

$$S_{z,\tau,L}^{(M)} = S_{z,\tau,L}^{+,(M)} - S_{z,\tau,L}^{-,(M)}. \quad (30)$$

These operators will provide our finite-rank approximation of $S_{z,\tau}$. This approximation converges spectrally in the sense of the following proposition.

Proposition 4.3. *With notation as above, let $M \in \mathbb{N}$ be such that $e_{M+1,\tau} \neq e_{M,\tau}$; that is, $\Psi_\tau^{(M)}$ projects onto an $2M$ -dimensional union of eigenspaces of $S_{z,\tau}^{(M)}$. Then, there exists $L_* \in \mathbb{N}$ such that for all $L > L_*$ the following hold.*

- (i) $S_{z,\tau,L}^{(M)}$ has rank $2M$.
- (ii) There exists a closed subinterval $\tilde{I}_{z,\tau}$ of $(-z^{-1}, z^{-1})$ that contains $\sigma(S_{z,\tau,L}^{(M)})$ and $\sigma(-S_{z,\tau}^-) \cup \sigma(S_{z,\tau}^+)$.
- (iii) As $L \rightarrow \infty$, $S_{z,\tau,L}^{(M)}$ converges in operator norm, and thus spectrally in the sense of theorem 4.1, to $S_{z,\tau}^{(M)}$.
- (iv) As $M \rightarrow \infty$, $S_{z,\tau}^{(M)}$ converges in operator norm, and thus spectrally in the sense of theorem 4.1, to $S_{z,\tau}$.

Proof. See section 4.3. □

By proposition 4.3(iii), for fixed M and sufficiently large L , $S_{z,\tau,L}^{(M)}$ has exactly $2M$ nonzero eigenvalues that lie in the interval $\tilde{I}_{z,\tau}$. We will denote these eigenvalues as $e_{j,\tau,L}^{(M)}$ with $j \in \{-M, \dots, -1, 1, \dots, M\}$, and order them as

$$e_{1,\tau,L}^{(M)} \geq \dots \geq e_{M,\tau,L}^{(M)} > 0 > e_{-M,\tau,L}^{(M)} \geq \dots \geq e_{-1,\tau,L}^{(M)}.$$

We let $\psi_{j,\tau,L}^{(M)} \in \tilde{H}$ be an orthonormal set of eigenfunctions corresponding to $e_{j,\tau,L}^{(M)}$. From (30), we see that the eigenvalues satisfy $e_{-j,\tau,L}^{(M)} = -e_{j,\tau,L}^{(M)}$, and the corresponding eigenfunctions can be chosen so as to satisfy $\psi_{-j,\tau,L}^{(M)} = \psi_{j,\tau,L}^{(M)*}$. Let $\Psi_{\tau,L}^{(M)} : \tilde{H} \rightarrow \tilde{H}$ be the orthogonal projection onto $\text{ran } S_{z,\tau,L}^{(M)}$ (i.e., the $2M$ -dimensional span of the $\psi_{j,\tau,L}^{(M)}$). By proposition 4.3(iv), we have that $\Psi_{\tau,L}^{(M)}$ converges strongly to $\Psi_{\tau}^{(M)}$ as $L \rightarrow \infty$.

Next, define the finite-rank operator $\tilde{R}_{z,\tau,L}^{(M)} = \gamma_z^{-1}(S_{z,\tau,L}^{(M)})$. Note that the well-definition of $\tilde{R}_{z,\tau,L}^{(M)}$ relies on the fact that the spectrum of $S_{z,\tau,L}^{(M)}$ is a subset of $\tilde{I}_{z,\tau}$. In particular, $\tilde{R}_{z,\tau,L}^{(M)}$ has exactly $2M$ nonzero eigenvalues

$$\vartheta_{j,\tau,L}^{(M)} := \gamma_z^{-1}(e_{j,\tau,L}^{(M)}), \tag{31}$$

which come in complex-conjugate pairs, $\vartheta_{j,\tau,L}^{(M)*} = \vartheta_{-j,\tau,L}^{(M)}$, and have $\psi_{j,\tau,L}^{(M)}$ as corresponding eigenfunctions. For these eigenvalues, we define the eigenfrequencies (cf. (19))

$$\omega_{j,\tau,L}^{(M)} = \frac{1}{i} \beta_z(\vartheta_{j,\tau,L}^{(M)}). \tag{32}$$

By continuity of γ_z^{-1} on the closed interval $\tilde{I}_{z,\tau}$ and proposition 4.3(iii), we have that $\tilde{R}_{z,\tau,L}^{(M)}$ converges in operator norm to $\tilde{R}_{z,\tau}^{(M)} := \Psi_{\tau}^{(M)} R_{z,\tau} \Psi_{\tau}^{(M)}$ as $L \rightarrow \infty$.

Letting $\Psi_{\tau}^{(M),\perp} = I - \Psi_{\tau}^{(M)}$ and $\Psi_{\tau,L}^{(M),\perp} = I - \Psi_{\tau,L}^{(M)}$ be the complementary projectors to $\Psi_{\tau}^{(M)}$ and $\Psi_{\tau,L}^{(M)}$, respectively, we define the operators

$$R_{z,\tau,L}^{(M)} = \tilde{R}_{z,\tau,L}^{(M)} + z^{-1} \Psi_{\tau,L}^{(M),\perp}, \quad R_{z,\tau}^{(M)} = \tilde{R}_{z,\tau}^{(M)} + z^{-1} \Psi_{\tau}^{(M),\perp}.$$

These operators have discrete spectra contained in $C_z \setminus \{0\}$ and are resolvents of skew-adjoint operators

$$V_{z,\tau,L}^{(M)} = \beta_z(R_{z,\tau,L}^{(M)}), \quad V_{z,\tau}^{(M)} = \beta_z(R_{z,\tau}^{(M)}) \equiv \Psi_{\tau}^{(M)} V_{z,\tau} \Psi_{\tau}^{(M)},$$

respectively, that have rank $2M$. In particular, the nonzero eigenfrequencies of $V_{z,\tau,L}^{(M)}$ are given by $\omega_{j,\tau,L}^{(M)}$ from (32), and have $\psi_{j,\tau,L}^{(M)}$ as corresponding orthonormal eigenfunctions. The nonzero eigenfrequencies of $V_{z,\tau}^{(M)}$ are identical to the first $2M$ eigenfrequencies $\omega_{j,\tau}$ of $V_{z,\tau}$ ranked in order of increasing modulus.

We will employ the resolvent $R_{z,\tau,L}^{(M)}$ as an approximation of the compactified resolvent $R_{z,\tau}$ that is accessible from the approximation spaces \tilde{H}_L . By the convergences $\tilde{R}_{z,\tau,L}^{(M)} \xrightarrow{n} \tilde{R}_{z,\tau}^{(M)}$ and $\Psi_{\tau,L}^{(M)} \xrightarrow{s} \Psi_{\tau}^{(M)}$, we have $R_{z,\tau,L}^{(M)} \xrightarrow{s} R_{z,\tau}^{(M)}$ as $L \rightarrow \infty$. Moreover, from $\Psi_{\tau}^{(M)} \xrightarrow{s} I$ (which implies $\tilde{R}_{z,\tau}^{(M)} \xrightarrow{n} R_{z,\tau}$) and $\Psi_{\tau}^{(M),\perp} \xrightarrow{s} 0$, we get $R_{z,\tau}^{(M)} \xrightarrow{s} R_{z,\tau}$ as $M \rightarrow \infty$. We therefore conclude that our approximation of $V_{z,\tau}$ by the finite-rank operators $V_{z,\tau,L}^{(M)}$ converges in strong resolvent sense in the iterated limit of $M \rightarrow \infty$ after $L \rightarrow \infty$.

4.3. Proof of proposition 4.3

We begin by recalling the following Hilbert space result.

Lemma 4.4. *Let $A : \mathbb{H} \rightarrow \mathbb{H}$ be a compact, self-adjoint operator on a Hilbert space \mathbb{H} and B_1, B_2, \dots a uniformly bounded sequence of self-adjoint operators on \mathbb{H} that converges strongly to the identity. Then, the sequence A_1, A_2, \dots with $A_n = B_n A B_n$ converges to A in operator norm.*

Proof. Since A is compact and B_n is a uniformly bounded sequence converging strongly to the identity, the sequence $B_n A$ converges to A in operator norm; that is,

$$\lim_{n \rightarrow \infty} \|(I - B_n)A\| = 0. \quad (33)$$

Letting $\beta = \sup_n \|B_n\|$, we have

$$\begin{aligned} \|A - A_n\| &= \|A - B_n A B_n\| = \|A - B_n A + B_n A - B_n A B_n\| \\ &\leq \|(I - B_n)A\| + \|B_n A(I - B_n)\| \leq \|(I - B_n)A\| + \beta \|A(I - B_n)\| \\ &= (1 + \beta) \|(I - B_n)A\|, \end{aligned}$$

where we have used self-adjointness of A and B_n to obtain the last equality. The claim of the lemma follows from (33). \square

We use lemma 4.4 to prove claims (iii) and (iv) of proposition 4.3.

Proof of claims (iii) and (iv). Consider first the operators $S_{z,\tau,L}^+$ from (28). Since $S_{z,\tau}^+$ is self-adjoint and compact, and Π_L is a sequence of orthogonal projections converging strongly to the identity on \tilde{H} , it follows from lemma 4.4 that, as $L \rightarrow \infty$, $S_{z,\tau,L}^+$ converges to $S_{z,\tau}^+$ in operator norm. It is known that operator norm convergence implies compact convergence [14, section 3.3]. Thus, $S_{z,\tau,L}^+$ converges spectrally to $S_{z,\tau}^+$ in the sense of theorem 4.1. In particular, for any M such that $\Psi_{\tau}^{+,(M)}$ projects onto a union of eigenspaces of $S_{z,\tau}^+$, we have that the projections $\Xi_{\tau,L}^{(M)}$ converge strongly to $\Psi_{\tau}^{+,(M)}$.

Together, the norm convergence of $S_{z,\tau,L}^+$ to $S_{z,\tau}^+$ and the strong convergence of $\Xi_{\tau,L}^{(M)}$ to $\Psi_{\tau}^{+, (M)}$ imply that, as $L \rightarrow \infty$, $S_{z,\tau,L}^{+, (M)}$ converges to $S_{z,\tau}^{+, (M)}$ in norm.

Repeating these arguments for $S_{z,\tau,L}^-$, we can deduce that $S_{z,\tau,L}^{-, (M)}$ converges to $S_{z,\tau}^{-, (M)}$ in norm. We therefore conclude that $S_{z,\tau,L}^{(M)}$ converges to $S_{z,\tau}^{(M)}$ in norm, and thus spectrally in the sense of theorem 4.1. This proves claim (iii). The norm convergence of $S_{z,\tau}^{(M)} = \Psi_{\tau}^{(M)} S_{z,\tau} \Psi_{\tau}^{(M)}$ in claim (iv) follows similarly from the fact that $S_{z,\tau}$ is self-adjoint and compact and $\Psi_{\tau}^{(M)}$ is a sequence of orthogonal projections converging strongly to the identity on \tilde{H} as $M \rightarrow \infty$.

We now continue with the proof of the remaining claims.

Proof of claims (i) and (ii). First, note that the nonzero eigenvalues $e_{j,\tau}^{(M)}$ of $S_{z,\tau}^{(M)}$ satisfy $|e_{j,\tau}^{(M)}| \leq e_{1,\tau}$ and $|e_{j,\tau}^{(M)}| \geq e_{M,\tau}$ by construction.

Fix any $e_{\max} \in (e_{1,\tau}, z^{-1})$, $e_{\min} \in (e_{M+1,\tau}, e_{M,\tau})$, and define $\tilde{I}_{z,\tau} = [-e_{\max}, e_{\max}]$. By claim (iii) and theorem 4.1(i), there exists $L_* \in \mathbb{N}$ such that for every $L > L_*$, the multiplicities of the eigenvalues of $S_{z,\tau,L}^{(M)}$ in the set $(-e_{\max}, -e_{\min}) \cup (e_{\min}, e_{\max})$ sum up to $2M$, i.e., $\text{rank } S_{z,\tau,L}^{(M)} \geq 2M$. Since $\text{rank } S_{z,\tau,L}^{(M)} \leq 2M$ by construction, we have $\text{rank } S_{z,\tau,L}^{(M)} = 2M$, proving claim (ii). Moreover, we have $\sigma(S_{z,\tau,L}^{(M)}) \subset (-e_{\max}, -e_{\min}) \cup \{0\} \cup (e_{\min}, e_{\max})$ and $\sigma(S_{z,\tau}) \subset I_{z,\tau} \subset \tilde{I}_{z,\tau}$. This verifies claim (i) and completes our proof of proposition 4.3.

5. Numerical implementation

In this section, we describe a numerical procedure for approximating the compactified resolvent and associated approximate generator from sections 3 and 4 using data sampled along dynamical trajectories. The first step in the procedure is to build a data-driven dictionary of observables that asymptotically approximates an orthonormal basis of the infinite-dimensional Hilbert space H using eigenfunctions of kernel integral operators. This step is identical to the procedure employed in [26]. In section 5.2, we give a cursory overview of the basis construction following a description of the training dataset in section 5.1. In section 5.3, we describe a scheme for data-driven operator approximation that employs this basis. Using this scheme and the finite-rank approximations developed in section 4, we build an approximation of the projection Π_+ to the positive-frequency subspace and an approximation of the integral formula (1) for the resolvent via numerical quadrature. These steps are discussed in sections 5.4 and 5.5, respectively. In section 5.6, we describe data-driven analogs of the resolvent compactification and rank reduction schemes from sections 3 and 4 leading to the approximate resolvent $R_{z,\tau,L}^{(M)}$ and finite-rank generator $V_{z,\tau,L}^{(M)}$. Finally, in section 5.7 we build data-driven approximations of $R_{z,\tau,L}^{(M)}$ and $V_{z,\tau,L}^{(M)}$, and compute the corresponding eigenfrequency–eigenfunction pairs. A high-level summary of the entire procedure is displayed in algorithm 1.

Algorithm 1 Numerical operator approximation for selected resolvent parameter $z > 0$, regularization parameter $\tau > 0$, number of basis functions $L \in \mathbb{N}$, rank parameter $M \leq L$, number of resolvent quadrature nodes $Q \in \mathbb{N}$, and number of samples $N \in \mathbb{N}$. The algorithm computes the $L \times L$ matrix representation $\mathbf{V}_{z,\tau,N}^{(M)}$ of the finite-rank generator $V_{z,\tau,L,N}^{(M)}$ from (56), along with its nonzero eigenfrequencies $\omega_{j,\tau,L,N}^{(M)}$ from (55) and the corresponding eigenfunctions $\psi_{j,\tau,L,N}^{(M)}$ from (54). $\overline{(\cdot)}$ denotes elementwise complex-conjugation of matrices.

- 1: Compute kernel eigenvectors $\{\phi_{j,N}\}_{j=1}^L$ and corresponding eigenvalues $\{\lambda_{j,N}^\tau\}_{j=1}^L$ from (35). Set $\mathbf{\Lambda}_{\tau,N} = \text{diag}(\lambda_{1,N}^\tau, \dots, \lambda_{L,N}^\tau) \in \mathbb{R}^{L \times L}$.
 - 2: Filter basis to have only positive Fourier frequencies using (47): $\phi_{j,N}^+ = \hat{\Pi}_{+,N} \phi_{j,N}$.
 - 3: Compute projected resolvent matrix $\mathbf{R}_{z,N}^+ \in \mathbb{C}^{L \times L}$ using the quadrature formula (52) or (53) with Q nodes and projected shift operator matrix \mathbf{U}_N^+ obtained from $\phi_{j,N}^+$.
 - 4: Compute polar decomposition $\mathbf{R}_{z,N}^+ = \mathbf{W}_{z,N} \mathbf{S}_{z,N}^+$, where $\mathbf{W}_{z,N}$ is unitary and $\mathbf{S}_{z,N}^+$ is positive.
 - 5: Compute matrix square root $\sqrt{\mathbf{S}_{z,N}^+}$.
 - 6: Apply regularization: $\mathbf{S}_{z,\tau,N}^+ = \sqrt{\mathbf{S}_{z,N}^+} \mathbf{\Lambda}_{\tau,N} \sqrt{\mathbf{S}_{z,N}^+}$.
 - 7: Compute eigendecomposition of $\mathbf{S}_{z,\tau,N}^+$, with eigenvalues $e_{l,\tau,L,N}$ and orthonormal eigenvectors $\mathbf{c}_{l,\tau,N} \in \mathbb{C}^L$.
 - 8: Set $\mathbf{C}_{\tau,N}^{(M)} = (\mathbf{c}_{1,\tau,N}, \dots, \mathbf{c}_{M,\tau,N}) \in \mathbb{C}^{L \times M}$ and $\mathbf{E}_{z,\tau,N}^{(M)} = \text{diag}(e_{1,\tau,L,N}, \dots, e_{M,\tau,L,N}) \in \mathbb{R}^{M \times M}$. Form the reduced-rank matrices $\mathbf{S}_{z,\tau,N}^{+, (M)} = \mathbf{C}_{\tau,N}^{(M)} \mathbf{E}_{z,\tau,N}^{(M)} \mathbf{C}_{\tau,N}^{(M)*}$, $\mathbf{S}_{z,\tau,N}^{-, (M)} = \overline{\mathbf{S}_{z,\tau,N}^{+, (M)}}$, and $\mathbf{S}_{z,\tau,N}^{(M)} = \mathbf{S}_{z,\tau,N}^{+, (M)} - \mathbf{S}_{z,\tau,N}^{-, (M)}$.
 - 9: Compute eigendecomposition of $\mathbf{S}_{z,\tau,N}^{(M)}$ with eigenvalues $\vartheta_{l,\tau,L,N}^{(M)}$ and orthonormal eigenvectors $\mathbf{q}_{l,\tau,N}^{(M)} \in \mathbb{C}^L$. Form eigenfunctions $\psi_{l,\tau,L,N}^{(M)}$ with expansion coefficients $\mathbf{q}_{l,\tau,N}^{(M)}$ with respect to the $\phi_{j,N}$ basis.
 - 10: Set $\mathbf{\Omega}_{\tau,N}^{(M)} = \text{diag}(\omega_{-M,\tau,L,N}^{(M)}, \dots, \omega_{-1,\tau,L,N}^{(M)}, \omega_{1,\tau,L,N}^{(M)}, \dots, \omega_{M,\tau,L,N}^{(M)}) \in \mathbb{R}^{L \times L}$, $\mathbf{Q}_{\tau,N}^{(M)} = (\mathbf{q}_{-M,\tau,N}^{(M)}, \dots, \mathbf{q}_{-1,\tau,N}^{(M)}, \mathbf{q}_{1,\tau,N}^{(M)}, \dots, \mathbf{q}_{M,\tau,N}^{(M)}) \in \mathbb{C}^{L \times 2M}$. Form the matrix $V_{z,\tau,N}^{(M)} = i \mathbf{Q}_{\tau,N}^{(M)} \mathbf{\Omega}_{\tau,N}^{(M)} \mathbf{Q}_{\tau,N}^{(M)*}$.
 - 11: **return** Generator matrix $\mathbf{V}_{z,\tau,N}^{(M)}$ and eigenpairs $\{(\omega_{j,\tau,L,N}^{(M)}, \psi_{j,\tau,L,N}^{(M)})\}$.
-

5.1. Training data

We make the following standing assumptions on the training data.

- (A1) We have access to time-ordered samples y_0, \dots, y_{N-1} in a data space Y obtained from a continuous map $F : \mathcal{M} \rightarrow Y$ that is injective on the forward-invariant set $M \subseteq \mathcal{M}$; that is, $y_n = F(x_n)$ with $x_n \in \mathcal{M}$. The samples are taken at a fixed sampling interval $\Delta t > 0$ along a dynamical trajectory $x_0, \dots, x_{N-1} \in \mathcal{M}$ with $x_n = \Phi^{n \Delta t}(x_0)$.
- (A2) The invariant measure μ is ergodic under the discrete-time map $\Phi^{\Delta t}$.

(A3) The initial point x_0 (and thus the entire orbit x_0, x_1, \dots) lies in M , and moreover it lies in the basin of μ . This means that

$$\lim_{N \rightarrow \infty} \frac{1}{N} \sum_{n=0}^{N-1} f(x_n) = \int_X f d\mu, \quad \forall f \in C(M). \quad (34)$$

Note that we do not require knowledge of the state space trajectory x_0, \dots, x_{N-1} . Moreover, while (34) holds for μ -a.e. $x_0 \in \mathcal{M}$ by ergodicity, we do not assume that the x_n lie in the support of μ (which may be a null set with respect to an ambient measure on \mathcal{M} , such as an attractor of a dissipative system). Invariant measures for which (34) holds for initial conditions x_0 drawn from a positive-measure set with respect to an ambient measure (e.g., Lebesgue measure) are called observable, or physical; e.g., [82, 8].

Henceforth, we will let $\mu_N = \sum_{n=0}^{N-1} \delta_{x_n}/N$ denote the sampling measure supported on the trajectory x_0, \dots, x_{N-1} . Equation (34) can then be understood as weak-* convergence of μ_N to μ as $N \rightarrow \infty$ at fixed Δt . We also let $\hat{H}_N = L^2(\mu_N)$ be the L^2 space associated with μ_N , equipped with the inner product $\langle f, g \rangle_N = \sum_{n=0}^{N-1} f^*(x_n)g(x_n)/N$, where the elements of \hat{H}_N are equivalence classes of complex-valued functions on \mathcal{M} with common values on the trajectory x_0, \dots, x_{N-1} . For simplicity, we shall assume that the points x_0, \dots, x_{N-1} are distinct—under assumptions (A1)–(A3) this holds aside from trivial cases such as μ being supported on a singleton set containing a fixed point. The Hilbert space \hat{H}_N is then N -dimensional, and there is a bijective correspondence between elements $f \in \hat{H}_N$ and N -dimensional column vectors $\mathbf{f} = (f(x_0), \dots, f(x_{N-1}))^\top \in \mathbb{C}^N$. Note that if f is a unit vector with $\|f\|_{\hat{H}_N} = 1$ then \mathbf{f} has 2-norm $\|\mathbf{f}\|_2 = \sqrt{N}$. We let $\iota_N : C(M) \rightarrow \hat{H}_N$ be the restriction map on continuous functions into \hat{H}_N , i.e., $\iota_N f = \hat{f}$ where $\hat{f}(x_n) = f(x_n)$ for all $n \in \{0, \dots, N-1\}$ (cf. $\iota : C(M) \rightarrow H$ from section 2.1). We also let \tilde{H}_N be the $(N-1)$ -dimensional subspace of \hat{H}_N consisting of zero-mean functions with respect to the sampling measure, i.e., $\tilde{H}_N = \{f \in \hat{H}_N : \langle \mathbf{1}, f \rangle_N \equiv \int_{\mathcal{M}} f d\mu_N = 0\}$ (cf. $\tilde{H} \subset H$ from section 2.1). In accordance with the notation laid out in section 2.1, $\|\hat{A}\|$ will denote the operator norm of $\hat{A} \in B(\hat{H}_N)$, which is equivalent in this case to any norm on $N \times N$ complex matrices.

Remark 5.1 (single vs. multiple trajectories). While in assumptions (A1)–(A3) we consider that the samples are taken on a single dynamical trajectory, the methods described below can be generalized to training with data from ensembles of shorter trajectories. The basic requirements are that the corresponding sampling measures converge to μ in the sense of (34) and the individual trajectories in the ensemble are sufficiently long for the frequency filtering and quadrature methods in sections 5.4 and 5.5 to be applied.

5.2. Basis construction

Recall from section 3.1 that the integral operators G_τ used for resolvent compactification are induced from Markovian kernels $p_\tau : \mathcal{M} \times \mathcal{M} \rightarrow \mathbb{R}_+$. For the purposes of data-driven

approximation, we assume that p_τ is the pullback of a kernel $q_\tau : Y \times Y \rightarrow \mathbb{R}_+$ on data space; that is, $p_\tau(x, x') = q_\tau(F(x), F(x'))$. We also assume that available to us is a family of continuous kernels $q_{\tau,N} : Y \times Y \rightarrow \mathbb{R}_+$ and their pullbacks $p_{\tau,N} : \mathcal{M} \times \mathcal{M} \rightarrow \mathbb{R}_+$, $p_{\tau,N}(x, x') = q_{\tau,N}(F(x), F(x'))$, such that $p_{\tau,N}$ is symmetric and Markovian with respect to μ_N , i.e.,

$$p_{\tau,N}(x, x') = p_{\tau,N}(x', x), \quad p_{\tau,N}(x, x') \geq 0, \quad \int_M p_{\tau,N}(x, \cdot) d\mu_N = 1, \quad \forall x, x' \in \mathcal{M}.$$

We require that, as $N \rightarrow \infty$, $p_{\tau,N}$ converges to p_τ , uniformly on $M \times M$. The data-dependent kernels $p_{\tau,N}$ can be constructed analogously to p_τ by normalization of a data-independent kernel $k : \mathcal{M} \times \mathcal{M} \rightarrow \mathbb{R}_+$; see Appendix A.

Associated with each $p_{\tau,N}$ is a self-adjoint Markov operator $G_{\tau,N} : \hat{H}_N \rightarrow \hat{H}_N$ defined as $G_{\tau,N}f = \int_M p_{\tau,N}(\cdot, x)f(x) d\mu_N(x)$. Concretely, we represent $G_{\tau,N}$ by the $N \times N$ kernel matrix $\mathbf{G}_\tau = [G_{ij}]$ with entries $G_{ij} = p_{\tau,N}(x_i, x_j)/N$. This matrix is a bistochastic matrix (i.e., $\mathbf{G}_\tau^\top = \mathbf{G}_\tau$ and $\sum_{j=0}^{N-1} G_{ij} = 1$ for all $i \in \{0, \dots, N-1\}$), and it has the property that if $f \in \hat{H}_N$ is represented by the column vector $\mathbf{f} = (f(x_0), \dots, f(x_{N-1}))^\top \in \mathbb{C}^N$, then $\mathbf{g} = \mathbf{G}_\tau \mathbf{f}$ with $\mathbf{g} = (g_0, \dots, g_{N-1})^\top$ is the column matrix representation of $g = G_{\tau,N}f$, i.e., $g_i = g(x_i)$.

Correspondingly, an eigendecomposition of \mathbf{G}_τ ,

$$\mathbf{G}_\tau \boldsymbol{\phi}_j = \lambda_{j,N}^\tau \boldsymbol{\phi}_j, \quad \boldsymbol{\phi}_j = (\phi_{0,j,N}, \dots, \phi_{N-1,j,N})^\top,$$

where the eigenvalues are ordered as $1 = \lambda_{0,N}^\tau \geq \lambda_{1,N}^\tau \geq \dots \geq \lambda_{N-1,N}^\tau$ and the eigenvectors are chosen such that $\boldsymbol{\phi}_0 = (1, \dots, 1)$ and $\boldsymbol{\phi}_i^\top \boldsymbol{\phi}_j = N\delta_{ij}$, provides an orthonormal basis $\{\phi_{0,N}, \dots, \phi_{N-1,N}\}$ of \hat{H}_N with $\phi_{j,N}(x_n) = \phi_{n,j,N}$, consisting of eigenvectors of $G_{\tau,N}$,

$$G_{\tau,N} \phi_{j,N} = \lambda_{j,N}^\tau \phi_{j,N}. \quad (35)$$

Similarly to the eigenvectors of G_τ corresponding to nonzero eigenvalues (see section 3.1), the eigenvectors $\phi_{j,N}$ corresponding to $\lambda_{j,N}^\tau \neq 0$ have continuous representatives $\varphi_{j,N} \in C(M)$ given by

$$\varphi_{j,N}(x) = \frac{1}{\lambda_{j,N}^\tau} \int_M p_{\tau,N}(x, x') \phi_{j,N}(x') d\mu_N(x') = \frac{1}{\lambda_{j,N}^\tau N} \sum_{n=0}^{N-1} p_{\tau,N}(x, x_n) \phi_{n,j,N}. \quad (36)$$

Note that since $p_{\tau,N}(x, x_n) = q_{\tau,N}(F(x), y_n)$ and $q_{\tau,N}(\cdot, y_n)$ are known functions, the eigenfunctions $\varphi_{j,N}$ can be evaluated at any $x \in M$ given the corresponding value $y = F(x)$ in data space.

The following convergence result for the eigenbasis of $G_{\tau,N}$ is based on spectral approximation techniques for kernel integral operators on spaces of continuous functions [79].

Lemma 5.2. *Under the assumptions on the kernel and training data stated in sections 3.1, 5.1 and 5.2 the following hold.*

- (i) For every (nonzero) eigenvalue λ_j^τ of G_τ , $\lim_{N \rightarrow \infty} \lambda_{j,N}^\tau = \lambda_j^\tau$, including multiplicities in the sense of theorem 4.1(i).
- (ii) For every eigenfunction $\phi_j \in H$ of G_τ corresponding to nonzero eigenvalue λ_j^τ , there exists a sequence of eigenfunctions $\phi_{j,N} \in \hat{H}_N$ of $G_{\tau,N}$ such that $\lim_{N \rightarrow \infty} \|\varphi_{j,N} - \varphi_j\|_{C(M)} = 0$, where $\varphi_j, \varphi_{j,N} \in C(M)$ are the continuous representatives of ϕ_j and $\phi_{j,N}$, respectively.

Proof. See [36, Appendix A]. □

Lemma 5.2 in conjunction with ergodicity of G_τ (property (K5)) imply that for sufficiently large N , $\lambda_{0,N}^\tau$ is a simple eigenvalue. Henceforth, we will assume that this is the case. A sufficient condition for $\lambda_{0,N}^\tau$ to be simple is that \mathbf{G}_τ has strictly positive elements.

5.3. Operator approximation

We use the results of section 5.2 to perform data-driven approximation of operators on \tilde{H} .

Similarly to section 4.2, for an integer parameter L consider the L -dimensional subspace $H_L \subset \tilde{H}$ spanned by the leading L nonconstant eigenfunctions of G_τ , i.e., $H_L = \text{span}\{\phi_1, \dots, \phi_L\}$ with corresponding orthogonal projection $\Pi_L : \tilde{H} \rightarrow \tilde{H}$. Henceforth, we shall assume that L is chosen such that $\lambda_L^\tau \neq \lambda_{L+1}^\tau$ so that H_L is a union of eigenspaces of G_τ . Given a bounded operator $A \in B(\tilde{H})$, we define its compression $A_L \in B(\tilde{H})$ as $A_L = \Pi_L A \Pi_L$. Since $\{\phi_1, \dots\}$ is an orthonormal basis of \tilde{H} , as $L \rightarrow \infty$, the operators A_L converge to A in the strong operator topology of $B(\tilde{H})$. Note that we can equivalently view A_L as an operator from H_L into itself. In particular, A_L is completely characterized through its $L \times L$ matrix representation $\mathbf{A} = [A_{ij}]_{i,j=1}^L$ with $A_{ij} = \langle \phi_i, A \phi_j \rangle$.

To make an analogous construction in the data-driven setting, we define $\hat{H}_{L,N} = \text{span}\{\phi_{1,N}, \dots, \phi_{L,N}\} \subseteq \tilde{H}_N$ via the eigenvectors $\phi_{j,N}$ of $G_{\tau,N}$, and use the orthogonal projections $\Pi_{L,N} : \hat{H}_N \rightarrow \hat{H}_N$ with $\text{ran } \Pi_{L,N} = \hat{H}_{L,N}$ to define compressions $\hat{A}_{L,N} := \Pi_{L,N} \hat{A}_N \Pi_{L,N}$ of operators $\hat{A}_N \in B(\hat{H}_N)$. The operators $\hat{A}_{L,N}$ are represented by $L \times L$ matrices $\mathbf{A}_N = [\hat{A}_{ij}]_{i,j=1}^L$ with entries $A_{ij} = \langle \phi_{i,N}, \hat{A}_N \phi_{j,N} \rangle_N$. Note that we do not ask that \hat{A}_N preserves the subspace of zero-mean functions $\tilde{H}_N \subset \hat{H}_N$. Note also that \mathbf{A}_N can be computed numerically so long as the action of \hat{A}_N on the basis elements $\phi_{j,N}$ is known.

Next, consider a bounded operator $A \in B(\tilde{H})$ and a sequence of operators $\hat{A}_1, \hat{A}_2, \dots$ on \hat{H}_N that approximates A in the following sense:

- (A4) The family \hat{A}_N is uniformly bounded, i.e., $\sup_N \|\hat{A}_N\| < \infty$.
- (A5) There is an operator $\tilde{A} : \tilde{C}(M) \rightarrow \tilde{C}(M)$ on zero-mean continuous functions such that
 - (a) $\iota \tilde{A} = A \iota$.

(b) For every $f \in \tilde{C}(M)$, $\lim_{N \rightarrow \infty} \|(\iota_N \tilde{A} - \hat{A}_N \iota_N) f\|_{\hat{H}_N} = 0$.

Given such an approximation, and a choice of dimension parameter L , the $L \times L$ matrix representations of the compressions $A_{L,N}$ consistently approximate the corresponding matrix representation of A_L .

Lemma 5.3. *Let \mathbf{A} and \mathbf{A}_N be the $L \times L$ matrix representations of \hat{A}_L and $\hat{A}_{L,N}$, respectively, constructed as above. Then under assumptions (A4) and (A5), and the assumptions of lemma 5.2, we have $\lim_{N \rightarrow \infty} \mathbf{A}_N = \mathbf{A}$ in any matrix norm.*

Proof. See Supplementary Information (SI) of ref. [31]. \square

For our purposes, the main utility of lemma 5.3 is that it allows us to consistently approximate Koopman operators on \tilde{H} by shift operators on \tilde{H}_N [6, 35]. For that, let $\hat{U}_N : \hat{H}_N \rightarrow \hat{H}_N$ be the circular left shift operator defined as

$$\hat{U}_N f(x_n) = \begin{cases} f(x_{n+1}), & 0 \leq n \leq N-2, \\ f(x_0), & n = N-1. \end{cases} \quad (37)$$

As \hat{U}_N is unitary, the family $\{\hat{U}_N\}_{N \geq 1}$ is uniformly bounded, $\|\hat{U}_N\| = 1$, and satisfies assumption (A4). Moreover, letting $\tilde{U}^t : \tilde{C}(M) \rightarrow \tilde{C}(M)$ be the time- t Koopman operator on zero-mean continuous functions, $\tilde{U}^t f = f \circ \Phi^t$, we have $\iota \tilde{U}^t = U^t \iota$ since μ is an invariant measure of the flow Φ^t . One also verifies using assumption (A3) that $\lim_{N \rightarrow \infty} \|(\iota_N \tilde{U}^{\Delta t} - \hat{U}_N \iota_N) f\|_{\hat{H}_N} = 0$ for any $f \in \tilde{C}(M)$, and thus that assumption (A5) holds.

By lemma 5.3, we conclude that the $L \times L$ projected shift operator matrices $\mathbf{U}_N = [\hat{U}_{ij}]_{i,j=1}^L$ with $\hat{U}_{ij} = \langle \phi_{i,N}, \hat{U}_N \phi_{j,N} \rangle_N$ consistently approximate the projected Koopman operator matrix $\mathbf{U} = [U_{ij}]_{i,j=1}^L$ with $U_{ij} = \langle \phi_i, U^{\Delta t} \phi_j \rangle$, i.e., $\lim_{N \rightarrow \infty} \mathbf{U}_N = \mathbf{U}$. Note that the matrix elements \hat{U}_{ij} can be computed directly by applying (37) to the kernel eigenvectors $\phi_{j,N}$; explicitly,

$$\hat{U}_{ij} = \frac{1}{N} \sum_{n=0}^{N-2} \phi_{n,i,N} \phi_{n+1,j,N} + \frac{1}{N} \phi_{N-1,i,N} \phi_{0,j,N}. \quad (38)$$

In the following two subsections we will use our data-driven approximation of the Koopman operator to derive an approximation of (i) the projection Π_+ onto the positive-frequency subspace (section 5.4); and (ii) the resolvent $R_z(V)$ of the generator (section 5.5).

Remark 5.4 (circular vs. non-circular shift operators). In addition to \hat{U}_N from (37), consistent approximations of the Koopman operator can also be obtained using non-circular shift operators, e.g., $\hat{U}'_N : \hat{H}_N \rightarrow \hat{H}_N$, where

$$\hat{U}'_N f(x_n) = \begin{cases} f(x_{n+1}), & 0 \leq n \leq N-2, \\ 0, & n = N-1. \end{cases} \quad (39)$$

The corresponding $L \times L$ shift operator matrices $\mathbf{U}'_N = [\hat{U}'_{ij}]_{i,j=1}^L$, $\hat{U}'_{ij} = \langle \phi_{i,N}, \hat{U}'_N \phi_{j,N} \rangle_N$, satisfy $\lim_{N \rightarrow \infty} \mathbf{U}'_N = \mathbf{U}$; however, the \hat{U}'_N are not unitary operators. Unitarity of

\hat{U}_N will turn out to be useful when we perform data-driven approximation of the resolvent $R_z(V)$ in section 5.5 (see, in particular, (52)). Therefore, in this work we opt to approximate the Koopman operator using the circular shift operator from (37).

5.4. Positive-frequency filtering

Let $\{A, \tilde{A}, \hat{A}_1, \hat{A}_2, \dots\}$ with $A : \tilde{H} \rightarrow \tilde{H}$, $\tilde{A} : \tilde{C}(M) \rightarrow \tilde{C}(M)$, and $\hat{A}_N : \hat{H}_N \rightarrow \hat{H}_N$ be a family of operators satisfying assumptions (A4) and (A5). In this subsection, we build a data-driven approximation of the projected operator

$$A_+ := \Pi_+ A \Pi_+ \quad (40)$$

onto the positive-frequency subspace H_+ . We will arrive at (46), which employs the discrete Fourier transform (DFT) to filter out negative frequencies.

For a time unit $S > 0$ and natural numbers m and n define the frequency and time domains

$$\Omega_m = \left[-\frac{2\pi m}{S}, \frac{2\pi m}{S} \right], \quad T_{m,n} = \left[-\frac{n^2 S}{m(2n+1)}, \frac{n^2 S}{m(2n+1)} \right], \quad (41)$$

respectively. Fix also a family $\{h_m : \mathbb{R} \rightarrow \mathbb{R}_+\}_{m \in \mathbb{N}}$ of smooth, compactly supported functions with $\text{supp } h_m \subseteq [0, 2\pi m/S]$ that converge pointwise to the characteristic function $\chi_{[0, \infty)}$, i.e., $\lim_{m \rightarrow \infty} h_m(\omega) = \chi_{[0, \infty)}(\omega)$ for every $\omega \in \mathbb{R}$. With this family, define the operators $P_{m,n} : H \rightarrow H$ as

$$P_{m,n} f = \int_{\mathbb{R}^2} h_m(\omega) \chi_{T_{m,n}}(t) e^{-i\omega t} U^t f \, d(\omega, t). \quad (42)$$

We then have the following approximation lemma.

Lemma 5.5. *The operators $P_{m,n}$ converge strongly to Π_+ in the sense of the iterated limit*

$$\Pi_+ f = \lim_{m \rightarrow \infty} \lim_{n \rightarrow \infty} P_{m,n} f, \quad \forall f \in H.$$

Proof. Define $\xi_{m,n} \in C_0(\mathbb{R})$ as

$$\xi_{m,n}(\omega) = \frac{1}{2\pi} \int_{-nS/m}^{nS/m} e^{-i\omega t} dt = \frac{1}{2\pi} \int_{\mathbb{R}} e^{-i\omega t} \chi_{T_{m,n}}(t) dt.$$

Since h_m is smooth and compactly supported, for every $\omega' \in \mathbb{R}$ we have $h_m(\omega') = \lim_{n \rightarrow \infty} h_{m,n}(\omega')$, where $h_{m,n} \in C_0(\mathbb{R})$ is defined by

$$h_{m,n}(\omega') = \int_{\mathbb{R}} \xi_{m,n}(\omega - \omega') h_m(\omega) d\omega = \int_{\mathbb{R}^2} h_m(\omega) \chi_{T_{m,n}}(t) e^{-i\omega t} e^{i\omega' t} d(\omega, t).$$

Since h_m converges to $\chi_{[0, \infty)}$ pointwise, for every $f \in H$ we have

$$\Pi_+ f = \chi_{i[0, \infty)}(V) f = \chi_{[0, \infty)}(V/i) f = \lim_{m \rightarrow \infty} h_m(V/i) f = \lim_{m \rightarrow \infty} \lim_{n \rightarrow \infty} h_{m,n}(V/i) f,$$

where

$$h_{m,n}(V/i)f = \int_{\mathbb{R}^2} h_m(\omega)\chi_{T_{m,n}}(t)e^{-i\omega t}e^{Vt}f d(\omega, t) = \int_{\mathbb{R}^2} h_m(\omega)\chi_{T_{m,n}}(t)e^{-i\omega t}U^t f d(\omega, t).$$

The claim of the lemma follows. \square

Remark 5.6. The particular choice of frequency–time domain in (41) is made in order to make contact between our approach and the DFT. The convergence results in lemma 5.5, as well as proposition 5.7 stated below, remain valid for other domain choices so long as Ω_m increases to \mathbb{R} as $m \rightarrow \infty$ and $T_{m,n}$ increases to \mathbb{R} as $n \rightarrow \infty$ at fixed m .

5.4.1. Numerical quadrature We approximate $P_{m,n}$ by a family of operators $\{P_{m,n,K}\}_{K \in \mathbb{N}}$ obtained by replacing the integral over the frequency–time domain $\Omega_m \times T_{m,n} \subseteq \mathbb{R}^2$ by quadrature. Defining $\tilde{N} = (2n+1)K^2/n^2$ and the gridpoints $\{(\omega_k, t_j)\}_{k,j=-K}^K$ where

$$\omega_k = \frac{\text{len}(\Omega_m)k}{2K} = \frac{2\pi mk}{SK}, \quad t_j = \frac{\text{len}(T_{m,n})j}{2K} = \frac{n^2 S j}{m(2n+1)K}, \quad \omega_k t_j = \frac{2\pi k j}{\tilde{N}},$$

we set

$$P_{m,n,K} := \frac{1}{\tilde{N}} \sum_{k,j=-K}^K h_m(\omega_k)\chi_{T_{m,n}}(t_j)e^{-2\pi i k j / \tilde{N}} U^{t_j}. \quad (43)$$

By continuity of the cross-correlation function $C_{fg}(t) = \langle g, U^t f \rangle$ for any $f, g \in H$, it follows that $\lim_{K \rightarrow \infty} \langle g, P_{m,n,K} f \rangle = \langle g, P_{m,n} f \rangle$, and thus that $P_{m,n,K}$ converges to $P_{m,n}$ strongly. Combining this fact with lemma 5.5, we can express the projected operator A_+ from (40) as the iterated strong limit

$$A_+ f = \lim_{m \rightarrow \infty} \lim_{n \rightarrow \infty} \lim_{K \rightarrow \infty} A_{m,n,K} f, \quad \forall f \in H,$$

where $A_{m,n,K} = P_{m,n,K}^* A P_{m,n,K}$.

Consider now the operators $\tilde{P}_{m,n,K} : \tilde{C}(M) \rightarrow \tilde{C}(M)$ $\tilde{P}'_{m,n,K} : \tilde{C}(M) \rightarrow \tilde{C}(M)$ and $\hat{P}_{m,n,K,N} : \hat{H}_N \rightarrow \hat{H}_N$ defined as

$$\begin{aligned} \tilde{P}_{m,n,K} &= \frac{1}{\tilde{N}} \sum_{k,j=-K}^K h_m(\omega_k) e^{-2\pi i k j / \tilde{N}} \tilde{U}^{t_j}, \\ \tilde{P}'_{m,n,K} &= \frac{1}{\tilde{N}} \sum_{k,j=-K}^K h_m(\omega_k) \chi_{T_{m,n}}(t_j) e^{2\pi i k j / \tilde{N}} \tilde{U}^{-t_j}, \\ \hat{P}_{m,n,K,N} &= \frac{1}{\tilde{N}} \sum_{k,j=-K}^K h_m(\omega_k) e^{-2\pi i k j / \tilde{N}} \hat{U}_N^j, \end{aligned} \quad (44)$$

where in the definition of $\hat{P}_{m,n,K,N}$ we used the shift operator \hat{U}_N based on the sampling interval $\Delta t = nS/(mK)$. One readily verifies that for

each $m, n, K \in \mathbb{N}$, the family of operators $\{P_{m,n,K}, \tilde{P}_{m,n,K}, \hat{P}_{m,n,K,1}, \hat{P}_{m,n,K,2}, \dots\}$ satisfies assumptions (A4) and (A5). Similarly, these assumptions are satisfied by the family $\{P_{m,n,K}^*, \tilde{P}'_{m,n,K}, \hat{P}_{m,n,K,1}^*, \hat{P}_{m,n,K,2}^*, \dots\}$. We thus conclude that $\{A_{m,n,K}^+, \tilde{A}_{m,n,K}^+, \hat{A}_{m,n,K,1}^+, \hat{A}_{m,n,K,2}^+, \dots\}$ with

$$\begin{aligned} A_{m,n,K}^+ &= P_{m,n,K}^* A \tilde{P}_{m,n,K}, & \tilde{A}_{m,n,K}^+ &= \tilde{P}_{m,n,K}^* \tilde{A} \tilde{P}_{m,n,K}, \\ \hat{A}_{m,n,K,N}^+ &= \hat{P}_{m,n,K,N}^* \hat{A}_N \hat{P}_{m,n,K,N} \end{aligned}$$

also satisfies assumptions (A4) and (A5).

Define now the functions $\{\phi_j^+ \in H_+\}_{j \in \mathbb{N}}$ and $\{\phi_{j,m,n,K,N}^+ \in \hat{H}_N\}_{j=1}^{N-1}$ as $\phi_j^+ = \Pi_+ \phi_j$ and $\phi_{j,m,n,K,N}^+ = \hat{P}_{m,n,K,N} \phi_{j,N}$. The following is a corollary of lemma 5.3 that summarizes our approximation of positive-frequency projected operators.

Proposition 5.7. *Given $m, n, K, L, N \in \mathbb{N}$ and with notation as above, let $\mathbf{A}^+ = [A_{ij}^+]_{i,j=1}^L$ and $\mathbf{A}_{m,n,K,N}^+ = [\hat{A}_{ij}^+]_{i,j=1}^L$ be the $L \times L$ matrix representations of $A_L^+ := \Pi_L A^+ \Pi_L$ and $A_{m,n,K,L,N}^+ := \Pi_{L,N} \hat{A}_{m,n,K,N} \Pi_{L,N}$, i.e.,*

$$\begin{aligned} A_{ij}^+ &= \langle \phi_i, A^+ \phi_j \rangle = \langle \phi_i^+, A \phi_j^+ \rangle, \\ \hat{A}_{ij}^+ &= \langle \phi_{i,N}, \hat{A}_{m,n,K,N}^+ \phi_{j,N} \rangle_N = \langle \phi_{i,m,n,K,N}^+, \hat{A}_{m,n,K,N} \phi_{j,m,n,K,N}^+ \rangle_N. \end{aligned}$$

Then, $\mathbf{A}_{m,n,K,N}^+$ converges to \mathbf{A}^+ in the iterated limit

$$\lim_{m \rightarrow \infty} \lim_{n \rightarrow \infty} \lim_{K \rightarrow \infty} \lim_{N \rightarrow \infty} \mathbf{A}_{m,n,K,N}^+ = \mathbf{A}^+.$$

Remark 5.8. Aside from (44), other schemes could be employed to build the approximate projections $\hat{P}_{m,n,K,N}$, e.g., high-order quadrature, or convolution-based methods [18]. Such methods may be able to attain a sufficiently fast rate of convergence with respect to K that allows combining the iterated limits of $n \rightarrow \infty$ after $K \rightarrow \infty$ to a single $K \rightarrow \infty$ limit over an increasing integration domain $T_{m,n,K}$. At the same time, however, the use of high-order quadrature imposes regularity conditions on the cross-correlation function C_{fg} that may not hold for arbitrary $f, g \in H$ (effectively restricting the class of basis functions for which proposition 5.7 holds). For instance, if g does not lie in the domain of the generator V then C_{fg} is not continuously differentiable, which creates obstacles to approximation of $\langle f, P_{m,n} g \rangle$ via high-order quadrature.

When convenient, we will use the abbreviated notations $\phi_{j,N}^+ \equiv \phi_{j,m,n,K,N}^+$ for the positive-frequency projected basis functions and $\mathbf{A}_N^+ \equiv \mathbf{A}_{m,n,K,N}^+$ for the corresponding projected operator matrices. Convergence of \mathbf{A}_N^+ to \mathbf{A}^+ will be understood in the sense of proposition 5.7.

5.4.2. Discrete Fourier transform In the experiments of section 6, we assume that we are given N samples at a fixed sampling interval Δt (see section 5.1), and we take N to be odd for simplicity. We then use the special case of $P_{m,n,K,N}$ with $S = 2 \Delta t$, $m = 1$,

and $n = K = (N - 1)/2$. With this choice, the frequency domain $\Omega_1 = [-\pi/\Delta t, \pi/\Delta t]$ is consistent with the Nyquist–Shannon theorem for the sampling interval Δt . Moreover, we have $\tilde{N} = N$ and the operator $P_{1,K,K,N}$ becomes

$$P_{1,K,K,N} = \frac{1}{N} \sum_{k,j=-K}^K h_1(\omega_k) e^{-2\pi i k j / N} \hat{U}_N^j.$$

Choosing, further, the window function h_1 such that $h_1(\omega_j) = 1$ for all $j = 1, \dots, K - 1$, our final approximation for the positive-frequency projection is given by $\hat{\Pi}_{+,N} : \hat{H}_N \rightarrow \hat{H}_N$, where

$$\hat{\Pi}_{+,N} = \frac{1}{N} \sum_{k=1}^K \sum_{j=-K}^K e^{-2\pi i k j / N} \hat{U}_N^j. \quad (45)$$

This leads to the projected operator

$$\hat{A}_{+,N} := \hat{\Pi}_{+,N}^* \hat{A}_N \hat{\Pi}_{+,N}, \quad (46)$$

which provides (through its matrix representation), a data-driven approximation of A_+ from (40). Since, for any $f \in \hat{H}_N$,

$$\hat{\Pi}_{+,N} f(x_l) = \frac{1}{N} \sum_{k=1}^K \sum_{j=-K}^K e^{-2\pi i k j / N} f(x_{j+l}), \quad (47)$$

$\hat{\Pi}_{+,N} f$ can be directly computed by applying a fast Fourier transform (FFT) to the N -dimensional vector representing f , zeroing-out the non-positive frequencies, and then applying an inverse FFT.

Aside from (47), DFT-based computation of $P_{m,n,K,N} f$ is possible for other values of $n, K > (N - 1)/2$, using zero-padding of the vector representing f as appropriate. Working with frequency window functions other than $h_1(\omega_j) = 1$ used in (45) would also be amenable to usage of DFT. Here, we do not consider such possibilities further since we found that (47) yields satisfactory results, but doing so would be an interesting direction for future work.

5.5. Approximation of the resolvent

Recall that the finite-rank approximation scheme discussed in section 4.2 employs finite-rank approximations $\tilde{R}_{z,L}^+$ and $\tilde{R}_{z,L}^-$ of the positive- and negative-frequency projected resolvents R_z^+ and R_z^- , respectively. In order to build data-driven analogs of these approximations, we take advantage of the integral representation of the resolvent eq. (1), reproduced here for convenience:

$$R_z(V) = \int_0^\infty e^{-zt} U^t dt, \quad \operatorname{Re} z > 0.$$

As with our approximation of the projection Π_+ in section 5.4, given a time unit $S' > 0$, we introduce an increasing sequence T_1, T_2, \dots of time domains, $T_\ell = [0, \ell S']$, and approximate $R_z(V) \in B(\tilde{H})$ by the operators $R_{z,\ell} \in B(\tilde{H})$, where

$$R_{z,\ell} = \int_0^{\ell S'} e^{-zt} U^t dt. \quad (48)$$

Due to the exponential decay of the e^{-zt} term in the integrand, as $\ell \rightarrow \infty$, $R_{z,\ell}$ converges to $R_z(V)$ in operator norm.

We further approximate $R_{z,\ell}$ by a sequence of operators $\{R_{z,\ell,1}, R_{z,\ell,2}, \dots\}$, where $R_{z,\ell,Q} : H \rightarrow H$ is obtained from a quadrature rule with nodes $t_0, \dots, t_Q \in T_\ell$ and corresponding weights $w_0, \dots, w_Q \in \mathbb{R}_+$, viz.

$$R_{z,\ell,Q} = \sum_{q=0}^Q w_q e^{-zt_q} U^{t_q}. \quad (49)$$

In the experiments of section 6, we use the composite Simpson rule where the nodes are equispaced, $t_q = (q-1)\Delta t$ with $\Delta t = \ell S'/Q$, and the weights have the values $w_0 = w_Q = \Delta t/3$, $w_{2q+1} = 2\Delta t/3$, and $w_{2q} = 4\Delta t/3$. The resulting approximations from (49) converge in the strong operator topology, i.e., $\lim_{Q \rightarrow \infty} R_{z,\ell,Q} f = R_{z,\ell} f$ for every $f \in \tilde{H}$. Explicit rates of convergence can be obtained under additional assumptions on f . For instance, if f lies in a finite-dimensional Koopman-invariant subspace of \tilde{H} , then $\mathbb{R} \ni t \mapsto U^t f$ is a C^∞ function in the norm of \tilde{H} and the error $\|(R_{z,\ell,Q} - R_{z,\ell})f\|_H$ is $O(Q^{-3})$. Of course, we may have to contend with slower rates of convergence as such assumptions may not hold in practice. A natural alternative to a composite Simpson scheme given the exponentially decaying integrand in (48) is Gauss–Laguerre quadrature.

Using $R_{z,\ell,Q}$, we obtain a strongly convergent approximation of the positive-frequency projected resolvent as

$$R_z^+(V)f = \lim_{\ell \rightarrow \infty} \lim_{Q \rightarrow \infty} R_{z,\ell,Q}^+ f, \quad \forall f \in \tilde{H}, \quad (50)$$

where $R_{z,\ell,Q}^+ = \Pi_+ R_{z,\ell,Q} \Pi_+$.

Next, passing to the data-driven setting, we approximate $R_{z,\ell,Q}$ by $\hat{R}_{z,\ell,Q,N} : \hat{H}_N \rightarrow \hat{H}_N$,

$$\hat{R}_{z,\ell,Q,N} = \sum_{q=0}^Q w_q e^{-zq\Delta t} \hat{U}_N^q, \quad (51)$$

where \hat{U}_N is the shift operator on \hat{H}_N from (37). In this last approximation we have tacitly identified the interval Δt used to build $R_{z,\ell,Q}$ in (49) with the sampling interval of the data. It is also natural to set $S' = \Delta t$ so that ℓ and Q represent the number of timesteps within the integration domain T_ℓ .

Since $R_{z,\ell,Q}$ and $\hat{R}_{z,\ell,Q,N}$ are given by finite linear combinations of Koopman and shift operators, respectively (i.e., they satisfy assumptions (A4) and (A5)), the projected

operators $R_{z,\ell,Q}^+$ can be approximated by positive-frequency projections of $\hat{R}_{z,\ell,Q,N}$ using proposition 5.7 in conjunction with (50). Specifically, given $L \leq N - 1$ and for each $q \in \{0, \dots, Q\}$, we can compute the $L \times L$ positive-frequency projected shift operator matrix $\mathbf{U}_N^{+,q} = [\hat{U}_{ij}^{+,q}]_{i,j=1}^{L-1}$ with elements $\hat{U}_{ij}^{+,q} = \langle \phi_{i,N}^+, \hat{U}_N^q \phi_{j,N}^+ \rangle_N$ (cf. (38)), i.e.,

$$\hat{U}_{ij}^{+,q} = \frac{1}{N} \sum_{n=0}^{N-1-q} \phi_{n,i,N}^+ \phi_{n+q,j,N}^+ + \frac{1}{N} \sum_{n=N-q}^{N-1} \phi_{n,i,N}^+ \phi_{n-N-q,j,N}^+,$$

and the matrix

$$\mathbf{R}_{z,N}^+ = \sum_{q=0}^Q w_q e^{-zq \Delta t} \mathbf{U}_N^{+,q}. \quad (52)$$

The matrix $\mathbf{R}_{z,N}^+$ represents the projected operator

$$\hat{R}_{z,\ell,Q,L,N}^+ = \Pi_{L,N} \hat{R}_{z,\ell,Q,N}^+ \Pi_{L,N}, \quad \hat{R}_{z,\ell,Q,N}^+ = \hat{\Pi}_{+,N} \hat{R}_{z,\ell,Q,N} \hat{\Pi}_{+,N},$$

in the $\{\phi_{j,N}\}$ basis of $\hat{H}_{L,N}$. Its computation completes step 3 of algorithm 1. By proposition 5.7 and (50), $\mathbf{R}_{z,N}^+$ converges to the $L \times L$ matrix representation $\mathbf{R}_z^+ = [R_{ij}^+]_{i,j=1}^L$ of $\tilde{R}_{z,L}^+ = \Pi_L R_z^+(V) \Pi_L$, with $R_{ij}^+ = \langle \phi_i^+, R_z(V) \phi_j^+ \rangle$ in the iterated limit $\lim_{\ell \rightarrow \infty} \lim_{Q \rightarrow \infty} \lim_{m \rightarrow \infty} \lim_{n \rightarrow \infty} \lim_{K \rightarrow \infty} \lim_{N \rightarrow \infty}$. (Recall that we have suppressed the dependence of the approximate positive-frequency projection $\hat{\Pi}_{+,N}$ on the parameters m , n , and K appearing in the iterated limit.)

In the ensuing subsections, we will use the abbreviated notation $R_{z,L,N}^+ \equiv \hat{R}_{z,L,\ell,Q,N}^+$ and interpret convergence of $R_{z,L,N}^+$ to $R_{z,L}^+$, as well as convergence of related data-driven operator approximations, in that limit. We also note that a variant of (52) is

$$\tilde{\mathbf{R}}_{z,N}^+ = \sum_{q=0}^Q w_q e^{-zq \Delta t} (\mathbf{U}_N^+)^q, \quad \mathbf{U}_N^+ \equiv \mathbf{U}_N^{+,1}, \quad (53)$$

which applies iteratively the 1-step shift matrix \mathbf{U}_N^+ rather than using the multi-step matrices $\mathbf{U}_N^{+,q}$. This approximation also consistently recovers \mathbf{R}_z^+ and has the computational benefit of having to form (and store) only a single shift operator matrix (as opposed to Q such matrices used in (52)). For this reason, in the experiments of section 6 we implement algorithm 1 using $\tilde{\mathbf{R}}_z^+$. We alert the reader to the fact that the numerical stability of (53) depends on the fact that \hat{U}_N is a unitary operator. In numerical implementations using on non-circular shift operators (e.g., \hat{U}'_N from (39)), we found that thresholding the singular values of the operator matrix to 1 is important to ensure stable behavior of the iterative approximation (53) as Q increases.

5.6. Compactification

Having computed the matrix representation $\mathbf{R}_{z,N}^+ \in \mathbb{C}^{L \times L}$, steps 4–6 of algorithm 1 approximate the compact operator $S_{z,\tau}^+$ and its negative-frequency counterpart, $S_{z,\tau}^-$.

Leveraging the results of sections 4 and 5.3, we build these approximation using data-driven approximations of the finite-rank operators $S_{z,\tau,L}^+$ and $S_{z,\tau,L}^-$, respectively, defined in (28). As one can verify using lemma 3.2 in conjunction with the fact that the basis functions ϕ_j are real, the matrix elements of $S_{z,\tau,L}^+$ and $S_{z,\tau,L}^-$ are complex conjugates of one another, i.e., $\langle \phi_i, S_{z,\tau,L}^- \phi_j \rangle = \langle \phi_i, S_{z,\tau,L}^+ \phi_j \rangle^*$. In light of that, it suffices to consider approximations of $S_{z,\tau,L}^+$ and obtain from them approximations of $S_{z,\tau,L}^-$ by complex conjugation.

First, we approximate $\tilde{S}_{z,L}^+ = |R_{z,L}^+|$ from (28) by $\tilde{S}_{z,L,N}^+ := |R_{z,L,N}^+|$. The latter operator is represented in the $\{\phi_{j,N}\}$ basis of $\hat{H}_{L,N}$ by the $L \times L$ matrix $\mathbf{S}_{z,N}^+ = |R_{z,N}^+|$, which we compute by a polar decomposition of $\mathbf{R}_{z,N}^+$; that is, $\mathbf{R}_{z,N}^+ = \mathbf{W}_{z,N} |\mathbf{R}_{z,N}^+|$ where $\mathbf{W}_{z,N}$ is a unitary matrix. We then approximate $\sqrt{\tilde{S}_{z,L}^+}$ by $\sqrt{\tilde{S}_{z,L,N}^+}$ which is represented by the matrix square root $\sqrt{\mathbf{S}_{z,N}^+}$. Since the modulus and square root functions are continuous on \mathbb{C} and $[0, \infty)$, respectively, it follows from the convergence of $R_{z,N}^+$ to R_z^+ (see lemma 5.5) that $\sqrt{\mathbf{S}_{z,N}^+}$ converges to the matrix representation $\sqrt{\mathbf{S}_z^+} = [\langle \phi_i, \sqrt{S_z^+} \phi_j \rangle]_{i,j=1}^L$ of $\sqrt{\tilde{S}_{z,L}^+}$.

The pre/post multiplication of $\sqrt{\tilde{S}_{z,L}^+}$ by G_τ to effect compactification (see (15)) is approximated by pre/post multiplication of $\sqrt{\tilde{S}_{z,L,N}^+}$ by $G_{\tau,N}$, giving

$$S_{z,\tau,L,N}^+ := \sqrt{\tilde{S}_{z,L,N}^+} G_{\tau,N} \sqrt{\tilde{S}_{z,L,N}^+}$$

as an operator on $\hat{H}_{L,N}$. The $L \times L$ matrix representation of this operator in the $\{\phi_{j,N}\}$ basis of $\hat{H}_{L,N}$ is given by

$$\mathbf{S}_{z,\tau,N}^+ = \sqrt{\mathbf{S}_{z,N}^+} \mathbf{\Lambda}_{\tau,N} \sqrt{\mathbf{S}_{z,N}^+},$$

where $\mathbf{\Lambda}_{\tau,N} := \text{diag}(\lambda_{1,N}^\tau, \dots, \lambda_{L,N}^\tau)$ and $\lambda_{j,N}^\tau$ are eigenvalues of $G_{\tau,N}$ (see Appendix A.3). By lemma 5.2 and the convergence of $\sqrt{\mathbf{S}_{z,N}^+}$ to $\sqrt{\mathbf{S}_z^+}$, it follows that $\mathbf{S}_{z,\tau,N}^+$ converges to the matrix representation $\mathbf{S}_{z,\tau}^+ = [\langle \phi_i, S_{z,\tau}^+ \phi_j \rangle]_{i,j=1}^L$ of $S_{z,\tau,L}^+$.

Defining $\mathbf{S}_{z,\tau,N}^- = \overline{\mathbf{S}_{z,\tau,N}^+}$, where $\overline{(\cdot)}$ denotes elementwise complex conjugation, we have that $\mathbf{S}_{z,\tau,N}^-$ is the matrix representation of $S_{z,\tau,L,N}^- := \sqrt{\tilde{S}_{z,L,N}^-} G_{\tau,N} \sqrt{\tilde{S}_{z,L,N}^-}$, where $\tilde{S}_{z,L,N}^- := |R_{z,L,N}^-|$. The matrices $\mathbf{S}_{z,\tau,N}^-$ converge to the matrix representation $\mathbf{S}_{z,\tau}^- = [\langle \phi_i, S_{z,\tau}^- \phi_j \rangle]_{i,j=1}^L$ of $S_{z,\tau,L}^-$.

5.7. Eigendecomposition

The rest of algorithm 1 (steps 7–11) involves (i) approximating the reduced-rank operators $S_{z,\tau,L}^{+,(M)}$ and $S_{z,\tau,L}^{-,(M)}$ from the eigendecompositions of $S_{z,\tau,L,N}^+$ and $S_{z,\tau,L,N}^-$, respectively; (ii) forming the corresponding approximation of $S_{z,\tau,L}^{(M)}$ in (30); and (iii) computing another eigendecomposition for that operator to yield our approximations of the resolvent $R_{z,\tau,L}^{(M)}$, the finite-rank generator $V_{z,\tau,L}^{(M)}$, and their associated eigenfrequencies and eigenfunctions.

We begin by computing an eigendecomposition of $\mathbf{S}_{z,\tau,N}^+$,

$$\mathbf{S}_{z,\tau,N}^+ \mathbf{c}_{l,\tau,N} = e_{l,\tau,L,N} \mathbf{c}_{l,\tau,N},$$

where the eigenvalues $e_{l,\tau,L,N}$ are ordered in decreasing order, $z^{-1} > e_{1,\tau,L,N} \geq e_{2,\tau,L,N} \geq \dots \geq e_{L,\tau,L,N} \geq 0$, and the corresponding eigenvectors $\mathbf{c}_{l,\tau,N} \in \mathbb{C}^L$ are chosen to be orthonormal with respect to the standard Euclidean inner product, $\mathbf{c}_{k,\tau,N} \cdot \mathbf{c}_{l,\tau,N} = \delta_{kl}$. The eigenvectors $\mathbf{c}_{l,\tau,N} = (c_{1l}, \dots, c_{Ll})^\top$ give the expansion coefficients of eigenfunctions $\xi_{l,\tau,L,N}$ of $S_{z,\tau,L,N}^+$ in the $\{\phi_{j,N}\}$ basis of $\hat{H}_{L,N}$; that is,

$$S_{z,\tau,L,N}^+ \xi_{l,\tau,L,N} = e_{l,\tau,L,N} \xi_{l,\tau,L,N},$$

where $\xi_{l,\tau,L,N} = \sum_{j=1}^L c_{jl} \phi_{j,N}$ and $\langle \xi_{k,\tau,L,N}, \xi_{l,\tau,L,N} \rangle_N = \delta_{kl}$. By convergence of $\mathbf{S}_{z,\tau,N}^+$ to $\mathbf{S}_{z,\tau}^+$, the eigenvalues $e_{l,\tau,L,N}$ of $S_{z,\tau,L,N}^+$ converge to the eigenvalues $e_{l,\tau,L}$ of $S_{z,\tau,L}^+$ in the sense of theorem 4.1(i), and for every eigenfunction $\xi_{l,\tau,L} \in H_L$ of $S_{z,\tau,L}^+$ there exists a sequence of eigenfunctions $\xi_{l,\tau,L,N} \in \hat{H}_{L,N}$ converging to it in the sense of uniform convergence of their corresponding representatives in $C(M)$.

Next, let $\mathbf{C}_{\tau,N}^{(M)} = (\mathbf{c}_{1,\tau,N}, \dots, \mathbf{c}_{L,\tau,N})$ be the $L \times M$ matrix whose columns are the leading M eigenvectors $\mathbf{c}_{l,\tau,N}$, and $\mathbf{E}_{\tau,N}^{(M)} = \text{diag}(e_{1,\tau,L,N}, \dots, e_{M,\tau,L,N})$ the diagonal matrix whose diagonal entries are the corresponding eigenvalues. Note that $\mathbf{\Xi}_{\tau,N}^{(M)} = \mathbf{C}_{\tau,N}^{(M)} \mathbf{C}_{\tau,N}^{(M)*}$ is the matrix representation of the orthogonal projection $\Xi_{\tau,L,N}^{(M)} : \hat{H}_{L,N} \rightarrow \hat{H}_{L,N}$ onto the M -dimensional subspace of $\hat{H}_{L,N}$ spanned by $\xi_{1,\tau,L,N}, \dots, \xi_{M,\tau,L,N}$. Define the matrix $\mathbf{S}_{z,\tau,N}^{+, (M)} = \mathbf{C}_{\tau,L,N}^{(M)} \mathbf{E}_{\tau,N}^{(M)} \mathbf{C}_{\tau,N}^{(M)*}$ that represents the reduced-rank operator $S_{z,\tau,L,N}^{+, (M)} := \Xi_{\tau,L,N}^{(M)} S_{z,\tau,L,N}^+ \Xi_{\tau,L,N}^{(M)}$. The elementwise complex conjugate $\overline{\mathbf{S}_{z,\tau,N}^{+, (M)}} =: \mathbf{S}_{z,\tau,N}^{-, (M)}$ is the matrix representation of the negative-frequency reduced-rank operator $S_{z,\tau,L,N}^{-, (M)} := \bar{\Xi}_{\tau,L,N}^{(M)} S_{z,\tau,L,N}^- \bar{\Xi}_{\tau,L,N}^{(M)}$. Correspondingly, $\mathbf{S}_{z,\tau,N}^{(M)} = \mathbf{S}_{z,\tau,N}^{+, (M)} - \mathbf{S}_{z,\tau,N}^{-, (M)}$ represents the operator $S_{z,\tau,L,N}^{(M)} = S_{z,\tau,L,N}^{+, (M)} - S_{z,\tau,L,N}^{-, (M)}$.

By the previous results, the matrices $\mathbf{S}_{z,\tau,N}^{+, (M)}$, $\mathbf{S}_{z,\tau,N}^{-, (M)}$, and $\mathbf{S}_{z,\tau,N}^{(M)}$ converge to the matrix representations of the operators $S_{z,\tau,L}^{+, (M)}$, $S_{z,\tau,L}^{-, (M)}$, and $S_{z,\tau,L}^{(M)}$, respectively, from (29) and (30). The operator $S_{z,\tau,L}^{(M)}$ has rank at most $2M$. By the convergence of its matrix representation to that of $S_{z,\tau,L}^{(M)}$ and proposition 4.3, for sufficiently large N and L , $\text{rank } S_{z,\tau,L,N}^{(M)}$ will be equal to $2M$, and $\sigma(S_{z,\tau,L,N}^{(M)})$ will lie in a (closed) proper subinterval of $[-z^{-1}, z^{-1}]$. Henceforth, we will assume that this is the case.

We now compute an eigendecomposition of $\mathbf{S}_{z,\tau,N}^{(M)}$,

$$\mathbf{S}_{z,\tau,N}^{(M)} \mathbf{q}_{j,\tau,N}^{(M)} = e_{j,\tau,L,N}^{(M)} \mathbf{q}_{j,\tau,N}^{(M)},$$

indexing, as in section 4.2, the nonzero eigenvalues by $j \in \{-M, \dots, -1, 1, \dots, M\}$ and ordering them as

$$e_{-M,\tau,L,N}^{(M)} \leq \dots \leq e_{-1,\tau,L,N}^{(M)} < 0 < e_{1,\tau,L,N}^{(M)} \leq \dots \leq e_{M,\tau,L,N}^{(M)}.$$

We choose the corresponding eigenvectors $\mathbf{q}_{j,\tau,N}^{(M)} = (q_{1j}, \dots, q_{Lj})^\top$ to be orthonormal on \mathbb{C}^L , $\mathbf{q}_{j,\tau,N}^{(M)} \cdot \mathbf{q}_{k,\tau,N}^{(M)} = \delta_{jk}$, and define associated eigenfunctions $\psi_{j,L,N}^{(M)}$ as

$$\psi_{j,L,N}^{(M)} = \sum_{i=1}^L q_{ij} \phi_{i,N}. \quad (54)$$

We also let $\mathbf{Q}_{\tau,N}^{(M)} = (\mathbf{q}_{-M,\tau,N}^{(M)}, \dots, \mathbf{q}_{-1,\tau,N}^{(M)}, \mathbf{q}_{1,\tau,N}^{(M)}, \dots, \mathbf{q}_{M,\tau,N}^{(M)})$ be the $L \times (2M)$ matrix containing the eigenvectors $\mathbf{q}_{j,\tau,N}^{(M)}$ in its columns. The matrix $\Psi_{\tau,N}^{(M)} = \mathbf{Q}_{\tau,N}^{(M)} \mathbf{Q}_{\tau,N}^{(M)*}$ is then a projection matrix that represents the orthogonal projection $\Psi_{L,N}^{(M)} : \hat{H}_{L,N} \rightarrow \hat{H}_{L,N}$ onto $\text{span}\{\psi_{j,L,N}^{(M)}\}_{j \in \{-M, \dots, -1, 1, \dots, M\}}$ with respect to the $\{\phi_{j,N}\}$ basis of $\hat{H}_{L,N}$. We denote the complementary projection operator to $\Psi_{L,N}^{(M)}$ as $\Psi_{L,N}^{(M),\perp} \equiv I - \Psi_{L,N}^{(M)}$. This operator is represented by the projection matrix $\Psi_{\tau,N}^{(M),\perp} := \mathbf{I} - \Psi_{\tau,N}^{(M)}$ where \mathbf{I} is the $L \times L$ identity matrix. By the convergence of the matrix representation of $S_{z,\tau,L,N}^{(M)}$ to the matrix representation of $S_{z,\tau,L}^{(M)}$, the eigenvalues $e_{j,\tau,L,N}^{(M)}$ of $S_{z,\tau,L,N}^{(M)}$ converge to the eigenvalues $e_{j,\tau,L}^{(M)}$ of $S_{z,\tau,L}^{(M)}$ in the sense of theorem 4.1(i). Moreover, by lemma 5.2, for every corresponding eigenfunctions $\psi_{j,\tau,L}^{(M)}$ of $S_{j,\tau,L}^{(M)}$, there is a family of eigenfunctions $\psi_{j,\tau,L,N}^{(M)}$ that converges to it in the sense of uniform convergence in $C(M)$ of their continuous representatives.

Next, similarly to (31) and (32), respectively, we define resolvent eigenvalues $\vartheta_{j,\tau,L,N}^{(M)} \in C_z$ and eigenfrequencies $\omega_{j,\tau,L,N}^{(M)} \in i\mathbb{R}$ as

$$\vartheta_{j,\tau,L,N}^{(M)} = \gamma_z^{-1}(e_{j,\tau,L,N}^{(M)}), \quad \omega_{j,\tau,L,N}^{(M)} = \frac{1}{i} \beta_z(\vartheta_{j,\tau,L,N}^{(M)}). \quad (55)$$

We assemble these eigenvalues and eigenfrequencies into $(2M) \times (2M)$ diagonal matrices

$$\begin{aligned} \Theta_{\tau,N}^{(M)} &= \text{diag}(\vartheta_{-M,\tau,L,N}^{(M)}, \dots, \vartheta_{-1,\tau,L,N}^{(M)}, \vartheta_{1,\tau,L,N}^{(M)}, \dots, \vartheta_{M,\tau,L,N}^{(M)}), \\ \Omega_{\tau,N}^{(M)} &= \text{diag}(\omega_{-M,\tau,L,N}^{(M)}, \dots, \omega_{-1,\tau,L,N}^{(M)}, \omega_{1,\tau,L,N}^{(M)}, \dots, \omega_{M,\tau,L,N}^{(M)}), \end{aligned}$$

and define

$$\mathbf{R}_{z,\tau,N}^{(M)} = \mathbf{Q}_{\tau,N}^{(M)} \Theta_{\tau,N}^{(M)} \mathbf{Q}_{\tau,N}^{(M)*} + z^{-1} \Psi_{\tau,N}^{(M),\perp}, \quad \mathbf{V}_{z,\tau,N}^{(M)} = i \mathbf{Q}_{\tau,N}^{(M)} \Omega_{\tau,N}^{(M)} \mathbf{Q}_{\tau,N}^{(M)*}. \quad (56)$$

The matrix $\mathbf{R}_{z,\tau,N}^{(M)}$ represents (with respect to the $\{\psi_{j,N}\}$ basis of $\hat{H}_{L,N}$) the resolvent $R_{z,\tau,L,N}^{(M)} : \hat{H}_{L,N} \rightarrow \hat{H}_{L,N}$ of a skew-adjoint operator $V_{z,\tau,L,N}^{(M)}$ on $\hat{H}_{L,N}$ of rank $2M$ that is represented by the (skew-adjoint) matrix $\mathbf{V}_{z,\tau,N}^{(M)}$.

By construction, the operators $R_{z,\tau,L,N}^{(M)}$ and $V_{z,\tau,L,N}^{(M)}$ have the eigendecompositions

$$R_{z,\tau,L,N}^{(M)} \psi_{j,\tau,L,N}^{(M)} = \vartheta_{j,\tau,L,N}^{(M)} \psi_{j,\tau,L,N}^{(M)}, \quad V_{z,\tau,L,N}^{(M)} \psi_{j,\tau,L,N}^{(M)} = i \omega_{j,\tau,L,N}^{(M)} \psi_{j,\tau,L,N}^{(M)},$$

respectively. Moreover, by continuity of the functions γ_z^{-1} and β_z , the eigenvalues $\vartheta_{j,\tau,L,N}^{(M)}$ and eigenfrequencies $\omega_{j,\tau,L,N}^{(M)}$ from (55) converge to $\vartheta_{j,\tau,L}^{(M)}$ and $\omega_{j,\tau,L}^{(M)}$ from (31) and (32), respectively.

To summarize, the asymptotic convergence of our scheme is as follows:

- (i) At fixed regularization parameter τ , rank parameter M , and approximation space dimension parameter L , the $L \times L$ matrix representations of $R_{z,\tau,L,N}^{(M)}$ and $V_{z,\tau,L,N}^{(M)}$ on $\tilde{H}_{L,N}$ converge to the $L \times L$ matrix representations of $R_{z,\tau,L}^{(M)} = \tilde{\Pi}_L R_{z,\tau}^{(M)} \tilde{\Pi}_L$ and $V_{z,\tau,L}^{(M)} = \tilde{\Pi}_L V_{z,\tau}^{(M)} \tilde{\Pi}_L$ on \tilde{H}_L , respectively, in the sense of proposition 5.7 and (50) (i.e., in the iterated limit $\lim_{m \rightarrow \infty} \lim_{n \rightarrow \infty} \lim_{K \rightarrow \infty} \lim_{\ell \rightarrow \infty} \lim_{Q \rightarrow \infty} \lim_{N \rightarrow \infty}$). As a result, the eigenvalues $\gamma_{l,\tau,L,N}^{(M)}$ and $\omega_{l,\tau,L,N}^{(M)}$ of $R_{z,\tau,L,N}^{(M)}$ and $V_{z,\tau,L,N}^{(M)}$ converge to eigenvalues $\gamma_{l,\tau,L}^{(M)}$ and $\omega_{l,\tau,L}^{(M)}$ of $R_{z,\tau,L}^{(M)}$ and $V_{z,\tau,L}^{(M)}$, respectively. The corresponding eigenfunctions $\psi_{l,\tau,L,N}^{(M)}$ converge to eigenfunctions $\psi_{l,\tau,L}^{(M)}$ of $R_{z,\tau,L}^{(M)}$ and $V_{z,\tau,L}^{(M)}$ in the sense of convergence of the corresponding continuous representatives in $C(M)$ (cf. lemma 5.2).
- (ii) At fixed regularization parameter τ and rank parameter M , $R_{z,\tau,L}^{(M)}$ converges as $L \rightarrow \infty$ strongly to the projected resolvent $R_{z,\tau}^{(M)}$. As a result, the corresponding skew-adjoint operators $V_{z,\tau,L}^{(M)}$ converge in strong resolvent sense, and thus spectrally in the sense of theorem 2.2, to $V_{z,\tau}^{(M)}$.
- (iii) At fixed regularization parameter τ , $R_{z,\tau}^{(M)}$ converges as $M \rightarrow \infty$ strongly to the compactified resolvent $R_{z,\tau}$. As a result, $V_{z,\tau}^{(M)}$ converges in strong resolvent sense, and thus spectrally in the sense of theorem 2.2, to $V_{z,\tau}$.
- (iv) As $\tau \rightarrow 0^+$ the compactified resolvents $R_{z,\tau}$ converge to $R_z(V)$ strongly. As a result, $V_{z,\tau}$ converges to the Koopman generator V in strong resolvent sense, and thus spectrally in the sense of theorem 2.2.

5.8. Practical computing considerations

There are several computational choices one makes when implementing algorithm 1, namely the choice of: basis functions $\phi_{j,N}$, the number L of such functions used, the rank parameter M , the choice of resolvent parameter z , the choice of regularization parameter τ , and the numerical integration time $T_\ell = Q \Delta t$ used for resolvent computation.

Choice of basis functions. The asymptotic convergence of algorithm 1 requires fairly mild assumptions on the kernel k (i.e., continuity, Markov normalizability, and strict positivity of the associated integral operator), which can be met using many of the popular classes of kernels in the literature [34]. In particular, our approach of using orthonormal basis functions derived by eigendecomposition of integral operators addresses an important problem in data-driven Koopman and transfer operator techniques, namely the choice of a well-conditioned dictionary adapted to the function space on which the Koopman/transfer operator acts [81, 47].

That being said, at any given L, M and number of samples N , the performance of algorithm 1 invariably depends on the choice of k . In broad terms, our approach is subject to usual bias–variance tradeoffs encountered in data-driven techniques—increasing L and/or M reduces the bias associated with the approximation of $R_{z,\tau}$ by the finite-rank operator $R_{z,\tau,L}^{(M)}$, but at the same time, increasing L and/or M at fixed

N increases the risk of sampling errors (“variance”) in the approximation of the matrix representation of $R_{z,\tau,L}^{(M)}$ by the matrix representation of $R_{z,\tau,L,N}^{(M)}$. Thus, for efficient and statistically robust spectral computations, it is advantageous that the leading basis vectors ϕ_j span subspaces of H which are approximately invariant under the action of the Koopman operator.

In specific cases, the kernel k can be explicitly chosen such that the ϕ_j span unions of Koopman eigenspaces (e.g., a translation-invariant kernel for systems on tori with pure point spectra; see section 6.1 and Appendix A.3). In such cases, accurate approximations of Koopman eigenfunctions can be obtained with small numbers of basis functions. In general, however, the more complex are the dynamics and/or observation modality F , the more basis functions are required. A possible empirical approach for increasing the efficiency of the basis functions in representing approximately Koopman-invariant subspaces is to lift the observation map to take values in a higher-dimensional space using delay embeddings. It can be shown that this approach leads to kernel integral operators G_τ that asymptotically commute with the Koopman operator, and as a result the eigenspaces of G_τ with sufficiently isolated corresponding eigenvalues become approximately Koopman-invariant [23, 36]. This approach may be particularly useful in high-dimensional applications (e.g., climate dynamics [33]).

Balance between resolvent parameter z and total integration time T_ℓ . The choice of z and T_ℓ will affect the accuracy of the numerical quadrature (51). As z increases, the rapidly decreasing term e^{-zt} will require finely spaced quadrature nodes for accuracy. Eventually, for t greater than a z -dependent value t_ϵ , e^{-zt} will decay to zero to machine precision; increasing T_ℓ beyond t_ϵ will not improve convergence of the numerical quadrature, and may in fact be detrimental due to injection of numerical noise to small matrix elements of $R_{z,\ell,Q,N}$ from (51). At the same time, for a given z , T_ℓ must be sufficiently large so that the truncated resolvent $R_{z,\ell}$ from (48) is a good approximation to $R_z(V)$ when projected onto the finite-dimensional approximation space H_L . We recommend that z is chosen so that z^{-1} is on the order of expected frequencies of the system.

Choice of regularization parameter τ . Choosing τ involves a similar tradeoff to the choice of number of basis functions L . That is, the smaller τ is the closer is the approximate generator $V_{z,\tau}$ to the true generator V is in a spectral sense, but, in general, the smaller τ is accurate approximation of $V_{z,\tau}$ requires larger numbers of basis functions and/or training samples. As one might expect, the sensitivity of the eigenvalues and eigenfunctions of $V_{z,\tau}$ on τ is higher in systems with non-diagonalizable Koopman operators (e.g., the L63 system studied in section 6.3), where the eigenspaces of $V_{z,\tau}$ along convergent sequences of eigenvalues may not have well-defined limits as τ decreases to 0. On the other hand, in systems with non-trivial Koopman eigenfunctions, like the torus rotation described in section 6.1, the results of spectral calculations appear to be more insensitive to the choice of τ .

As a practical guideline, τ can be tuned by minimization of the pseudospectral bound ε_{T_c} from eq. (24) for the leading eigenfunctions of $V_{z,\tau}$ over candidate τ values. Fortunately, varying τ takes relatively few computation resources as the use of $G_{\tau/2,N}$ (algorithm 1, step 5) happens after the expensive basis function computation (the first step of algorithm 1).

Choice of rank parameter M . In the numerical experiments detailed in section 6, we found that we could obtain sufficient results when the rank parameter M was chosen to be no larger than $L/3$, however smaller values of M can improve results, particularly when L is large. For the second example (skew-product flow on the torus; section 6.2), we found that $M = 266 \approx L/3$ yields less than optimal results, and instead use $M \approx L/20$. (Using values of $M = L/6$ and $M = L/10$ gave very similar results in the sense of eigenfrequency accuracy and the magnitude ε_{T_c} .) Ultimately, we recommend making an initial choice of $M = L/6$, with the possibility of tuning this parameter through minimizing ε_{T_c} and maintaining M large enough such that the eigendecomposition can capture relevant dynamics of the system.

6. Examples

In this section, we apply the technique described in section 5 to three ergodic systems of increasing complexity: a linear rotation on the torus, a skew rotation on the torus, and the Lorenz 63 (L63) system [57] on \mathbb{R}^3 . The linear and skew torus rotations have pure point spectra which we can compute analytically. The L63 system is mixing with an associated continuous spectrum of the Koopman operator.

In each example, we numerically generate state space trajectory data $x_0, \dots, x_{N-1} \in X$ at a fixed interval Δt . We embed the state space trajectory in data space $Y = \mathbb{R}^d$ via an embedding $F : X \rightarrow Y$ to produce time-ordered samples y_0, \dots, y_{N-1} with $y_n = F(x_n)$. Using the samples y_n , we compute kernel eigenvectors $\phi_{j,N}$ and associated eigenvalues via the approach described in section 5.2 and Appendix A. We then execute algorithm 1 to compute eigenfunctions $\psi_{j,\tau,L,N}^{(M)}$ of the approximate generator $V_{z,\tau,L,N}^{(M)}$ and their corresponding eigenfrequencies $\omega_{j,\tau,L,N}^{(M)}$. For the remainder of this section, if there is no risk of confusion we suppress τ , L , M , and N subscripts/superscripts from our notation for eigenfunctions and eigenfrequencies, i.e., $\phi_{j,N} \equiv \phi_j$, $\psi_{j,\tau,L,N}^{(M)} \equiv \psi_j$, and $\omega_{j,\tau,L,N}^{(M)} \equiv \omega_j$.

Our main experimental objectives are to verify that our approach (i) yields consistent results with analytical solutions for systems with known spectra (linear and skew torus rotations); and (ii) identifies observables that behave as approximate Koopman eigenfunctions, i.e., have strong cyclicity and slow correlation decay, under mixing dynamics. Given these objectives, we order our computed eigenpairs $(\omega_1, \psi_1), (\omega_2, \psi_2), \dots$ using the pseudospectral criteria described in section 3.5; that is, ψ_1 is the non-constant eigenfunction with the smallest pseudospectral bound $\varepsilon_{T_c}(\omega_j, \psi_j)$ from (24), ψ_2 has the second-smallest $\varepsilon_{T_c}(\omega_j, \psi_j)$ value, and so on.

System	Observation Map	N	T_c	Computed ω_j	Known ω_j	Relative Error	$\varepsilon_{T_c}(\omega_j, \psi_j)$
Linear rotation	\mathbb{R}^4	40962	49.10	1.0001	1.0000	0.01%	0.01175
				5.4784	5.4772	0.02%	0.01176
				6.4787	6.4772	0.02%	0.01133
		4098	49.10	1.0001	1.0000	0.01%	0.12167
				5.478	5.4772	0.01%	0.12179
				6.4774	6.4772	0.00%	0.12160
	\mathbb{R}^3	40962	49.10	1.0002	1.0000	0.02%	0.01203
				5.4811	5.4772	0.07%	0.01176
				6.4819	6.4772	0.07%	0.01163
		4098	49.10	1.0002	1.0000	0.02%	0.12344
				5.4823	5.4772	0.09%	0.16230
				6.481	6.4772	0.06%	0.13050
Skew rotation	\mathbb{R}^4	40962	19.64	1.0001	1.0000	0.01%	0.00974
				5.4882	5.4772	0.20%	0.01244
				6.5149	6.4772	0.58%	0.02215
		4098	19.64	1.0002	1.0000	0.02%	0.98219
				5.4837	5.4772	0.12%	0.10718
				6.5075	6.4772	0.47%	0.11348
	\mathbb{R}^3	40962	19.64	1.0019	1.0000	0.19%	0.00951
				5.4899	5.4772	0.23%	0.10952
				6.6956	6.4772	3.37%	0.30054
		4098	19.64	1.0025	1.0000	0.25%	0.09899
				5.4677	5.4772	0.17%	0.20315
				6.6596	6.4772	2.82%	0.32353
163	Id	64000	2.00	7.4639	NA	NA	0.15949
				14.2152	NA	NA	0.35803
				4.7587	NA	NA	0.78442

Table 1. Representative eigenfrequencies ω_j for the linear rotation, skew rotation, and L63 system. We print numerically computed eigenfrequencies, analytically known eigenfrequencies (for the torus rotation and skew rotation), and the corresponding relative error. The table also shows the value of the pseudospectral bound $\varepsilon_{T_c}(\omega_j, \psi_j)$ from (24) for the corresponding eigenfunctions ψ_j and the time parameter T_c for which $\varepsilon_{T_c}(\psi_j)$ was computed. The quantity N denotes the number of training data points for each experiment.

Representative numerical eigenfrequencies computed for the three systems under study using datasets of different lengths, along with corresponding values of ε_{T_c} and error relative to analytically known eigenfrequencies (when available) are listed in table 1.

6.1. Linear rotation on the torus

A linear rotation on the torus is the simplest system studied and is defined by the flow $\Phi^t : \mathbb{T}^2 \rightarrow \mathbb{T}^2$,

$$\Phi^t(\theta_1, \theta_2) = (\theta_1 + \alpha_1 t, \theta_2 + \alpha_2 t) \pmod{2\pi},$$

where $\alpha_1, \alpha_2 \in \mathbb{R}$ are frequency parameters, and $(\theta_1, \theta_2) \in [0, 2\pi)^2$ are standard angle coordinates. For any $\alpha_1, \alpha_2 \in \mathbb{R}$, the flow Φ^t preserves the normalized Haar measure μ on \mathbb{T}^2 , and when α_1 and α_2 are incommensurate μ is ergodic (in that case, μ is the unique Borel invariant probability measure under Φ^t). The eigenfrequency (ω_j) and

eigenfunction (ψ_j) pairs for the Koopman generator V on $L^2(\mu)$ can be written as

$$\omega_j = \alpha_1 m_j + \alpha_2 n_j, \quad \psi_j(\theta_1, \theta_2) = e^{i(m_j \theta_1 + n_j \theta_2)} \quad (57)$$

for some integers m_j, n_j . Thus, when Φ^t is ergodic, the set of eigenfrequencies has the structure of an additive abelian group generated by α_1 and α_2 , and forms a dense subset of the real line. The eigenfunctions ψ_j have the form of Fourier functions, i.e., they correspond to characters of \mathbb{T}^2 viewed as an abelian group.

In the following experiments, we set $\alpha_1 = 1$ and $\alpha_2 = \sqrt{30}$. We additionally split this case into two experiments: one where the torus \mathbb{T}^2 is embedded into \mathbb{R}^4 and one where the embedding is into \mathbb{R}^3 . The observation map $F_4 : \mathbb{T}^2 \rightarrow \mathbb{R}^4$ is the standard “flat” embedding of the torus,

$$F_4(\theta_1, \theta_2) = (\cos \theta_1, \sin \theta_1, \cos \theta_2, \sin \theta_2). \quad (58)$$

The observation map $F_3 : \mathbb{T}^2 \rightarrow \mathbb{R}^3$ is given by

$$F_3(\theta_1, \theta_2) = ((1 + R \cos \theta_1) \cos \theta_2, (1 + R \cos \theta_1) \sin \theta_2, R \sin \theta_1), \quad (59)$$

where R is a radius parameter set to 0.5. While the Koopman eigenfunctions of the system do not change with the observation map, one could anticipate that computing these from data sampled in \mathbb{R}^4 will be easier since in this case the integral operator G_τ commutes with the Koopman operator U^t (by translation invariance of the kernel; see Appendix A.3), which means that Koopman eigenfunctions can be represented as finite linear combinations of basis functions ϕ_j .

Generated data Data was generated with a time step of $\Delta t = 0.0491 \approx 2\pi/28$ for 2011 time units ($N = 40,962$ samples), and we compute the approximate Koopman eigenfunctions with the following parameters for both observation maps: $z = 1$ (resolvent parameter), $\tau = 10^{-4}$ (regularization parameter), $L = 101$ (number of basis functions ϕ_j), $M = 33$ (rank parameter), and $T_\ell = 50$ (resolvent integration time). We compute the pseudospectral bound $\varepsilon_{T_c}(\omega_j, \psi_j)$ with the time parameter $T_c = 49.1$. To assess the robustness of our results, we also compute eigenfunctions using a time series of $N = 4,098$ samples rather than 40,962.

Numerical results Figures 4 and 5 show representative numerical eigenfunctions ψ_j computed from the dataset with $N = 40,962$ samples using the F_4 and F_3 observation maps, respectively. These eigenfunctions were selected on the basis of their low corresponding $\varepsilon_{T_c}(\omega_j, \psi_j)$ values and the proximity of the corresponding eigenfrequencies ω_j with the theoretical values ω_j from (57) equal to $\alpha_1 = 1$ ($m_j = 1, n_j = 0$), $\alpha_2 = \sqrt{30} \approx 5.48$ ($m_j = 0, n_j = 1$), and $\alpha_1 + \alpha_2 \approx 6.48$ ($m_j = n_j = 1$). In the case of the F_4 experiments, the plotted eigenfunctions are ψ_{56} , ψ_{58} , and ψ_{54} ; in the case of the F_3 experiments, they are ψ_{16} , ψ_8 , and ψ_4 . The numerically computed eigenfrequencies match the true eigenfrequencies between two and five significant digits

(see table 1). Note that, in general, there is no correspondence between our ordering of the eigenfunctions based on $\varepsilon_{T_c}(\psi_j)$ and an ordering based on the corresponding eigenfrequencies. In the case of the F_4 observation map, the ordering places the generating eigenfrequencies near the end of list of eigenfrequencies at the 56th and 58th places of the $2M = 66$ nontrivial eigenfrequencies. In this case, the ε_{T_c} ordering becomes somewhat arbitrary as the eigenfunctions are well resolved, with $0.0082 \leq \varepsilon_{T_c} \leq 0.0118$ for the first 60 eigenfrequencies. Eigenfrequency errors are generally more significant in the F_3 experiments—this is expected from the fact that in this case the embedding yields a manifold with curvature, and the corresponding kernel integral operator G_τ does not commute with the Koopman operator.

The bottom rows of figs. 4 and 5 show scatterplots of the real parts of ψ_j on the sampled states x_n on the torus. These scatterplots have the structure of plane waves and are in good agreement with the theoretical eigenfunctions in (57); see fig. B1(top) for comparison. The middle row shows traceplots of the time series $\psi_j(x_0), \psi_j(x_1), \dots$ in the complex plane. Theoretically, the time series should trace the unit circle in the complex plane. The numerical results in figs. 4 and 5 demonstrate that this is the case to a very good approximation. Some discrepancy from the unit circle is visible in the ψ_{16} results in fig. 5, which is likely due to the fact that the basis functions ϕ_j derived from the F_3 embedding cannot represent general Koopman eigenfunctions through finite basis expansions. The top rows of figs. 4 and 5 show time series of the real parts of $\psi_j(x_n)$. These time series have the structure of sinusoidal waves with frequencies close to the corresponding eigenfrequencies, as expected theoretically.

In separate calculations, we have computed eigenfunctions and eigenfrequencies using the $N = 4098$ -sample datasets (with either F_4 or F_3 embeddings). The reduction of the number of samples was found to impart a modest loss of accuracy compared to the $N = 40,962$ datasets (evidenced by the higher values of ε_{T_c} in table 1), but overall the computed eigenfunctions are in good qualitative agreement with those depicted in figs. 4 and 5.

6.2. Skew rotation on the torus

We consider the skew-product flow $\Phi^t : \mathbb{T}^2 \rightarrow \mathbb{T}^2$ defined by the system of differential equations

$$\frac{d\theta_1}{dt} = \alpha_1, \quad \frac{d\theta_2}{dt} = \alpha_2(1 + \beta \sin \theta_1). \quad (60)$$

As with the linear rotation example in section 6.1, α_1 and α_2 are real frequency parameters, and the system is measure-preserving and ergodic for the Haar probability measure when α_1 and α_2 are incommensurate. The parameter $\beta \in [0, 1)$ controls the strength of the influence of the θ_1 evolution to the θ_2 dynamics.

One can verify by solving (60) that the Koopman generator of this system admits the eigenfrequencies ω_j and corresponding eigenfunctions ψ_j given by

$$\omega_j = \alpha_1 m_j + \alpha_2 n_j, \quad \psi_j(\theta_1, \theta_2) = e^{im_j \theta_1} e^{in_j(\theta_2 + \beta \frac{\alpha_2}{\alpha_1} \cos(\alpha_1 \theta_1))}$$

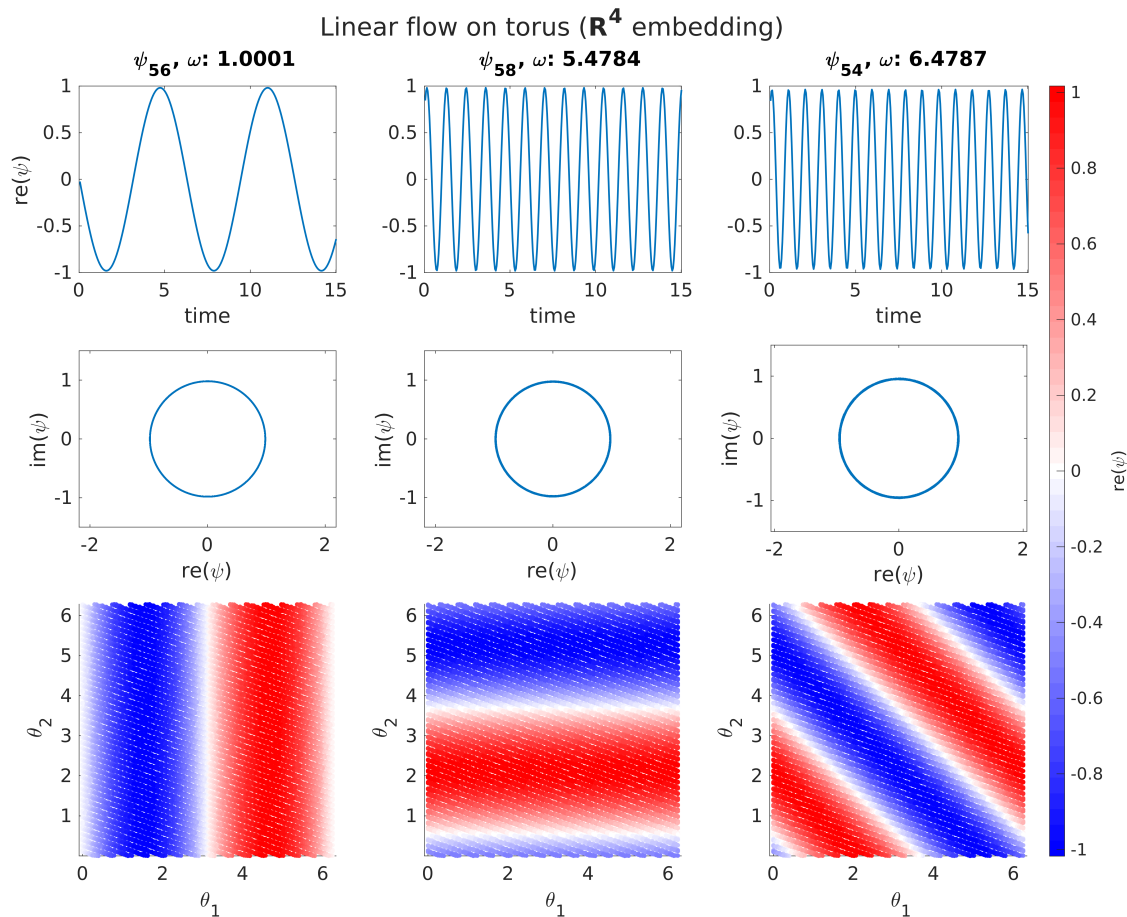


Figure 4. Eigenfunctions of the approximate Koopman generator for the linear torus rotation computed using trajectory data in \mathbb{R}^4 from the embedding F_4 in (58). Each column shows a different eigenfunction ψ_j , with eigenfrequency ω_j given in the title. The index j represents the eigenfunction order which corresponds to a sorting of smallest $\epsilon_{T_c}(\psi_j)$ as computed in (24). Top row: Real part of ψ_j versus time along a portion of the dynamical trajectory. Middle row: Evolution of ψ_j along a portion of the dynamical trajectory plotted in the complex plane. Bottom row: Scatterplot of the real part of ψ_j on the 2-torus parameterized by the angle coordinates $\theta_1, \theta_2 \in [0, 2\pi)$. Notice that eigenfunction ψ_{54} , shown in the right column, has an eigenfrequency that is approximately an integer linear combination of the eigenfrequencies of ψ_{56} and ψ_{58} , shown in the left and middle columns, respectively.

with $m_j, n_j \in \mathbb{Z}$. Thus, the eigenfrequencies of this system are the same as those of the linear rotation in section 6.1, whereas the eigenfunctions have the structure of distorted Fourier functions with the amount of distortion depending on β . See fig. B1 in Appendix B for plots of selected eigenfunctions. One can also verify that $\{\psi_j\}$ forms an orthonormal basis of $L^2(\mu)$.

In fact, the system (60) is topologically conjugate to the linear torus rotation. We can define this conjugacy explicitly by setting z_1 and z_2 to the eigenfunctions ψ_j

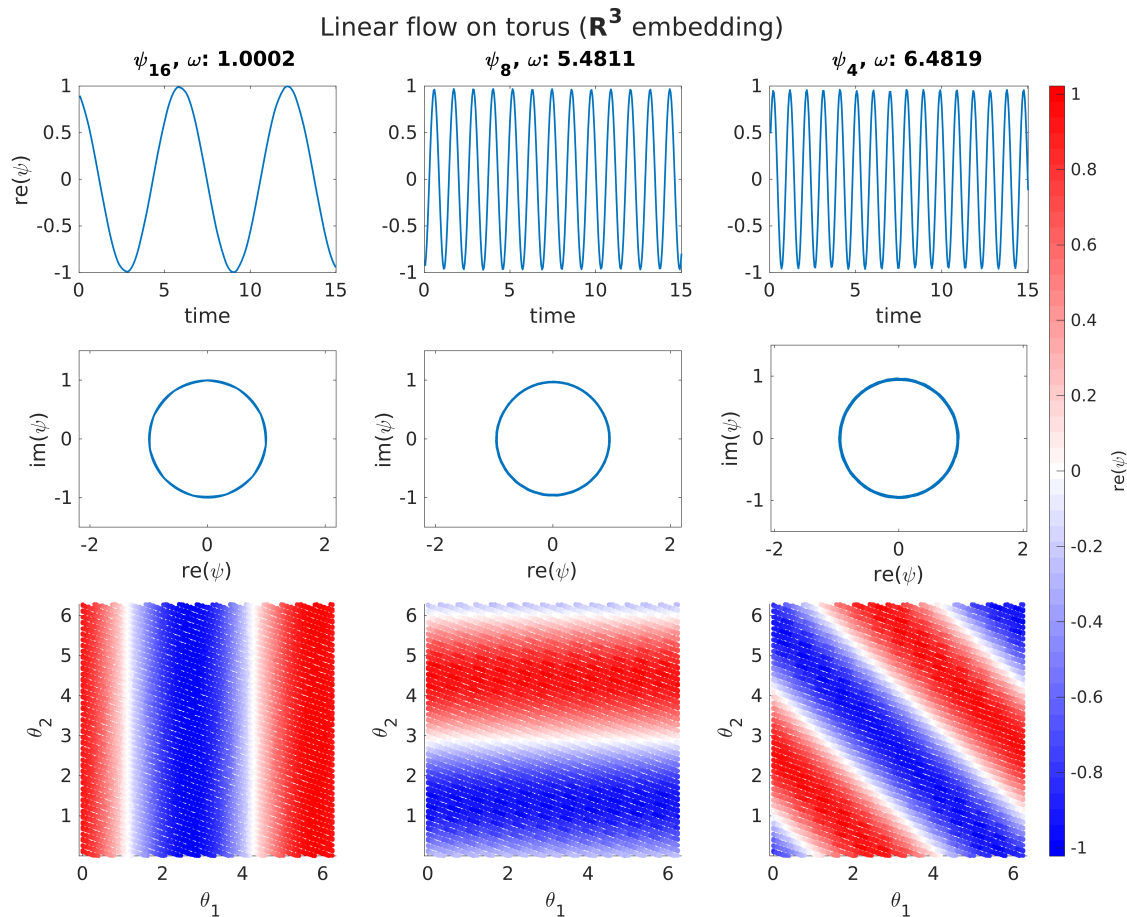


Figure 5. Eigenfunctions of the approximate generator for the linear torus rotation, with trajectory data given in \mathbb{R}^3 . Figure organized as described in fig. 4. As one would expect, the eigenfrequencies and eigenfunctions associated with this system are nearly identical to those found in the \mathbb{R}^4 embedding of the same system.

corresponding to the generating eigenfrequencies α_1 and α_2 , respectively, and defining $h : \mathbb{T}^2 \rightarrow \mathbb{C}^2$ as the map $h(\theta_1, \theta_2) = (z_1(\theta_1), z_2(\theta_2))$. It can then be shown that h is a continuous injective map with image $\mathbb{T}^2 \subset \mathbb{C}^2$ that satisfies the conjugacy relationship $h \circ \Phi^t = \Phi_{\text{rot}}^t \circ h$. Here, Φ_{rot} stands for the linear rotation from section 6.1 with the same generating frequencies as the skew rotation Φ^t generated by (60). More generally, the existence of h follows from the Halmos–von Neumann theorem [41], which states that any two spectrally isomorphic systems with pure point spectra are measure-theoretically isomorphic. In this case, the isomorphism is realized by the continuous function h so it becomes a topological conjugacy.

Generated data We set $\beta = 0.5$ and use the same frequency parameters $\alpha_1 = 1$ and $\alpha_2 = \sqrt{30}$ as in section 6.1. Similarly to section 6.1, the data used was generated with a time step of $\Delta t = 0.0491 \approx 2\pi/28$ for $N = 40,962$ or 4098 samples. The eigenfunctions

of the approximate Koopman generator are computed with parameters $z = 1$, $L = 800$, $\tau = 10^{-4}$, $M = 40$, and $T_\ell = 50$. We order the eigendecomposition using ε_{T_c} as in the previous example, with $T_c = 19.64$.

Numerical results We have computed eigenfunctions from data embedded in either \mathbb{R}^4 or \mathbb{R}^3 using the observation maps F_4 and F_3 from (58) and (59), respectively. The experiments with different numbers of samples and observation maps yielded broadly similar results, so in what follows we focus on results from the F_4 observation map with $N = 40,962$ samples. See table 1 for summary results from all four experiments.

In fig. 6, we plot three representative eigenfunctions ψ_j in a similar manner as the linear rotation eigenfunctions shown in figs. 4 and 5. The three plotted eigenfunctions, ψ_{22} , ψ_2 , and ψ_{16} , have eigenfrequencies approximately equal to α_1 , α_2 , and $\alpha_1 + \alpha_2$, respectively, similarly to figs. 4 and 5. These eigenfunctions match analytical expectations: the computed eigenfunctions plotted on the trajectory of the flow are similar to the true eigenfunctions shown in fig. B1(bottom) and oscillate at approximately the correct frequency.

6.3. Lorenz 63 system

The L63 system is generated by the smooth vector field $\vec{V} : \mathbb{R}^3 \rightarrow \mathbb{R}^3$ defined as

$$\vec{V}(x, y, z) = (-\sigma(y - x), x(\rho - z) - y, xy - \beta z).$$

We use the standard parameter values $\beta = 8/3$, $\rho = 28$, $\sigma = 10$, and the identity for the observation map $F : \mathbb{R}^3 \rightarrow \mathbb{R}^3$. For this choice of parameters, the L63 system is known to have a compact attractor $X \subset \mathbb{R}^3$ with fractal dimension ≈ 2.06 that supports a unique SRB measure μ (which is physical) [76]. The system is also known to be mixing with respect to μ [58], which implies that the associated unitary Koopman group has no nonzero eigenfrequencies. The H_p subspace is then a one-dimensional space of constant functions, while H_c contains all zero-mean functions in $L^2(\mu)$ (i.e., $H_c = \tilde{H}$; see section 2.2). The L63 system with the standard parameter values is dissipative, $\text{div } \vec{V} < 0$, and can be shown to possess compact absorbing balls containing X [55]. Setting the forward invariant set M to such an absorbing ball, all assumptions for data-driven approximation stated in section 5.1 are rigorously satisfied. Yet, unlike the examples in sections 6.1 and 6.2, it is not obvious how the discrete spectra of the approximate Koopman generator $V_{z,\tau,L}^{(M)}$ should behave.

Generated data Data was generated with a time step of $\Delta t = 0.01$ for 4096 time units. We compute eigenfunctions of the approximate Koopman generator using the parameters $z = 1$, $\tau = 2 \times 10^{-6}$, $L = 2000$, $M = 333$, and $T_\ell = 50$. We use the pseudospectral bound $\varepsilon_{T_c}(\omega_k, \psi_j)$ computed with $T_c = 2$ to order the eigenpairs (ω_j, ψ_j) .

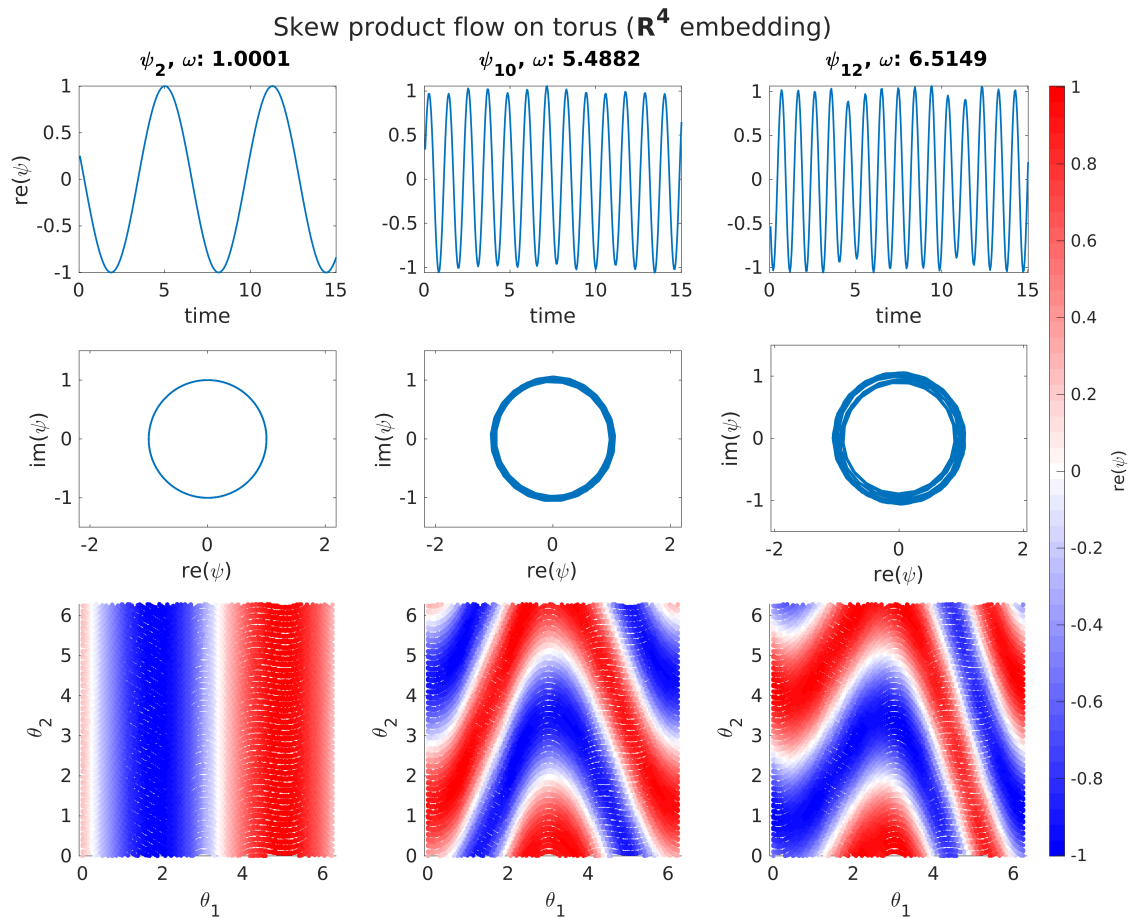


Figure 6. Eigenfunctions of the approximate Koopman generator for the skew torus rotation, with trajectory data given in \mathbf{R}^4 . Organized as in fig. 4.

Numerical results Representative eigenfrequencies ω_j and their corresponding eigenfunctions ψ_j are displayed in table 1 and fig. 7. Despite the mixing nature of the dynamics, the eigenfunctions appear to oscillate regularly and behave as Koopman eigenfunctions for sufficiently short times (see table 1). Additionally, many of the eigenfunctions remain predictable well beyond the Lyapunov time. The positive Lyapunov exponent of the system, approximately 0.90566, corresponds to a Lyapunov time of approximately 1.104 time units [78]. In contrast, many of the computed eigenfunctions remain correlated, thus predictable, for up to 5 time units. Some of these eigenfunctions – namely ψ_2 and ψ_4 plotted in fig. 7 – remain correlated for up to 20 time units. Notable also is that results similar to ψ_2 (where the similarity is most evident in the scatterplot of $\text{Re } \psi_2$ on the attractor) have been found in the L63 system by other methods, including [26, 33, 36, 53]. The period associated with ψ_2 , $2\pi/\omega_1 \approx 0.84$ time units, appears to capture the timescale of approximate periodic orbits around the fixed points centered at the “holes” in the L63 attractor lobes. In contrast, eigenfunction ψ_{30} ,

which is also shown in fig. 7, appears to be of a qualitatively nature and is associated with a longer period of $2\pi/\omega_{30} \approx 1.32$ time units. A possible interpretation of this eigenfunction is that it represents mixing between the two attractor lobes.

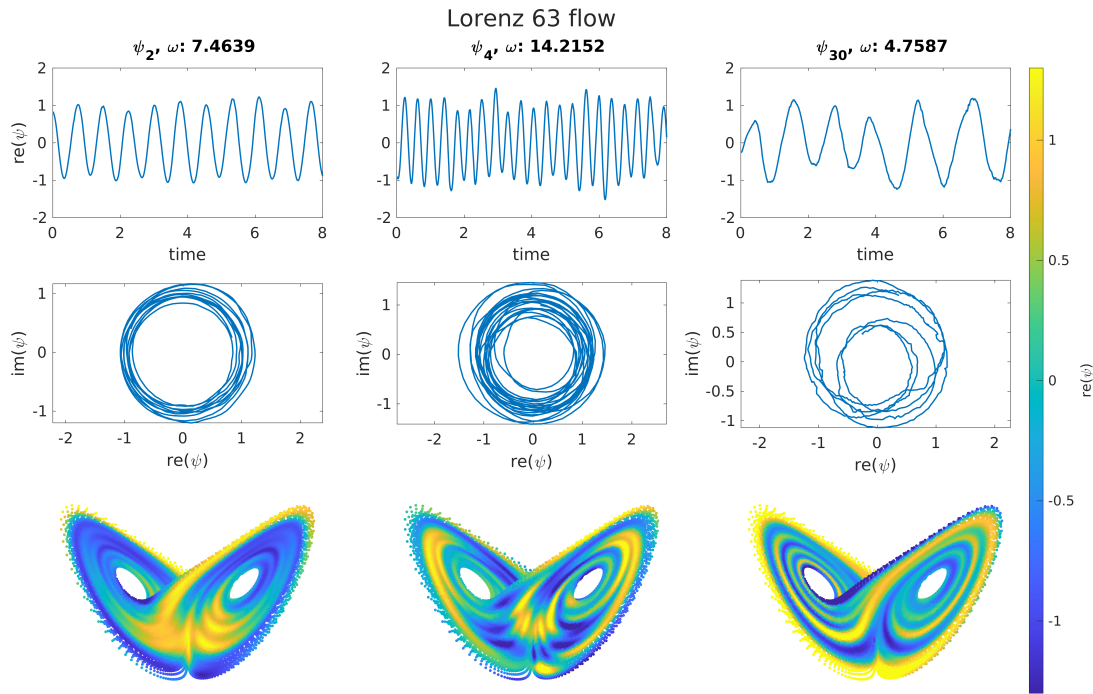


Figure 7. Eigenfunctions of the approximate generator for the Lorenz 63 system, organized as described in fig. 4. Eigenfunction ψ_2 , plotted in the center column, appears to be an approximate harmonic of the eigenfunction in the left column, as $2\omega_2 \approx \omega_4$ and the eigenfunctions behave as such on the attractor. The rightmost eigenfunction, ψ_{30} , appears to be less smooth, but still has qualitatively good behavior (oscillates regularly at about the frequency of ω_{30}).

6.4. Approximation of correlations

To further test the convergence of our approximations, we examine if we can reproduce the time-autocorrelation functions $C_f(t)$ from (22). Defining, for $f \in \tilde{H}$ and for $t \in \mathbb{R}$, the Borel probability measure $\nu_f : \mathcal{B}(i\mathbb{R}) \rightarrow [0, 1]$ and bounded Borel-measurable function $h_t : i\mathbb{R} \rightarrow \mathbb{C}$ as $\nu_f(\Theta) = \langle f, E(\Theta)f \rangle$ and $h_t(i\omega) = e^{i\omega t}$, we have $C_f(t) = \int_{i\mathbb{R}} h_t d\nu_f$ (here, $E : \mathcal{B}(i\mathbb{R}) \rightarrow B(H)$ is the spectral measure of the generator V ; see section 2.1). Similarly, the time-autocorrelation function $C_{f,\tau} : \mathbb{R} \rightarrow \mathbb{C}$ under $V_{z,\tau}$ can be expressed as

$$C_{f,\tau}(t) = \langle f, U_\tau^t f \rangle = \int_{i\mathbb{R}} h_t d\nu_{f,\tau}, \quad (61)$$

where $\nu_{f,\tau} : \mathcal{B}(i\mathbb{R}) \rightarrow [0, 1]$ is the Borel probability measure $\nu_{f,\tau}(\Theta) = \langle f, E_\tau(\Theta) \rangle$ induced by the (discrete) spectral measure $E_\tau : \mathcal{B}(i\mathbb{R}) \rightarrow B(H)$ of $V_{z,\tau}$,

$$E_\tau(\Theta) = \sum_{l: i\omega_{l,\tau} \in \Theta} \langle \psi_{l,\tau}, \cdot \rangle \psi_{l,\tau}. \quad (62)$$

Thus, testing for approximation of $C_f(t)$ by $C_{f,\tau}(t)$ amounts to testing for approximation of the spectral measure of the generator for specific observables (f) and test functions (h_t). Combining (61) and (62) leads to the formula

$$C_{f,\tau}(t) = \sum_{l \in \mathbb{Z}} e^{i\omega_{l,\tau}t} |c_{l,\tau}|^2, \quad c_{l,\tau} = \langle \psi_{l,\tau}, f \rangle, \quad (63)$$

giving the autocorrelation function in terms of the expansion coefficients $c_{l,\tau}$ of f in the $\psi_{l,\tau}$ basis of H and the corresponding eigenvalues $\omega_{l,\tau}$.

In the numerical setting of this section, we consider the empirical normalized anomaly correlation function computed for times $t_j = j \Delta t$, $j \in \mathbb{N}_0$, from samples of an observable $f : \mathcal{M} \rightarrow \mathbb{R}$ on the training data,

$$\hat{C}_f(t_j) = \frac{1}{N \|\hat{f}'\|_{\hat{H}_N}^2} \sum_{n=0}^{N-1} \hat{f}'(x_n) \hat{f}'(x_{n+j}), \quad \hat{f}' = f - \frac{1}{N} \sum_{n=0}^{N-1} f(x_n).$$

If f represents a unit vector in \tilde{H} then $\hat{C}_f(t_j)$ converges to $C_f(t_j)$ as $N \rightarrow \infty$ by ergodicity. We further approximate $C_{f,\tau}(t_j)$ by the autocorrelation function $\hat{C}_{f,\tau}(t_j)$ associated with the spectral measure of $V_{z,\tau,L,N}^{(M)}$, computed using an analogous formula to (63) applied to the unit vector $\hat{f}' / \|\hat{f}'\|_{\hat{H}_N} \in \hat{H}_N$ using the eigenfrequencies $\omega_{l,\tau,L,N}^{(M)}$ and the corresponding eigenfunctions $\psi_{l,\tau,L,N}^{(M)}$.

In fig. 8, we compare the empirical autocorrelation \hat{C}_f with the approximated autocorrelation $\hat{C}_{f,\tau}$ with f set to selected components $F^{(j)} : X \rightarrow \mathbb{R}$ of the embedding maps $F = (F^{(1)}, \dots, F^{(d)}) : X \rightarrow \mathbb{R}^d$ for the linear rotation, skew-product rotation, and L63 examples from sections 6.1–6.3, respectively.

In all examples considered, $\hat{C}_{f,\tau}$ tracks \hat{C}_f relatively well (at least for short times), with the case of the linear torus flow exhibiting the most accurate reconstruction (perhaps unsurprisingly due to the simplicity of the dynamics and observation map). A noticeable discrepancy between $\hat{C}_{f,\tau}(t_j)$ and $\hat{C}_f(t_j)$ is an apparent buildup of phase error as t_j increases for the $F^{(3)}$ component of the embedding map for the skew-product rotation and L63 system. In the case of the $F^{(1)}$ and $F^{(2)}$ components of the L63 system, we see that $\hat{C}_{f,\tau}$ captures the initial decay of correlations, but on longer times exhibits oscillations which are not seen in the true system. This re-emergence of correlations is likely due to the fact that $\hat{C}_{f,\tau}$ is given by a superposition of at most $2M$ periodic components (see algorithm 1), and thus cannot decay to 0 as $t_j \rightarrow \infty$. Nonetheless, for any $T > 0$, $\hat{C}_{f,\tau}(t_j)$ can be made arbitrarily close to the true autocorrelation $C_f(t_j)$ for all $t_j \in [0, T]$ for sufficiently large N, M, L and sufficiently small τ .

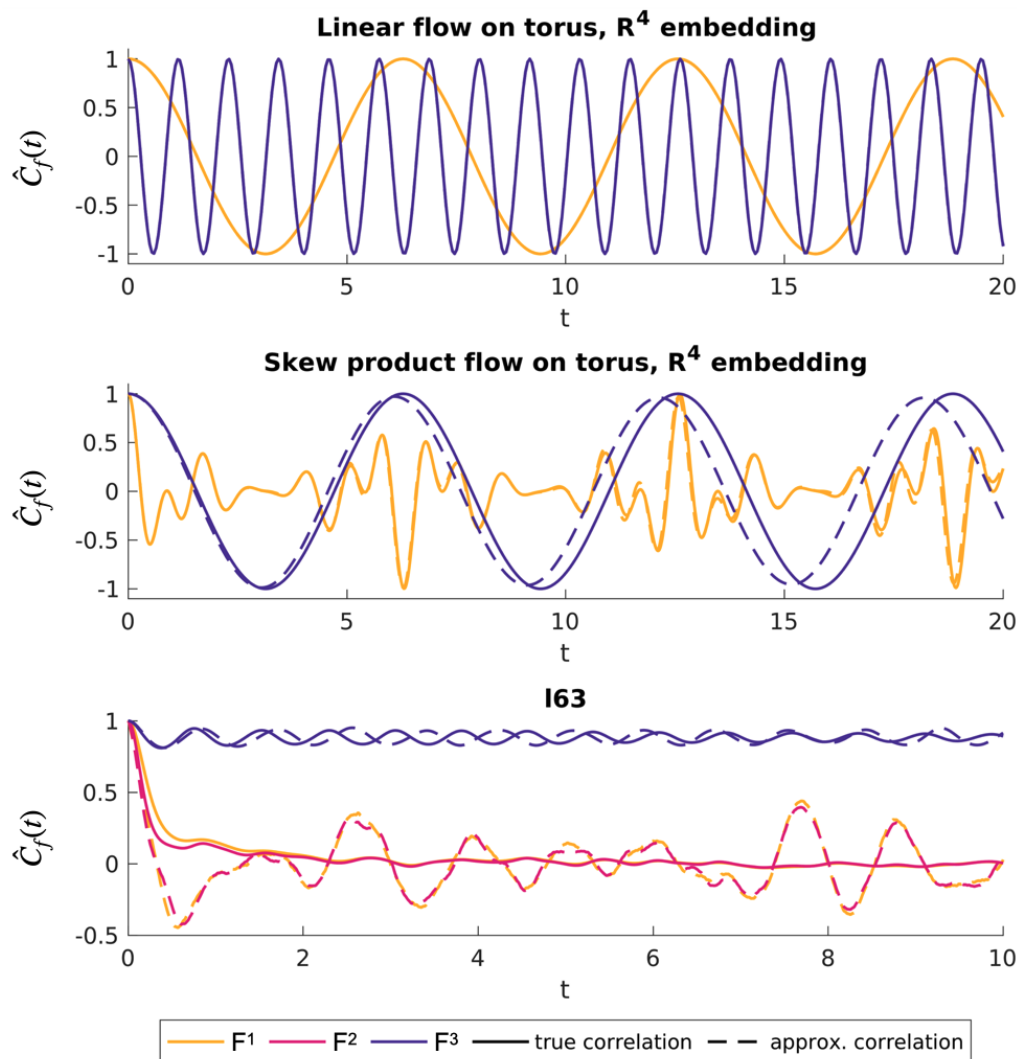


Figure 8. Comparison of the empirical autocorrelation functions \hat{C}_f (dashed lines) of selected coordinate functions $F^{(j)}$ to the autocorrelation functions $\hat{C}_{f,\tau}$ calculated from the approximated generator $V_{z,\tau}$ (solid lines). Only $F^{(1)}$ and $F^{(3)}$ are plotted in the two torus systems, as the correlation functions are the same in the \mathbb{R}^4 embedding for $j = 1$ and $j = 2$ as well as $j = 3$ and $j = 4$.

7. Conclusions

In this paper, we have developed a method for spectrally-accurate approximations of the Koopman generator on L^2 for continuous-time, ergodic, measure-preserving dynamical systems. The primary element of this method is a regularization of the Koopman resolvent using a semigroup of Markovian kernel integral operators which produces a one-parameter family of compact operators with discrete spectra and complete orthonormal families of associated eigenfunctions. These compactified operators act as resolvents of approximations $V_{z,\tau}$ to the generator that preserve important properties (namely, skew-adjointness and unboundedness) and converge spectrally to the generator in a limit of vanishing regularization parameter, $\tau \searrow 0$. In particular, the family $V_{z,\tau}$

generates unitary evolution groups with discrete spectra that converge strongly to the Koopman group on L^2 . Using a posteriori pseudospectral criteria, we identify elements of the spectra of $V_{z,\tau}$ whose corresponding eigenfunctions evolve with approximately cyclic behavior and slow correlation decay (i.e., behave as approximate Koopman eigenfunctions).

This method translates well to the data-driven setting. In particular, the use of the integral representation of the resolvent allows the use of integral quadrature methods with a resolvent parameter $z > 0$ that can be tuned to the time-resolution of the observed data (which, in practice, is difficult to control). Moreover, our use of data-driven basis functions obtained by eigendecomposition of kernel integral operators naturally addresses the problem of constructing well-conditioned dictionaries for Koopman operator approximation with asymptotic convergence guarantees in the large data limit. Using examples with pure point spectra (torus rotation and skew-rotation) and mixing dynamics (Lorenz 63 system), we have demonstrated this method can accurately approximate Koopman eigenvalues and eigenfunctions for those systems that have them, and is also effective at identify slowly decorrelating observables in systems with mixing dynamics and non-trivial continuous Koopman spectra.

A possible topic for future work would be to characterize aspects of the dependence of the eigenvalues and eigenfunctions of $V_{z,\tau}$ on the regularization parameter τ . As mentioned in section 1, the fact that $V_{z,\tau}$ is a family of operators with compact resolvent (rather than compact operators as in the approach of [26]) opens the possibility that this dependence is analytic, which could lead to new data-driven algorithms that take advantage of this analyticity. It would also be fruitful to explore applications of higher-order quadrature schemes for resolvent approximation and/or positive-frequency projection, as well as applications of recently-proposed residual-based criteria for filtering spurious eigenvalues from the spectra of $V_{z,\tau}$ [20]. Finally, while the focus of this work has been on L^2 spaces, implementations of our approach with positive-definite kernels should have natural analogs in RKHSs (cf. [26]). Working in an RKHS setting should be useful for supervised learning of models for predicting observables, which we plan to pursue in future work.

Appendix A. Kernel construction

In this appendix, we outline the construction of the families of Markov kernels $p_\tau : \mathcal{M} \times \mathcal{M} \rightarrow \mathbb{R}_+$ and $p_{\tau,N} : \mathcal{M} \times \mathcal{M} \rightarrow \mathbb{R}_+$, $\tau > 0$, associated with the integral operators $G_\tau : H \rightarrow H$ and $G_{\tau,N} : \hat{H}_N \rightarrow \hat{H}_N$, respectively. Our approach follows closely [35, 26], who use results of [79, 15, 7] to build these kernels and study their properties. Here, we summarize the main steps of the construction, referring the reader to [35, 26] for further details.

Appendix A.1. Choice of kernel

Our starting point is a strictly positive, measurable kernel function $k : \mathcal{M} \times \mathcal{M} \rightarrow \mathbb{R}_+$ that is continuous on the compact set M . In data-driven applications, we define k as the pullback of a kernel $\kappa : Y \times Y \rightarrow \mathbb{R}_+$ on data space, i.e.,

$$k(x, x') = \kappa(F(x), F(x')); \quad (\text{A.1})$$

see section 5. As a concrete example, the Gaussian radial basis function (RBF) kernel,

$$\kappa(y, y') = e^{-\|y-y'\|^2/\epsilon^2}, \quad \epsilon > 0, \quad (\text{A.2})$$

is continuous and strictly positive on $Y = \mathbb{R}^d$, and thus leads to a pullback kernel k from (A.1) that meets our requirements under the continuity and injectivity assumptions on the observation map F from section 5.1.

In the experiments of section 6 we work with a variable-bandwidth generalization of (A.2) proposed in [7],

$$\kappa(y, y') = \exp\left(-\frac{\|y - y'\|^2}{\epsilon^2 \sigma(y) \sigma(y')}\right), \quad \epsilon > 0, \quad (\text{A.3})$$

where $\sigma : Y \rightarrow \mathbb{R}_+$ is a continuous, strictly positive bandwidth function obtained via a kernel density estimation procedure. Intuitively, the role of σ is to increase (decrease) the locality of the kernel in regions of high (low) sampling density with respect to the Lebesgue measure on data space. See [26, Appendix A] and [35, Algorithm 1] for a precise definition and pseudocode. We tune the kernel bandwidth parameter ϵ automatically using the method described in [17, 7]; see again [35, Algorithm 1].

We should note that in applications the bandwidth function σ depends on the sampling measure μ_N underlying the training data; however, it converges uniformly to a data-independent function in the large data limit, $N \rightarrow \infty$. In this appendix, we suppress the dependence of σ on μ_N from our notation for κ from (A.3) for simplicity.

Appendix A.2. Markov normalization

With the kernel k from (A.1), we apply a normalization procedure based on the approach of [15] to obtain a symmetric Markov kernel $p : \mathcal{M} \times \mathcal{M} \rightarrow \mathbb{R}_+$ with respect to the invariant measure μ , as well as Markov kernels $p_N : \mathcal{M} \times \mathcal{M} \rightarrow \mathbb{R}_+$ with respect to the sampling measures μ_N .

Given a Borel probability measure ν with support contained in M , we construct a symmetric Markov kernel $p^{(\nu)} : \mathcal{M} \times \mathcal{M} \rightarrow \mathbb{R}_+$ with respect to ν through the sequence of operations

$$\begin{aligned} d(x) &= \int_M k(x, x') d\nu(x'), & q(x) &= \int_M \frac{k(x, x')}{d(x')} d\nu(x'), \\ p^{(\nu)}(x, x') &= \int_M \frac{k(x, x'')k(x'', x')}{d(x)q(x'')d(x')} d\nu(x''). \end{aligned} \quad (\text{A.4})$$

One readily verifies that $p^{(\nu)}$ is symmetric, strictly positive, and continuous on $M \times M$, and satisfies the Markov condition

$$\int_M p^{(\nu)}(x, \cdot) d\nu = 1, \quad \forall x \in \mathcal{M}.$$

Moreover, it can be shown that the corresponding integral operator $G^{(\nu)} : L^2(\nu) \rightarrow L^2(\nu)$ defined as

$$G^{(\nu)} f = \int_M p^{(\nu)}(\cdot, x) f(x) d\nu(x) \quad (\text{A.5})$$

is a trace class, strictly positive, ergodic Markov operator on $L^2(\nu)$.

Henceforth, we will let $p \equiv p^{(\mu)}$ and $\hat{p}_N \equiv p^{(\mu_N)}$ be the kernels obtained via (A.4) for the invariant measure μ and sampling measure μ_N , respectively, and $G \equiv G^{(\mu)}$ and $\hat{G}_N \equiv G^{(\mu_N)}$ be the corresponding integral operators on $H = L^2(\mu)$ and $\hat{H}_N = L^2(\mu_N)$, respectively, defined via (A.5). We will also let

$$G\phi_j = \lambda_j\phi_j, \quad \hat{G}_N\phi_{j,N} = \lambda_{j,N}\phi_{j,N} \quad (\text{A.6})$$

be eigendecompositions of G and \hat{G}_N , where $\{\phi_j\}_{j=0}^\infty$ and $\{\phi_{j,N}\}_{j=0}^{N-1}$ are real orthonormal bases of H and \hat{H}_N , and the corresponding eigenvalues are ordered as $1 = \lambda_0 > \lambda_1 \geq \lambda_2 \geq \dots \searrow 0^+$ and $1 = \lambda_{0,N} > \lambda_{1,N} \geq \lambda_{2,N} \geq \dots \lambda_{N-1,N} > 0$, respectively. Note that \hat{G}_N is represented by an $N \times N$ bistochastic matrix $\mathbf{G} = [\hat{p}_N(x_i, x_j)]_{i,j=0}^{N-1}$ computed from the training data $y_i = F(x_i)$, and the eigenvalues and eigenvectors of \hat{G}_N can be obtained by eigendecomposition of \mathbf{G} (cf. section 5.2). However, it turns out that for the class of kernels from (A.4) the eigendecomposition of \hat{G}_N can be computed from the singular value decomposition of an $N \times N$ non-symmetric kernel matrix $\hat{\mathbf{K}}$ that factorizes \mathbf{G} as $\mathbf{G} = \hat{\mathbf{K}}\hat{\mathbf{K}}^\top$; see [26, Appendix B]. We use the latter approach in our numerical experiments as it avoids explicit formation of the kernel matrix \mathbf{G} .

Appendix A.3. Markov semigroups

We use the integral operators G and \hat{G}_N from Appendix A.2 to define semigroups of Markov operators $G_\tau : H \rightarrow H$ and $G_{\tau,N} : \hat{H}_N \rightarrow \hat{H}_N$ parameterized by the regularization parameter $\tau \geq 0$. To that end, we first define the non-negative numbers

$$\eta_j = \left(\frac{1}{\lambda_j} - 1 \right) \frac{1}{\lambda_1}, \quad \eta_{j,N} = \left(\frac{1}{\lambda_{j,N}} - 1 \right) \frac{1}{\lambda_{1,N}},$$

and the self-adjoint operators $\Delta : D(\Delta) \rightarrow H$ and $\Delta_N : \hat{H}_N \rightarrow \hat{H}_N$ with

$$\Delta = \frac{G^{-1} - I}{\lambda_1}, \quad \Delta_N = \frac{\hat{G}_N^{-1} - I}{\lambda_{1,N}},$$

where the domain $D(\Delta) \subset H$ of Δ is given by $D(\Delta) = \{f \in H : \sum_{j=0}^\infty \eta_j |\langle \phi_j, f \rangle|^2 < \infty\}$.

The operators Δ and Δ_N are positive operators with discrete spectra $\{\eta_j\}_{j=0}^\infty$ and $\{\eta_{j,N}\}_{j=0}^{N-1}$ that generate semigroups $\{G_\tau\}_{\tau \geq 0}$ and $\{G_{\tau,N}\}_{\tau \geq 0}$ of compact self-adjoint

operators $G_\tau = e^{-\tau\Delta}$ and $G_{\tau,N} = e^{-\tau\Delta_N}$, respectively. One readily verifies the eigendecompositions

$$G_\tau\phi_j = \lambda_j^\tau\phi_j, \quad G_{\tau,N}\phi_{j,N} = \lambda_{j,N}^\tau\phi_{j,N},$$

where $\lambda_j^\tau = e^{-\tau\eta_j}$ and $\lambda_{j,N}^\tau = e^{-\tau\eta_{j,N}}$ are strictly positive eigenvalues for every $\tau \geq 0$. Moreover, it can be shown [26, Theorem 1] that for any $\tau > 0$, G_τ and $G_{\tau,N}$ are trace class integral operators,

$$G_\tau f = \int_M p_\tau(\cdot, x)f(x) d\mu(x), \quad G_{\tau,N}f = \int_M p_{\tau,N}(\cdot, x)f(x) d\mu_N(x).$$

Here, $p_\tau : \mathcal{M} \times \mathcal{M} \rightarrow \mathbb{R}_+$ and $p_{\tau,N} : \mathcal{M} \times \mathcal{M} \rightarrow \mathbb{R}_+$ are Markov kernels that are continuous on $M \times M$, and are given by uniformly convergent Mercer expansions

$$p_\tau(x, x') = \sum_{j=0}^{\infty} \lambda_j^\tau \varphi_j(x) \varphi_j(x'), \quad p_{\tau,N}(x, x') = \sum_{j=0}^{N-1} \lambda_{j,N}^\tau \varphi_{j,N}(x) \varphi_{j,N}(x'), \quad \forall x, x' \in M. \quad (\text{A.7})$$

In (A.7), $\varphi_j, \varphi_{j,N} \in C(M)$ are the continuous representatives of ϕ_j and $\phi_{j,N}$, respectively (cf. (36)),

$$\varphi_j = \frac{1}{\lambda_j^\tau} \int_M p(\cdot, x) \phi_j(x) d\mu(x), \quad \varphi_{j,N} = \frac{1}{\lambda_{j,N}^\tau} \int_M \hat{p}_N(\cdot, x) \phi_{j,N}(x) d\mu_N(x).$$

In summary, the kernels p_τ and $p_{\tau,N}$ satisfy all requirements laid out in sections 3.1 and 5.2.

Before closing this appendix, we note that the Gaussian RBF kernel (A.2) on \mathbb{R}^d is translation-invariant (i.e., $\kappa(y+s, y'+s) = \kappa(y, y')$ for all $y, y', s \in \mathbb{R}^d$), but the variable-bandwidth kernel (A.3) is not translation-invariant if σ is a non-constant function. In the linear torus rotation and skew torus rotation examples in sections 6.1 and 6.2, respectively, the data-dependent bandwidth function σ is, in general, non-constant but converges as $N \rightarrow \infty$ to a constant function on the support of the sampling distribution of the data when using the F_4 (“flat”) embedding (58). The latter, implies that the associated kernel integral operator G_τ commutes with the Koopman operators of the linear and skew torus rotations, and thus that any given Koopman eigenspace can be spanned by finitely many basis functions ϕ_j . In the case of the torus examples using the F_3 embedding (59) into \mathbb{R}^3 or the L63 system (section 6.3), the bandwidth function σ is nonconstant even in the $N \rightarrow \infty$ limit. In such cases, we cannot expect to completely recover Koopman eigenspaces with finite basis expansions.

Appendix B. Koopman eigenfunctions for linear and skew torus rotations

We plot selected known eigenfunctions for the Koopman generator of the systems described in section 6.1 and section 6.2 for ease of comparison between the analytically known eigenfunctions and the approximate numerical eigenfunctions. See fig. B1.

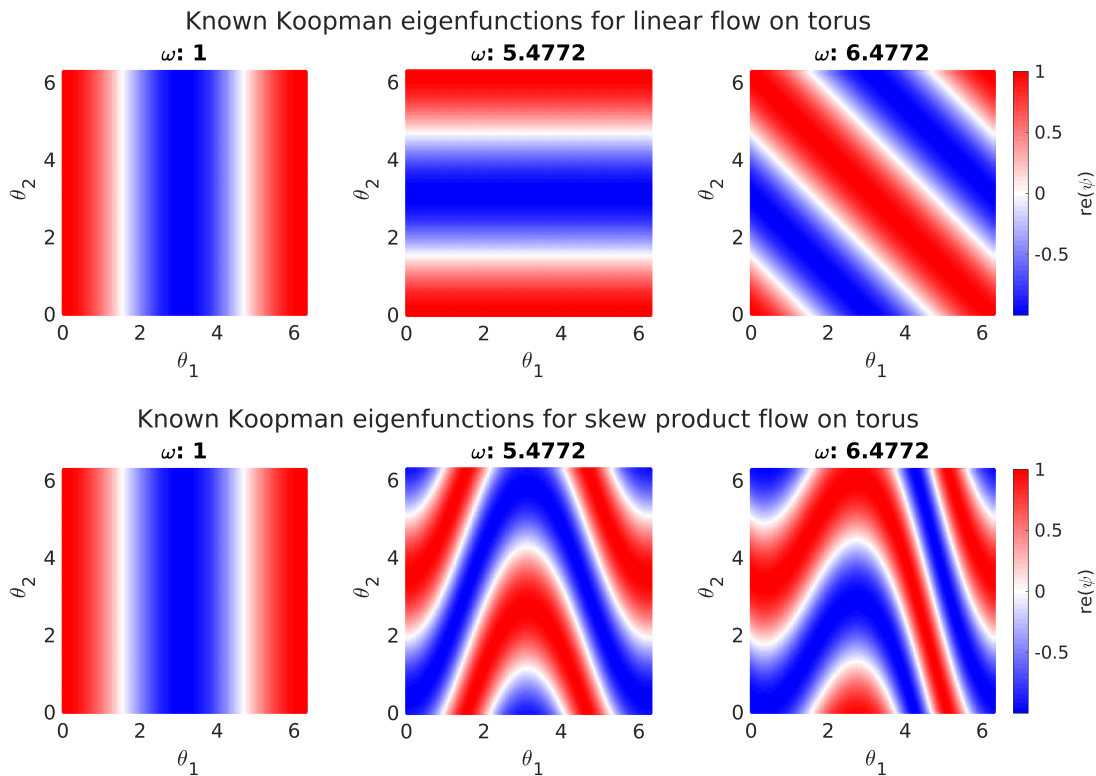


Figure B1. Scatterplots of real parts of Koopman eigenfunctions ψ_j on the torus parameterized by θ_1 and θ_2 for eigenfrequencies equal to $\omega_j = 1$ (left), $\omega_j = \sqrt{30}$ (middle), and $\omega_j = 1 + \sqrt{30}$ (right) with the same colormaps as the figures in section 6. Top: Koopman eigenfunctions for the linear flow on the torus. Bottom: Koopman eigenfunctions for the skew-product flow on the torus

Acknowledgments

We thank Michael Montgomery, Keefer Rowan, and Travis Russell for helpful conversations. DG acknowledges support from the US National Science Foundation under grant DMS-1854383, the US Office of Naval Research under MURI grant N00014-19-1-242, and the US Department of Defense, Basic Research Office under Vannevar Bush Faculty Fellowship grant N00014-21-1-2946. CV was supported by the US National Science Foundation Graduate Research Fellowship under grant DGE-1839302.

References

- [1] R. Alexander and D. Giannakis. Operator-theoretic framework for forecasting nonlinear time series with kernel analog techniques. *Phys. D*, 409, 2020.
- [2] P. J. Badoo, B. Herrmann, B. J. McKeon, J. N. Kutz, and S. L. Brunton. Physics-informed dynamic mode decomposition. *Proc. R. Soc. A*, 479, 2023.
- [3] P. B. Bailey, W. N. Everitt, J. Weidmann, and A. Zettl. Regular approximations of singular Sturm-Liouville problems. *Results Math.*, 23(1-2):3-22, 1993.

- [4] V. Baladi. *Positive Transfer Operators and Decay of Correlations*, volume 16 of *Advanced Series in Nonlinear Dynamics*. World Scientific, Singapore, 2000.
- [5] T. Berry, R. Cressman, Z. Gregurić-Ferenček, and T. Sauer. Time-scale separation from diffusion-mapped delay coordinates. *SIAM J. Appl. Dyn. Sys.*, 12:618–649, 2013.
- [6] T. Berry, D. Giannakis, and J. Harlim. Nonparametric forecasting of low-dimensional dynamical systems. *Phys. Rev. E.*, 91, 2015.
- [7] T. Berry and J. Harlim. Variable bandwidth diffusion kernels. *Appl. Comput. Harmon. Anal.*, 40(1):68–96, 2016.
- [8] M. Blank. Egodic averaging with and without invariant measures. *Nonlinearity*, 30:4649–4664, 2017.
- [9] M. Blank, G. Keller, and C. Liverani. Ruelle–Perron–Frobenius spectrum for Anosov maps. *Nonlinearity*, 15(6):1905–1973, 2002.
- [10] S. Bögli. Convergence of sequences of linear operators and their spectra. *Integr. Equ. Oper. Theory*, 88:559–599, 2017.
- [11] S. L. Brunton, B. W. Brunton, J. L. Proctor, E. Kaiser, and J. N. Kutz. Chaos as an intermittently forced linear system. *Nat. Commun.*, 8, 2017.
- [12] S. L. Brunton, M. Budisić, E. Kaiser, and J. N. Kutz. Modern Koopman theory for dynamical systems. *SIAM Rev.*, 64(2):229–340, 2022.
- [13] F. Chaitin-Chatelin and A. Harrabi. About definitions of pseudospectra of closed operators in Banach spaces. Technical Report TR/PA/98/08, CERFACS, Toulouse, France, 1998.
- [14] F. Chatelin. *Spectral Approximation of Linear Operators*. Classics in Applied Mathematics. Society for Industrial and Applied Mathematics, Philadelphia, 2011.
- [15] R. Coifman and M. Hirn. Bi-stochastic kernels via asymmetric affinity functions. *Appl. Comput. Harmon. Anal.*, 35(1):177–180, 2013.
- [16] R. R. Coifman and S. Lafon. Diffusion maps. *Appl. Comput. Harmon. Anal.*, 21:5–30, 2006.
- [17] R. R. Coifman, Y. Shkolnisky, F. J. Sigworth, and A. Singer. Graph Laplacian tomography from unknown random projections. *IEEE Trans. Image Process.*, 17(10):1891–1899, 2008.
- [18] M. Colbrook, A. Horning, and A. Townsend. Computing spectral measures of self-adjoint operators. *SIAM Rev.*, 63(3):489–524, 2021.
- [19] M. J. Colbrook. The mpEDMD algorithm for data-driven computations of measure-preserving dynamical systems. *SIAM J. Numer. Anal.*, 61(3):1585–1608, 2023.
- [20] M. J. Colbrook and A. Townsend. Rigorous data-driven computation of spectral properties of Koopman operators for dynamical systems. *Commun. Pure Appl. Math.*, 77:221–283, 2024.
- [21] P. Constantin, C. Foias, B. Nicolaenko, and R. Témam. *Integral Manifolds and Inertial Manifolds for Dissipative Partial Differential Equations*. Springer, New York, 1989.
- [22] F. Cucker and S. Smale. On the mathematical foundations of learning. *Bull. Amer. Math. Soc.*, 39(1):1–49, 2001.
- [23] S. Das and D. Giannakis. Delay-coordinate maps and the spectra of Koopman operators. *J. Stat. Phys.*, 175(6):1107–1145, 2019.
- [24] S. Das and D. Giannakis. Koopman spectra in reproducing kernel Hilbert spaces. *Appl. Comput. Harmon. Anal.*, 49(2):573–607, 2020.
- [25] S. Das and D. Giannakis. On harmonic Hilbert spaces on compact abelian groups. *J. Fourier Anal. Appl.*, 29(1):12, 2023.
- [26] S. Das, D. Giannakis, and J. Slawinska. Reproducing kernel Hilbert space compactification of unitary evolution groups. *Appl. Comput. Harmon. Anal.*, 54:75–136, 2021.
- [27] C. R. de Oliveira. *Intermediate Spectral Theory and Quantum Dynamics*, volume 54 of *Progress in Mathematical Physics*. Birkhäuser, Basel, 2009.
- [28] M. Dellnitz and O. Junge. On the approximation of complicated dynamical behavior. *SIAM J. Numer. Anal.*, 36:491, 1999.
- [29] T. Eisner, B. Farkas, M. Haase, and R. Nagel. *Operator Theoretic Aspects of Ergodic Theory*, volume 272 of *Graduate Texts in Mathematics*. Springer, Cham, 2015.

- [30] K.-J. Engel and R. Nagel. *One-Parameter Semigroups for Linear Evolution Equations*, volume 194 of *Graduate Texts in Mathematics*. Springer, Berlin, 2000.
- [31] D. C. Freeman, D. Giannakis, B. Mintz, A. Ourmazd, and J. Slawinska. Data assimilation in operator algebras. *Proc. Natl. Acad. Sci.*, 120(8), 2023.
- [32] G. Froyland. Computer-assisted bounds for the rate of decay of correlations. *Commun. Math. Phys.*, 189(NN):237–257, 1997.
- [33] G. Froyland, D. Giannakis, B. Lintner, M. Pike, and J. Slawinska. Spectral analysis of climate dynamics with operator-theoretic approaches. *Nat. Commun.*, 12, 2021.
- [34] M. C. Genton. Classes of kernels for machine learning: A statistics perspective. *J. Mach. Learn. Res.*, 2:299–312, 2001.
- [35] D. Giannakis. Data-driven spectral decomposition and forecasting of ergodic dynamical systems. *Appl. Comput. Harmon. Anal.*, 47(2):338–396, 2019.
- [36] D. Giannakis. Delay-coordinate maps, coherence, and approximate spectra of evolution operators. *Res. Math. Sci.*, 8, 2021.
- [37] D. Giannakis and A. J. Majda. Nonlinear Laplacian spectral analysis for time series with intermittency and low-frequency variability. *Proc. Natl. Acad. Sci.*, 109(7):2222–2227, 2012.
- [38] D. Giannakis, J. Slawinska, and Z. Zhao. Spatiotemporal feature extraction with data-driven Koopman operators. In D. Storcheus, A. Rostamizadeh, and S. Kumar, editors, *Proceedings of the 1st International Workshop on Feature Extraction: Modern Questions and Challenges at NIPS 2015*, volume 44 of *Proceedings of Machine Learning Research*, pages 103–115, Montreal, Canada, 2015. PMLR.
- [39] N. Govindarajan, R. Mohr, S. Chandrasekaran, and I. Mezić. On the approximation of Koopman spectra of measure-preserving flows. *SIAM J. Appl. Dyn. Syst.*, 20(1):232–261, 2021.
- [40] P. R. Halmos. *Lectures on Ergodic Theory*. American Mathematical Society, Providence, 1956.
- [41] P. R. Halmos and J. von Neumann. Operator methods in classical mechanics, II. *Ann. Math.*, 43(2):332–350, 1942.
- [42] M. Ikeda, I. Ishikawa, and C. Schlosser. Koopman and Perron–Frobenius operators on reproducing kernel Banach spaces. *Chaos*, 32, 2022.
- [43] O. Junge and P. Koltai. Discretization of the Frobenius–Perron operator using a sparse Haar tensor basis: The sparse Ulam method. *SIAM J. Numer. Anal.*, 47:3464–2485, 2009.
- [44] O. Junge, D. Matthes, and B. Schmitzer. Entropic transfer operators, 2022.
- [45] T. Kato. *Perturbation Theory for Linear Operators*. Classics in Mathematics. Springer-Verlag, Berlin, 2 edition, 1995.
- [46] Y. Kawahara. Dynamic mode decomposition with reproducing kernels for Koopman spectral analysis. In D. D. Lee, M. Sugiyama, U. von Luxburg, I. Guyon, and R. Garnett, editors, *Advances in Neural Information Processing Systems*, pages 911–919. Curran Associates, 2016.
- [47] S. Klus and C. Koltai, P. Schütte. On the numerical approximation of the Perron-Frobenius and Koopman operator. *J. Comput. Dyn.*, 3(1):51–79, 2016.
- [48] S. Klus, F. Nüske, P. Koltai, H. Wu, I. Kevrekidis, C. Schütte, and F. Noé. Data-driven model reduction and transfer operator approximation. *J. Nonlinear Sci.*, 28:985–1010, 2018.
- [49] S. Klus, I. Schuster, and K. Muandet. Eigendecomposition of transfer operators in reproducing kernel Hilbert spaces. *J. Nonlinear Sci.*, 30:283–315, 2020.
- [50] P. Koltai, J. von Lindheim, S. Neumayer, and G. Steidl. Transfer operators from optimal transport plans for coherent set detection. *Phys. D*, 426, 2021.
- [51] B. O. Koopman. Hamiltonian systems and transformation in Hilbert space. *Proc. Natl. Acad. Sci.*, 17(5):315–318, 1931.
- [52] B. O. Koopman and J. von Neumann. Dynamical systems of continuous spectra. *Proc. Natl. Acad. Sci.*, 18(3):255–263, 1932.
- [53] M. Korda, M. Putinar, and I. Mezić. Data-driven spectral analysis of the Koopman operator. *Appl. Comput. Harmon. Anal.*, 48(2):599–629, 2020.
- [54] V. R. Kostic, P. Novelli, A. Mauer, C. Ciliberto, L. Rosasco, and M. Pontil. Learning dynamical

- systems with Koopman operator regression in reproducing kernel Hilbert spaces. In S. Koyejo, S. Mohamed, A. Agarwal, D. Belgrave, K. Cho, and A. Oh, editors, *Advances in Neural Information Processing Systems 35 (NeurIPS 2022)*, 2022.
- [55] K. Law, A. Shukla, and A. M. Stuart. Analysis of the 3DVAR filter for the partially observed Lorenz'63 model. *Discrete Contin. Dyn. Syst.*, 34(3):1061–10178, 2013.
- [56] K. Law, A. Stuart, and K. Zygalakis. *Data Assimilation: A Mathematical Introduction*, volume 62 of *Texts in Applied Mathematics*. Springer, New York, 2015.
- [57] E. N. Lorenz. Deterministic nonperiodic flow. *J. Atmos. Sci.*, 20:130–141, 1963.
- [58] S. Luzzatto, I. Melbourne, and F. Paccaut. The Lorenz attractor is mixing. *Comm. Math. Phys.*, 260(2):393–401, 2005.
- [59] I. Mezić. Spectral properties of dynamical systems, model reduction and decompositions. *Nonlinear Dyn.*, 41:309–325, 2005.
- [60] I. Mezić. Analysis of fluid flows via spectral properties of the Koopman operator. *Annu. Rev. Fluid Mech.*, 45:357—378, 2013.
- [61] I. Mezić and A. Banaszuk. Comparison of systems with complex behavior. *Phys. D.*, 197:101–133, 2004.
- [62] S. E. Otto and C. W. Rowley. Koopman operators for estimation and control of dynamical systems. *Annu. Rev. Control Robot. Auton. Syst.*, 4:59–87, 2021.
- [63] C. Penland. Random forcing and forecasting using principal oscillation pattern analysis. *Mon. Weather Rev.*, 117(10):2165–2185, 1989.
- [64] J. A. Rosenfeld, R. Kamalapurkar, L. F. Gruss, and T. T. Johnson. Dynamic mode decomposition for continuous time systems with the Liouville operator. *J. Nonlinear Sci.*, 32, 2022.
- [65] J. A. Rosenfeld, R. Kamalapurkar, B. Russo, and T. T. Johnson. Occupation kernels and densely defined liouville operators for system identification. In *2019 IEEE 58th Conference on Decision and Control (CDC)*, pages 6455–6460, 2019.
- [66] C. W. Rowley, I. Mezić, S. Bagheri, P. Schlatter, and D. S. Henningson. Spectral analysis of nonlinear flows. *J. Fluid Mech.*, 641:115–127, 2009.
- [67] T. Sauer, J. A. Yorke, and M. Casdagli. Embedology. *J. Stat. Phys.*, 65(3–4):579–616, 1991.
- [68] P. J. Schmid. Dynamic mode decomposition of numerical and experimental data. *J. Fluid Mech.*, 656:5–28, 2010.
- [69] P. J. Schmid and J. L. Sesterhenn. Dynamic mode decomposition of numerical and experimental data. In *Bull. Amer. Phys. Soc., 61st APS meeting*, page 208, San Antonio, 2008.
- [70] M. H. Stone. On one-parameter unitary groups in Hilbert space. *Ann. Math.*, 33(3):643–648, 1932.
- [71] Y. Susuki, A. Mauroy, and I. Mezić. Koopman resolvent: A Laplace-domain analysis of nonlinear autonomous dynamical systems. *SIAM J. Appl. Dyn. Syst.*, 20(4):2013–2036, 2021.
- [72] F. Takens. Detecting strange attractors in turbulence. In *Dynamical Systems and Turbulence*, volume 898 of *Lecture Notes in Mathematics*, pages 366–381. Springer, Berlin, 1981.
- [73] L. N. Trefethen and M. Embree. *Spectra and Pseudospectra: The Behavior of Nonnormal Matrices and Operators*. Princeton University Press, Princeton, 2005.
- [74] N. G. Trillos, M. Gerlach, M. Hein, and D. Slepčev. Error estimates for spectral convergence of the graph Laplacian on random geometric graphs towards the Laplace–Beltrami operator. *Found. Comput. Math.*, 20:827–887, 2020.
- [75] J. H. Tu, C. W. Rowley, C. M. Luchenburg, S. L. Brunton, and J. N. Kutz. On dynamic mode decomposition: Theory and applications. *J. Comput. Dyn.*, 1(2):391–421, 2014.
- [76] W. Tucker. The Lorenz attractor exists. *C. R. Acad. Sci. Paris, Ser. I*, 328:1197–1202, 1999.
- [77] S. M. Ulam. *Problems in Modern Mathematics*. Dover Publications, Mineola, 1964.
- [78] Divakar Viswanath. *Lyapunov exponents from random Fibonacci sequences to the Lorenz equations*. Cornell University, 1998.
- [79] U. von Luxburg, M. Belkin, and O. Bousquet. Consistency of spectral clustering. *Ann. Stat.*, 26(2):555–586, 2008.
- [80] P. Walters. *An Introduction to Ergodic Theory*, volume 79 of *Graduate Texts in Mathematics*.

Springer-Verlag, New York, 1981.

- [81] M. O. Williams, I. G. Kevrekidis, and C. W. Rowley. A data-driven approximation of the Koopman operator: Extending dynamic mode decomposition. *J. Nonlinear Sci.*, 25(6):1307–1346, 2015.
- [82] L.-S. Young. What are SRB measures, and which dynamical systems have them? *J. Stat. Phys.*, 108:733–754, 2002.